UNIVERSITY OF CALIFORNIA,
IRVINE

Elucidating the biomechanical aspects of mammalian Notch Signaling

DISSERTATION

submitted in partial satisfaction of the requirements
for the degree of

DOCTOR OF PHILOSOPHY

in Biomedical Engineering

by

Shreyas Raj Ravindranath

Dissertation Committee:
Associate Professor Elliot Botvinick, Chair
Assistant Professor Elliot E. Hui
Assistant Professor Olivier Cinquin

DEDICATION

To

my parents, sister and friends

TABLE OF CONTENTS

LIST OF FIGURES

LIST OF ABBREVIATIONS

Δ	deleted
ADAM	a disintegrin and metalloprotease
ANK	Ankyrin
BB94	Batimastat; 4-(N-hydroxylamino)-2R-isobutyl-3S
CSL	CBF1/Su(H)/Lag-2
D1Fc	Dll1 extracellular domain fused in frame with human IgG Fc without the CH2-CH3 hinge
DLL/ Dll	Delta Like Ligand
DMEM	Dulbecco's Modified Eagle Medium
DNA	Deoxyribonucleic Acid
DSL	Delta, Serrate, Lag-2
E10.5	Embryonic day 10.5
EDTA	Ethylenediaminetetraacetic acid
EGF	Epidermal growth factor
EMT	Endothelial to mesenchymal transition (or transformation)
ET	Energy Trace
FEC	Force Extension Curve
FI	Furin Inhibitor – Decanoyl Chloromethyl Ketone
Jag	Jagged
MNNL	Module at the N-terminus of Notch Ligand
MRI	magnetic resonance imaging
N1	Notch 1

N1Fc	Ligand binding domain of Notch containing EGF repeats 1-15 fused in frame (contains the human IgG Fc with the CH2-CH3 hinge)
N1ΔFC	Notch 1 with deleted Furin Cleavage
NECD	Notch extracellular domain
NICD	Notch intracellular domain
NRR	Negative Regulatory Region
OCDN	Notch without intracellular domain
OT	Optical Tweezers
PF	Pulling Force
RFS	Rupture Force Spectra
S1	Site 1 – Furin Cleavage site
S1 Rupture	Breakage at the HD-A and HD-B non-covalent links
S2	Site 2 – ADAM10/17 cleavage site
S2 Rupture	Rupture of Notch due to ADAM cleavage upon ligand pulling
S3	Site 3 – γ-Secretase cleavage site
TAPI-2	TNF-α processing Inhibitor-2 – broad spectrum metalloproteinase & ADAM inhibitor
TM	Transmembrane
TMHA	N1-EGFr-(1-15)-TM-HA
VSD	ventricular septal defect
WT	Wild type
γ	Gamma

ACKNOWLEDGMENTS

I would like to express my deep gratitude to Prof. Elliot Botvinick who inducted me into his lab to pursue on such an interesting project with so many unanswered questions. He instilled dedication and motivation in me since the early days. His mentorship has enabled me to navigate calm waters and tormenting storms of the research voyage with focus and meticulous effort. I would definitely wish him the best on his future projects and endeavors at the BEAMS lab. I would like to thank my collaborator and mentor Prof. Gerry Weinmaster (retd.) from UCLA whose wealth of knowledge, encouragement and support was unrivalled. I would like to thank my committee members Prof. Elliot Hui and Prof. Olivier Cinquin for overseeing my thesis and dissertation and guidance.

I would like to thank my mentors Dr. Bhupinder Shergill, Dr. Abhishek Kurup and Dr. Martha Alvarez for their excellent teaching, coaching and guidance. I thank my peers Breanna Padilla, Drs. Sean White, John Weidling, Seema Ehsan, Lei Tian, Luis Alonzo, and Mark Keating, Rachel Gurlin, Avid Najdahmadi, Todd Thorson and Jessica Hsieh for their support, help and critique on my work and research. I would like to thank my junior researchers Janelle Halog, Eashani Sathialingam and Tim Tran for performing critical aspects of my projects and helping me with several lab related tasks and duties. I would like to thank my fellow BEAMs lab members for their encouragement, cooperation, support and comraderie-ship during my tenure as a graduate student. Their contribution to the intellectual stream ideas and suggestions was perennial and unending. I express my gratitude. I also thank UCLA members Dr. Laurence Meloty-Kapella, Dr. Meredith Oltmann

and Helen Yu for their assistance during the early years of my project. I would like to express my gratitude to Ann Fain for managing Administrating affairs of the Department and helping me with several clearances and procedures. I would also like to thank the Department Chair Dr. Abe Lee and Chair of Edwards Lifesciences Center of Advanced Cardiovascular Technology Dr. Chris Hughes and Dr. Steven George (previous) for enabling a thriving center of facilities for cutting edge Biomedical research.

I would like to thank my parents, sister and her family, and my friends who have stood by me during all the times. I would have never been able to accomplish anything without their constant support and guidance.

I would finally like to thank the National Institutes of Health and National Science Foundation for supporting the Notch signaling project at the Weinmaster lab and the BEAMS lab.

CURRICULUM VITAE

Shreyas Raj Ravindranath

Education

Winter 2017 **University of California, Irvine, Ph.D.,** *Biomedical Engineering*, **GPA-3.86**

August 2011 **Indian Institute of Technology(IIT), Kharagpur, B.Tech (Honors) & M.Tech,** *Biotechnology & Biochemical Engineering*, **CGPA – 7.97/10**

Academic Projects

Mechanotransduction of ligand mediated forces in Notch Signaling pathway (2011-Present)

P.I.-: Prof. Elliot Botvinick (UCI); Collaborator-: Prof. Gerry Weinmaster (UCLA, retd.)

- Performed receptor ligand interaction force spectroscopy to understand core mechanistic aspects of the pathway
- Elucidated the biomechanical dependency of mammalian Notch receptor activation in detail
- Performed experiments on, built, repaired and maintained laser tweezers instrumentation

The Role of Mechanical Asymmetry in 3D Breast Cancer Culture Models (2015)

P.I. -: Prof. Elliot Botvinick (UCI); Collaborator-: Prof. Thea Tlsty (UCSF)

- Conducted protein extraction from 3D cell and tissue cultures
- Performed quantitative analysis of signaling protein markers (normal and oncogenic) in 2 different culture models

Measurement of ICAM1 and anti-ICAM1-Antibody bond mechanical properties using optical tweezers based dynamic force spectroscopy (2015 - 2016)

P.I. -: Prof. Elliot Botvinick (UCI); Collaborator-: Prof. Jered Haun (UCI)

- Performed force measurements of bond strengths between ICAM and its antibody for characterizing adhesion dynamics of nanoparticles for targeted delivery.

Cloning and Analysis of Genome Segment 4 & 5 of *Antheraea mylitta* cytoplasmic polyhedrosis virus (AmCPV) (2009-11)

P.I.-: Prof. Ananta K. Ghosh

- Trained in and utilized several molecular biology tools to understand the function of cypoviral non-structural genes
- Involved in the experiments proving the Guanylyl transferase activity of AmCPVS5

Performed extensive gene manipulation to express the protein with proper glycosylation and function in bacterial and bicoloviral expression system

Internships

	University of Bath, Bath, UK
May – July 2009	Investigated Neurosphere growth and assay conditions for Flaviviral gene transfections
	University of Agricultural Sciences (GKVK), Bengaluru, India
May – July 2008	Performed DNA Fingerprinting of 20 novel inbred rice varieties using RAPD markers

Teaching Experience

- Teaching assistant for two Undergraduate courses, viz. Tissue Engineering (BME1(Cell and Molecular Engineering (BME 50A) at UCI (2012-2013); held discussions, hours and lectures for 100 above students
- Mentored 3 UGs and 1 graduate student leading to 2 UGs applying to law schoc authorship on a publication and several UG merit awards
- Teaching assistant for recombinant DNA laboratory at IIT Kharagpur (2011)
- Tutored several high school students in Mathematics & Science

Publications

- **S.Ravindranath** & M.Oltmann et al., "The Role of Furin Processing in Mammalian Notch Signaling". *Nature Communications* 2016 (Submitted)
- Kurup, **S. Ravindranath** et al., "Novel insights from 3D models: the pivotal role of physical symmetry in epithelial organization". *Scientific Reports*. 5, 15153 (2015).
- M. Wang, **S.Ravindranath**, et al., "The evolution of multivalent nanoparticle adhesion via specific molecular interactions". *Langmuir*. (2016) (Accepted for publication)

Other organizational roles

2013-2016	**Safety on Site Representative** Maintained SOPs, conducted safety training, documented and implemented updated procedures for storage, handling and usage of Chemicals and Biologicals with routine assessment and certification from EH&S
2006-2008	**Student Volunteer – National Service Scheme, IIT Kharagpur** Conducted workshops on sanitation, child education, eradication of social evils; maintained and organized demographics and health survey data of rural Kharagpur, India.

ABSTRACT OF THE DISSERTATION

Elucidating the biomechanical aspects of mammalian Notch Signaling

By

Shreyas Raj Ravindranath

Doctor of Philosophy in Biomedical Enginerring

University of California, Irvine, 2016

Associate Professor Elliot Botvinick,, Chair

Canonical Notch Signaling Pathway is a critical signaling pathway that is required for cell fate specification and as such for the development of cells of almost all type of tissues. This seemingly linear but increasingly complicated pathway has been implicated in several disorders and cancers. This is because both losses and gains in Notch signals are associated with improper downstream target gene activation leading to disorders. This peculiar signaling pathway comprises of Notch receptors (Notch) transactivated by its ligands on the apposing cells. In the basal state Notch exists in an auto-inhibited, unligated state and is activated only by ligand binding in trans. Upon binding, ligand exerts a physical pulling force to expose ADAM10 (A Disintegrin And Metalloproteinase) cleavage site (also known as S2 site) deeply buried inside three globular domains of the Notch mechano-sensitive unit known as Negative Regulatory Region (NRR). ADAM10 cleavage is immediately followed by intramembrane γ-secretase cleavage releasing the Notch intracellular domain (NICD). NICD translocates to nucleus and associates with transcription factors and activates several target genes in a global or a context dependent fashion. During maturation, Notch is cleaved into a heterodimer by furin in the trans-golgi network at a

region known as S1 cleavage site within the NRR just few amino acids upstream of the S2 site. Abrogation of heterodimerization process by deletion of S1 cleavage leads to reduced signaling in mice causing cardiovascular abnormalities. Here using optical tweezers based dynamic force spectroscopy, we study the response of S1 deleted Notch compared to wild type heterodimerized Notch to observe differences in response to ligand generated forces. I have found that S1 deleted Notch requires more mechanical work reflective of transactivation energetics upon ligand pulling compared to wild type Notch highly correlating with the loss of signaling in the S1 deleted Notch mice. Another important aspect of mammalian Notch receptors is the existence of several receptors and ligand which exhibit combinatorial effects in a context dependent fashion. I have also explored the possibility of each receptor-ligand bond strength and pulling mechanics to explain signaling outcomes and effects of the pair in a particular context.

CHAPTER 1

INTRODUCTION

The Notch gene was discovered in 1917 by Thomas Hunt Morgan after the loss of this gene caused the "Notch-ed" wing phenotype in *Drosophila*[1]. In the later part of 20th century, the relevance of this gene became associated with a number of developmental aspects in *Drosophila*[2]. Soon after the mammalian homologue of Drosophila Notch was reported[3] there was an explosion of studies of the relevance of this gene in mammalian development and disease[4]. Since the last two decades there have been several findings on unique aspects of the gene and its number of pathway components leading to its nomination as one among the "ivy league" or "aristocrat" pathways important for development, regulation and maintenance of cells and cell fates in most of the multi-cellular organisms[5,6].

NOTCH SIGNALING COMPONENTS

Notch Signaling is a juxtacrine signaling pathway that consists of Notch receptors and corresponding ligands. Canonical Notch signaling is the most commonly reported and cited mechanism while non-canonical activation like ligand independent signaling, non-canonical ligands etc. are also known[7–9]. In canonical or typical Notch signaling, the active ingredients are membrane bound receptors and ligands which are type-II transmembrane proteins as shown in Fig. 1.1. In a group of cells with equivalent potential to send or receive signals, Notch receptors (henceforth called as Notch) bind ligands on the apposing cell in a trans fashion establishing a signaling unit dependent upon cell-cell contact[10–13] (Fig. 1.1). Whereas, ligands expressed in same cell as Notch, inhibits its activation by reinforcing its auto-inhibited state[14]. In cell expressing Notch and ligands, when differential expression

drives a change in receptor -ligand interaction in the same and opposing cells, a sudden transition of signaling states occurs where one cell predominantly sends signal while another receives signals[15]. Both receptors and ligands are recycled at the cell surface and it has been shown that recycling has no effect in the binding properties of receptor-ligand pairs[16]. However, the ligand cell endocytosis is shown to have a unique role in driving activation of Notch on the Notch expressing cell[17,18].

ULTRA-STRUCTURE OF NOTCH AND LIGAND

Notch receptor is a 300kDa protein with several domains homologous for common reported motifs[10,19]. The Notch Extra Cellular Domain (NECD) consists of three main regions- a "tail" N-terminal tandemly repeating 29- 36 EGF like repeats (EGFRs), the globular *L*in12/*N*otch *R*epeats (LNR), the signal transducing unit – heterodimerization (HD) domain which is in turn made of two subdomains – HD-A & HD-B. The LNR is comprised of three globular domains that wrap around HD domains (A&B) to protect the ADAM 10 cleavage site housed within the β-5 sheet of HD-B domain[20,21]. The LNR and HD domains together are called as the Negative Regulatory Region (Fig. 1.2) and are the mechanosensitive, signal transducing part of Notch. The HD domain extends C-terminally into Transmembrane Domain (TD) and Notch Intracellular Domain (NICD) which is the transcription factor binding region. The TD houses the cleavage site for presenilin dependent S3 cleavage. The NICD has the nuclear localization signal, PEST, TAD, Ankyrin repeats with various functions and most importantly the RAM domain that binds RBPjκ to form an active transcription module.

Notch Ligands like Notch have several EGF repeats some of which contribute to the binding of Notch (Fig 1.3). Regions at the N-terminal face of Notch ligands known as MNNL and DSL domains have been shown to be important for binding to Notch interfaces with first three EGF repeats playing a role in receptor ligand bond formation[9,22,23]. The intracellular domains of Notch ligands are known to associate with cellular endocytosis machinery, that links ligands to the force generating actin-cytoskeleton[18].

NOTCH TRANSACTIVATION: PULLING FORCE MODEL

In canonical signaling, Notch expressed on the cell surface is bound by ligand on the apposing cell to form link at the EGF repeats- EGF 8-12 on the Notch with DSL/MNNL domains of the ligand[9,23,24]. Transactivation model proposed by our lab in collaboration with Prof. Gerry Weinmaster's lab, as shown in Fig. 1.4 introduces ligand endocytosis as the force generating machinery that tugs and pulls on Notch to dislocate and unravel the closed LNR structure shielding the S2 cleavage site[13,18]. At this juncture, the exposed S2 cleavage site can be accessed by ADAM10 for cleavage leading to subsequent S3 cleavage and NICD release. This is the pulling force model of Notch transactivation in which Notch-Ligand interactions have evolved to exhibit very strong binding at multiple EGF repeats[16,25] to potentiate disengagement of LNR to expose S2 cleavage with a sufficient force lesser than the bond strength at the EGF repeats[18,26]. The intracellular domain of the ligand associates with adaptors like Epsins for clathrin dependent endocytosis to tap into cellular forces generated by actin cytoskeleton as described by Meloty-Kapella et. al. 2012[18].

MAMMALIAN NOTCH SIGNALING

Vertebrate Notch signaling is different from diptherans in the fact that there are several Notch receptor homologues and several ligands. Drosophila has predominantly a single Notch receptor that is capable of generating all Notch dependent phenotypes[9,27] which stands markedly different to vertebrates like mammals which have four Notch receptors viz. Notch 1/2/3/4. There are two classes of Drosophila ligands – the Delta and the Serrate which have redundant or differential effects but act on the same single type of Notch receptor[9,24]. However, in mammals there are several ligands belonging to the Delta class or the Serrate (also Jagged) class; the Delta class consists of Delta-like ligand (DLL) 1/3/4 and Jagged class consists of Jagged 1/2. All these ligands are capable of signaling in trans and inhibiting in cis[9]. However, Dll-3 is the only divergent ligand that is shown not to activate but perhaps only cis-inhibit[28,29]. The different receptors and ligands are represented in Fig. 1.5

FURIN CLEAVAGE OF NOTCH

Notch receptors after translation are transported to the cell surface in trans-Golgi network (TGN). Notch receptors are proteolytically processed in the TGN by a broad spectrum furin like convertase (henceforth furin)[30] as represented in Fig 1.6. Furin belongs to bacterial subtilisin/kexin class of proteins that have broad spectrum of substrates[30,31]. Notch is cleaved at a dibasic RxRR amino acid site which lies on the S1 loop that connects HD-A and HD-B just tens of amino acid sequence N-terminal to S2 cleavage site[30]. Cleavage at S1 site generates a Notch that is heterodimeric that is held by non-covalent linkages[32]. The function of furin cleavage of Notch has been under speculation since its discovery. Transgenic studies in flies have identified the role of furin cleavage of Drosophila Notch

(dNotch) to be vestigial in function and that dNotch can signal without causing any remarkable phenotypes when S1 cleavage was deleted[33]. In fact, dNotch doesn't appear to have an obvious consensus sequence for furin cleavage and mouse Notch expressed in Drosophila and murine Notch with Drosophila S1 site wasn't processed by mouse furin, but nevertheless reached the cell surface[33,34]. This is significant because in cell culture studies, an over-expressed ectopic Notch with S1 deletion displayed reduced surface expression compared to its wild type counterpart raising the speculation that S1 cleavage of Notch was required for intra-cellular trafficking of Notch to the cell surface[35]. However, given other studies that S1 deleted Notch do appear on the cell surface but signal in a CSL independent manner shows that furin processing of Notch may not be a major determinant for Notch trafficking to the cell surface[36]. Further, given that Notch 1 and Notch 2 both have primary S1 cleavage site, and that Notch 2 transports to the cell surface it is difficult to conclude if S1 deletion leads to a trafficking defect[35]. Another most important aspect is that S1 deleted NRR preserves the molecular logic of the wild type NRR thereby showing that effect of S1 deletion doesn't significantly destabilize the NRR ultrastructure[20,37]. This is in line with the previously mentioned evidence that Drosophila Notch doesn't require S1 cleavage to signal[33]. However, does S1 cleavage serve a specific purpose, especially in mammalian Notch signaling? Deletion of S1 cleavage leads to *in vivo* phenotypic defects in Drosophila[38] showing that there exists confusion in the understanding of the relevance of S1 cleavage on Notch dependent processes.

ANIMAL MODEL TO UNDERSTAND THE ROLE OF S1 CLEAVAGE OF NOTCH

To remove the ambiguity surrounding the absolute requirement of S1 cleavage of Notch, our collaborator Prof. Gerry Weinmaster suggested an approach of generating a mice defective in S1 cleavage. To understand if the S1 cleavage of Notch is relevant for mammalian development and to elucidate the in vivo relevance of furin on Notch signaling, Weinmaster's lab generated a mutant mice with a precise deletion of 108 base pairs on exon 26 of mouse Notch 1 gene which codes for a protein without a 36 amino acid sequence on the S1 loop previously discussed. The is 36 amino acid deletion contains the conserved S1 site RxRR and the upstream sequences reported to be the cleavage site for furin[38] (Fig. 1.7) . The mutant mice were named as N1ΔFC (N1 with *d*eleted *F*urin *C*leavage) and obtained by intercrossing mice heterozygous for the mutation- $N1^{WT/\Delta FC}$. The Fig. 1.8 shows the survival probabilities of the embryos at different embryonic stages and the pups at birth. During the first wave of mesoderm differentiation the $N1^{\Delta FC/\Delta FC}$ embryos display survival rate similar to that of N1WT/WT. However, after mid-gestation i.e., post E14.5, the homozygous $N1^{\Delta FC/\Delta FC}$ show increased lethality and only 12% of the pups are born than the expected Mendelian 25%. Further, all these pups failed to thrive and died within two weeks. Tissue analyses of the yolk sac reveal that N1ΔFC is a full-length protein compared to wild type Notch in which both full length and heterodimer forms are present (Fig. 1.9).

A N1ΔFC with Notch null background ($N1^{-/\Delta FC}$) survived till E15 compared to homozygous Notch null ($N1^{-/-}$) which die around E10 and are resorbed by E11. This shows that N1ΔFC protein – the product of $N1^{\Delta FC}$ gene is a functional receptor capable of supporting Notch

dependent processes till E15 but soon as advanced stages become increasingly Notch reliant, N1ΔFC is incapable of recapitulating the signaling levels generated by wild type N1.

To further analyze the Notch dependency of the tissue development processes, specifically the dependency of furin cleaved Notch on embryonic stages past E15, Dr. Meredith Oltmann of Weinmaster lab analyzed the cardiovascular system which is heavily dependent on Notch as reviewed in Gridley et al. 2010[39] and High & Epstein, 2008[40]. Reflecting the high lethality associated with the N1ΔFC mutants, the N1ΔFC cardiovascular system displayed several defective phenotypes as illustrated in Fig. 1.10. To summarize the defects, the N1ΔFC hearts showed enlarged ventricles with ventricular septal defects, hypoplastic aortic arches, excessive sprouting of micro-vasculature and deficient epithelial to mesenchymal transition.

The in vivo relevance of the S1 cleaved receptor was elucidated by these animal mutation experiments. It was still unclear as to how the signaling deficiency was propagated by furin resistant mutant N1ΔFC, which can be detected on the cell surface, when several studies dismissed that furin cleavage of Notch was not "required" for signal activation[33,35]. In the following chapters, I will elucidate how furin processing of Notch into heterodimers is a critical process to generate biophysically efficient receptors that otherwise could be mechanically resistant to ligand pulling. And this "relief" of biophysical convenience is provided by S1 cleavage when demand for Notch signals become increasingly higher.

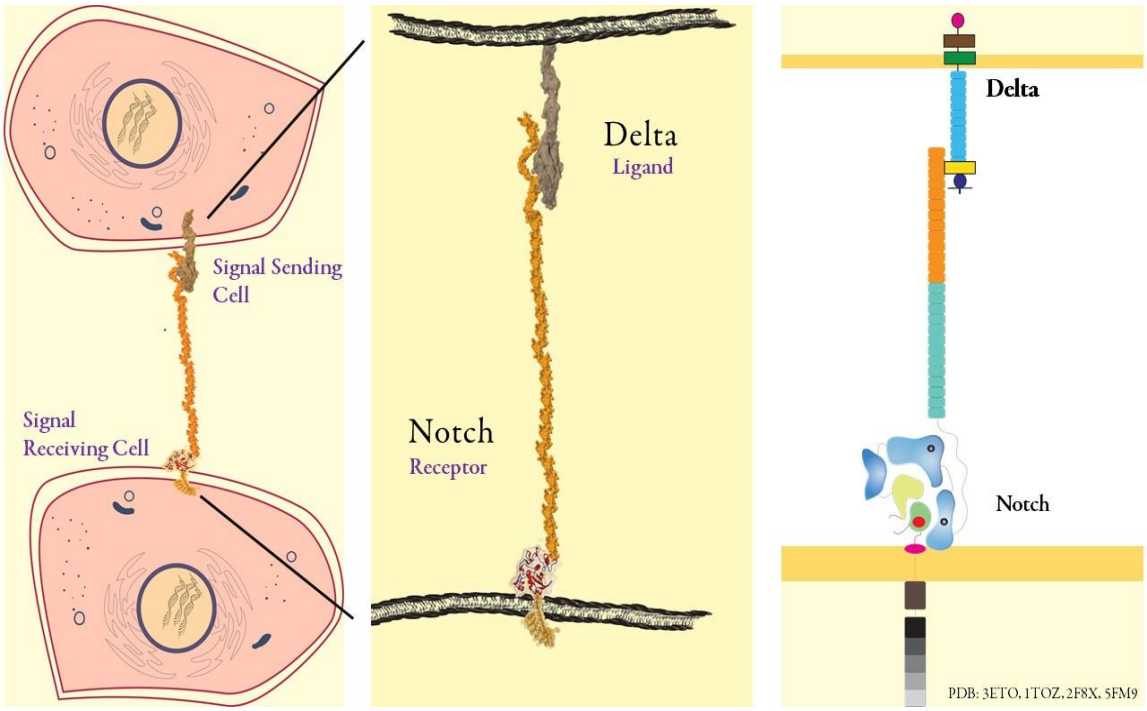

Figure 1.1: Schematic of components of Notch Signaling: **a.** Notch signaling is a juxtacrine signaling unit dependent upon cell-cell contact. **b.** Notch-Ligand juxtacrine interaction zoomed in. Structures were drawn from protein structure cartoons from PDB: 3ETO, 1TOZ, 2F8X, 5FM9, 4XBM, 2RR0 **c.** Cartoon representation of **b.**

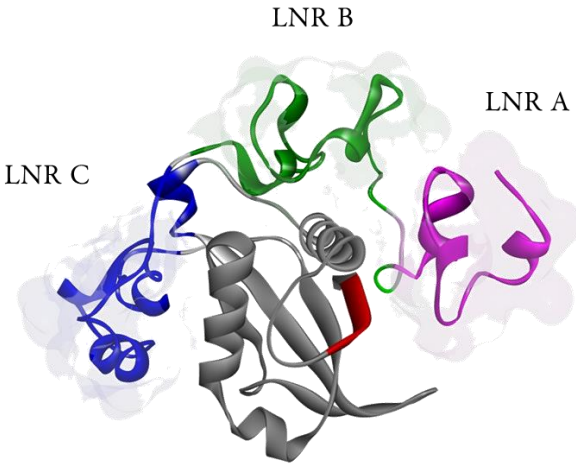

Figure 1.2: The ultrastructure of Negative Regulatory Region (NRR) from Gordon. W., et al. 2009[20] (PDB: 3ETO) . The NRR is made of LNRs A, B & C (pink, green and blue). The S2 cleavage site (red) remains buried deep inside the LNR shield.

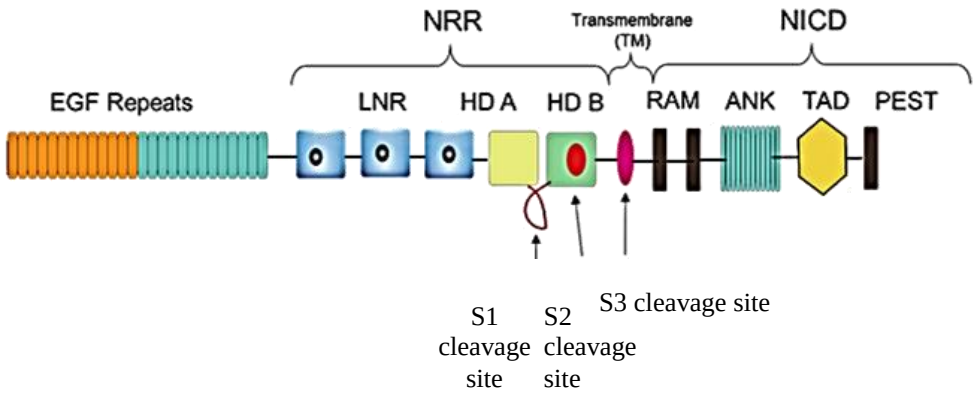

Figure 1.3: The components and domains of Notch.

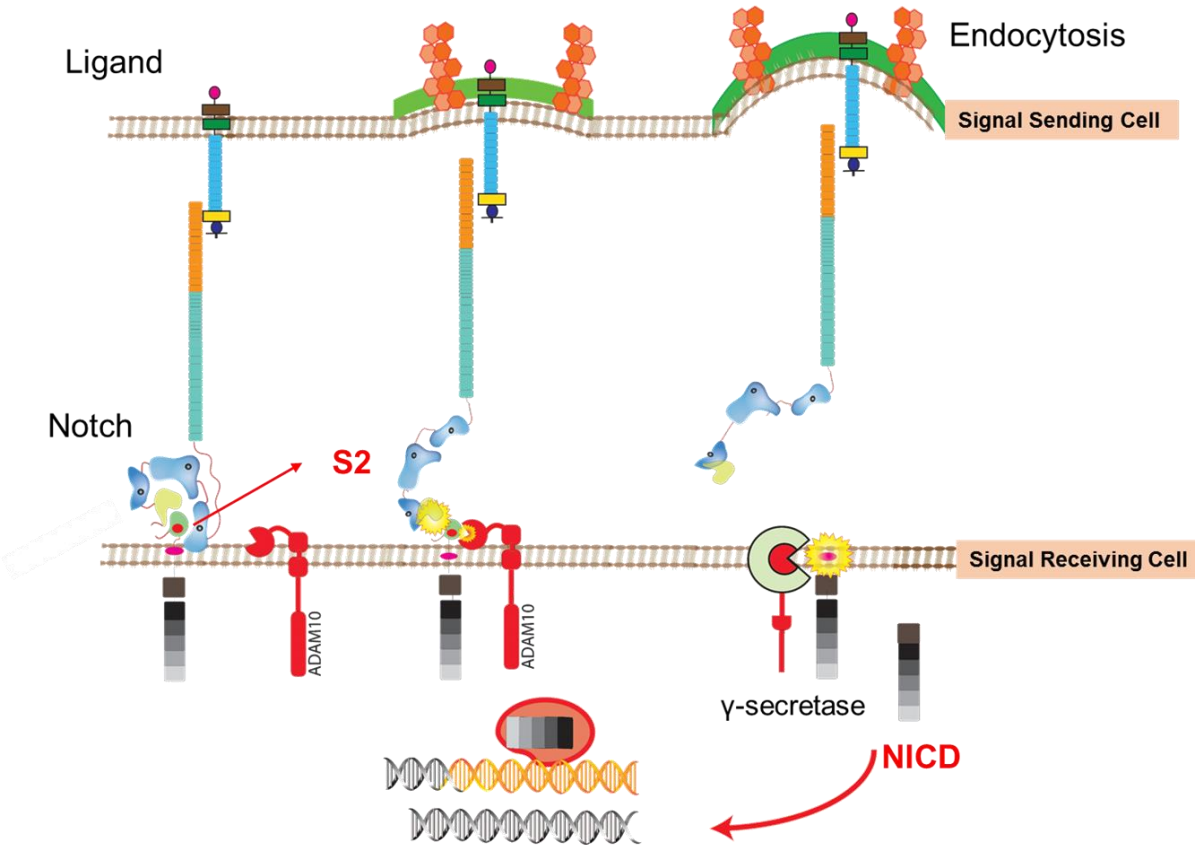

Figure 1.4: Pulling Force Model of Notch Transactivation. The Ligand exerts pulling force generated by endocytosis leading to exposure of S2 cleavage site for ADAM10 proteolysis followed by γ-secretase cleavage releasing the NICD which translocates to the nucleus to activate target genes.

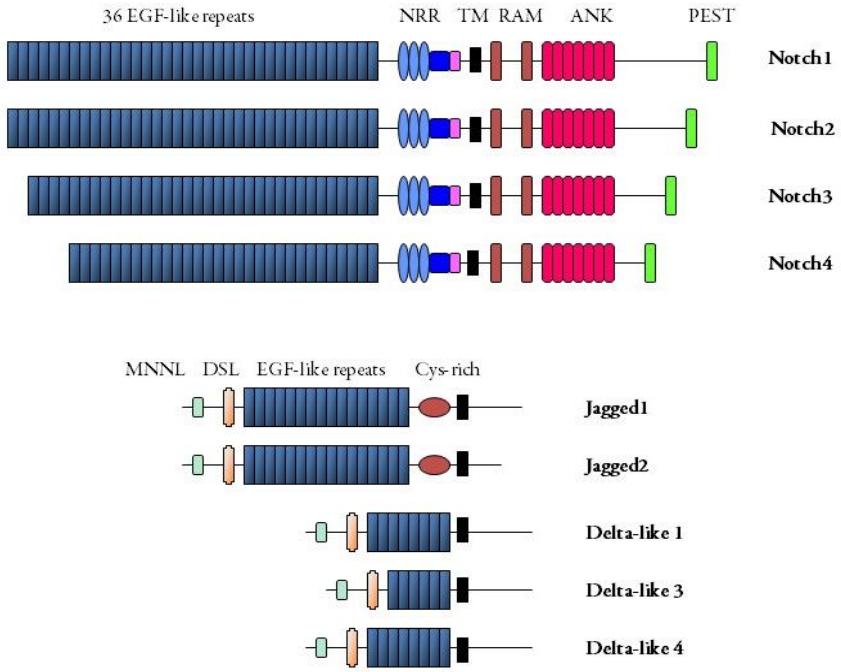

Figure 1.5: The components and domains of Mammalian Notch and Ligands. There are four mammalian Notch receptors 1-4. Notch 4 has the lowest number of EGF repeats (29) compared to the other homologs. There are two classes of Notch ligands- Delta class and the Serrate/ Jagged class. Each of these ligands send signals to Notch receptors in a context dependent manner. Also, the ligands within the same class may or may not be interchangeable. Further, Dll-3 a ligand relatively close Dll-4 which is a strong Notch activator is predominantly a Cis-inhibitor. **Courtesy: *Weinmaster lab***

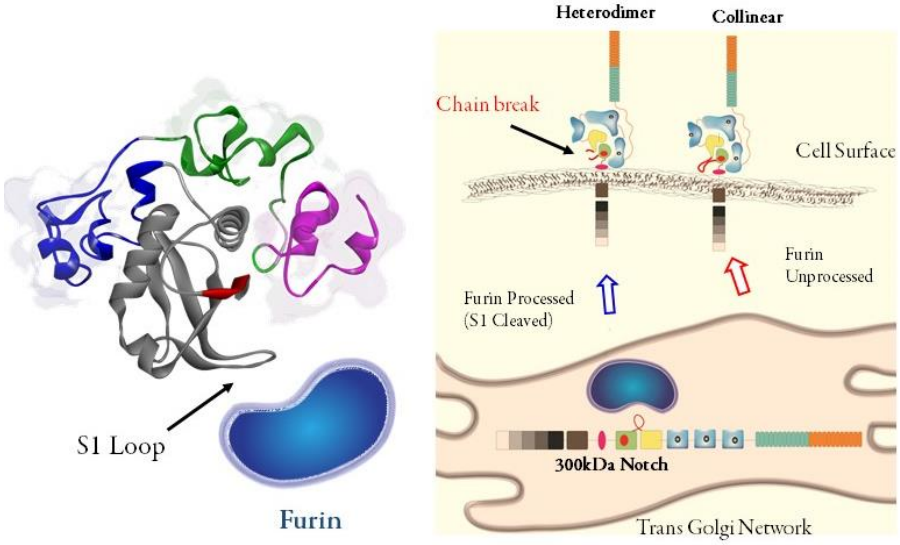

Figure 1.6: Schematic of furin processing of Notch (PDB: 3ETO)

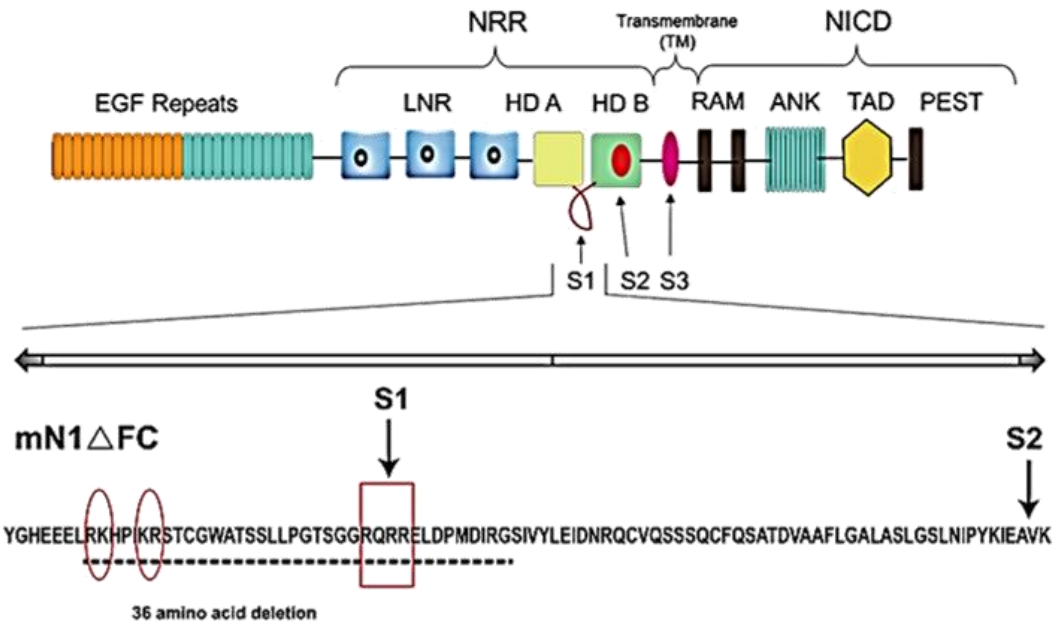

Figure 1.7: Schematic of Notch1 structural motifs and Exon 26 and 27 containing coding sequence of the NRR heterodimeric (HD) region. The furin cleavage consensus sequence is boxed and upstream positive charged residues are circled. The S1 and S2 sites are also indicated. **Courtesy:** ***Weinmaster lab***

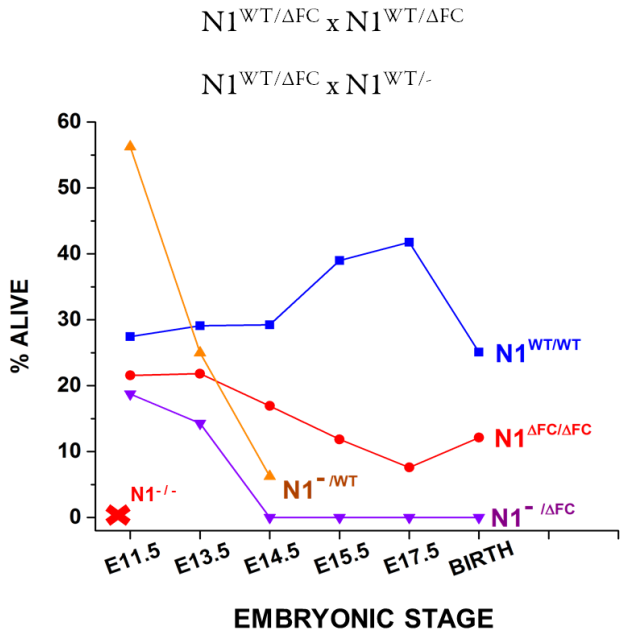

Figure 1.8: Generation and analysis of N1ΔFC mutant mice. Line graph comparing viability between Notch null (N1in32) and engineered furin cleavage heterozygous and homozygous mutants. **Courtesy: Dr. Meredith Oltmann,** ***Weinmaster lab***

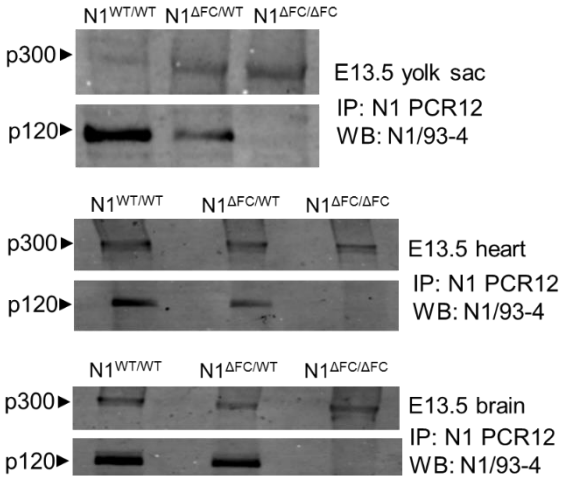

Figure 1.9: Furin processing of N1ΔFC mutants. Immunoblots of furin cleaved p120 and uncleaved p300 fractions immunoprecipitated and detected by antibodies raised against Notch intracellular domain. **Courtesy: Dr. Meredith Oltmann, *Weinmaster lab***

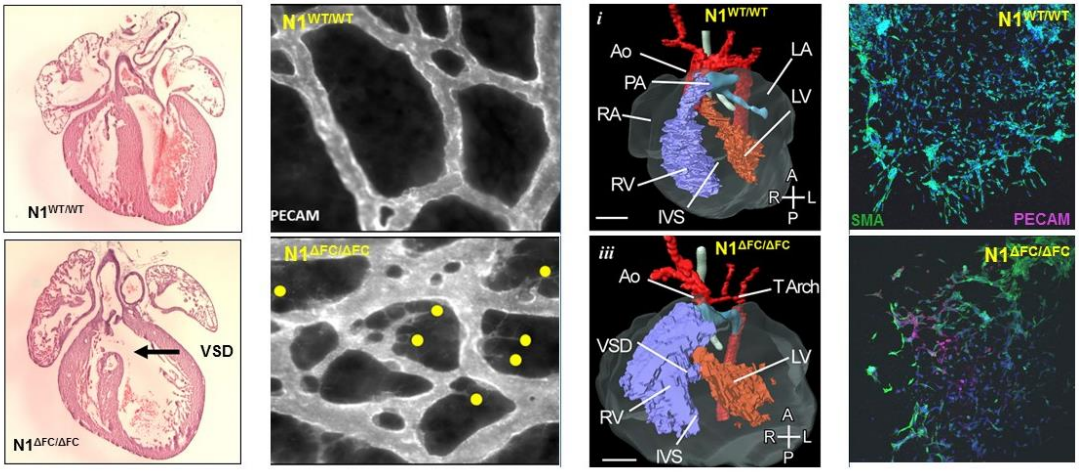

Figure 1.10: Cardiovascular defects in N1ΔFC mice (bottom panel) – from left to right- Ventricular Septal Defects (VSD), excessive sprouting in microvasculature, enlarged heart with aortic arches, incomplete epithelial to mesenchymal transition compared to wild type (top panel). **Courtesy: *Weinmaster lab***

CHAPTER 2

MATERIALS AND METHODS

OPTICAL TWEEZERS

A highly focused laser microbeam traps transparent and translucent particles in a fluid medium due to transferring and conservation of photonic momentum of light entering and passing through the bead[41]. When a polystyrene microbead is brought near the center of a laser beam shone through a high numerical aperture, the net force produced by change in momentum of photons entering from either side of a Gaussian profile beam lift the microbead upwards as shown in Fig. 2.1. This force is balanced by the photonic transfer of scattered light around the bead pushing the bead downward till all the forces acting on the bead are balanced. This levitates the bead at the trap center and the bead is said to be held by optical "tweezers". When the bead is displaced from the center of the trap, the trap exerts forces equal and opposite to the displacement till the linear region permits[41–43].

CELL CULTURE AND BEAD PREPARATION

L cells transfected with pBOS-HANotch1 or pBOS-HANotch1ΔFC (with the provided 36 aa S1 loop deletion) or N1-EGFR-TM-HA (N1 EGF repeats 1 -15 fused with Transmembrane domain and intracellular 3xHA tag) were cultured to cell lines stably expressing the wild type or the respective mutant proteins. Other clones used in the studies are L cells transfected with pBOS-Notch1 (LN1-A) or OCDN1 (NICD deleted). The cell lines were generated by Weimaster lab using methods described by Nichols et al. 2007[44] and Shergill et al. 2012[16]. The obtained cell lines were cultured in DMEM (Gibco) + 10% Fetal Bovine Serum (Atlanta Biologicals) and plated on 35 mm glass bottom dishes (MatTek). The cells

were supplemented with pre-warmed CO_2 independent media (Life Technologies) before placing it on the tweezers system for rupture experiments. For drug treatment experiments, the cells cultured in 35 mm dishes were supplemented with media containing 100 μM final concentration TAPI-2 (Enzo lifesciences) or 100 μM final concentration Dodecyl Chloromethyl ketone (Enzo lifesciences) for 4 hours to inhibit ADAMs or Furin respectively. The treatment time was restricted to 4 hours to minimize the impact of the Furin inhibitor on ADAM processing which is shown to occur past 4 hours[45].

Polystyrene microbeads (Bang's Laboratories) functionalized with Protein A on the surface were washed several times with Advanced DMEM (Life Technologies) and incubated with known concentration of Fc fusion proteins. For experiments on Notch expressing cells, the Protein A beads were incubated with 0.75 μg/ml D1Fc or 0.75 μg/ml Fc (Control). For Rupture Force Experiments on L cells expressing ligands, the Protein A beads were incubated with incubated with 0.5 μg/ml N1Fc that displayed significant ruptures in bead titration experiments reported by Shergill et al. 2012[16]. Microbeads for endocytic pulling force experiments were incubated with highest concentration of Fringe modified N1Fc conditioned media. The incubated microbeads were washed in PBS without ions (Life Technologies) and Advanced DMEM stored in CO_2 independent media or Advanced DMEM until further use.

CONDITIONED MEDIA GENERATION FOR LUNATIC FRINGE MODIFIED N1Fc

293 T cells were transfected with Lunatic Fringe and N1Fc cassettes, donated generously by Weinmaster lab, in the ratio 1:2 using Lipofectamine-2000 (ThermoFisher Scientific) following manufacturer's protocol and conditioned media generation described previously

by Weinmaster lab[36,46,47]. The cells were incubated in fresh media after 48 hours post-transfection for five days and supernatant was collected, centrifuged to remove debris and stored in 4°C until further use.

RUPTURE FORCE SPECTRA USING OPTICAL TWEEZERS

Cell lines expressing ectopic wild type N1 or mutant N1s were sparsely grown on 35 mm glass bottom dishes (MatTek) and mounted on the piezoelectric (Physicke Instruments) stage fitted to the custom built optical tweezers system for the experiments. The instrumentation used for the measurements are described in Kotlarchyk, et al. 2011[48] and Shergill et al. 2012[16]. Cells on the dishes were probed using 5μm diameter Protein-A coated beads (Bangs Lab) which were previously incubated in 0.75 μg/ml D1Fc. Each bead was trapped by a co-aligned trapping- detection laser system and brought close to the cells as shown in Fig. 2.2. An N1 (or N1 mutant) expressing cell is advanced to a D1Fc bead by the movement of the stage till contact is established for less than 0.1s after which the stage recedes from the bead at constant velocity of 24 μm/s. If an interaction is formed, the bead will be gently pulled away from the center of the trap under the influence of forces generated by the stage acting through the molecular interaction. The laser trap exerts equal and opposite force onto the D1Fc bead inducing tension through the molecular interaction. The tension increases over time as the stage continues to recede until it reaches a value that is sufficient to break the N1-Dll1 interaction, and the bead is pulled back to the center of the trap. Several such cycles were performed on several cell bead pairs to construct the Rupture Force Spectra as described by Shergill et al. 2012[16] for each particular cell line. A typical Force waveform is shown in Fig. 2.3. The 785 nm detection laser of the co-aligned laser system was used to record the deflections produced in the beads during such cell

loading experiments and data was acquired using instrumentation programs built using LabView software. The voltage signals were converted to Force by multiplying the voltage with volts-to-meter constant and trap stiffness. The stiffness of the trap was calculated using the power density spectrum method by observing random brownian displacements of a trapped bead in media[16,43,48]. A sample power spectrum is shown in Fig. 2.4. All experiments, including calibration was performed 5-6 μm above glass surface. Faxèn's correction was applied to the recorded rupture forces and force-extension curves[49]. The Rupture Force Spectra was constructed after collection and analysis of the data using program written in Matlab. All cell bead experiments were conducted within a custom built on-stage microscope incubator that maintained 37°C temperature. However, due to the microscope objective of the set up acting as a large heat sink, the equilibrium dish temperature was 33°C. Cells bead experiments were conducted in CO_2 independent media (Life Technologies). Similar experiments were performed on ligand expressing cells – Dll1, Dll-4, SN39 (Jagged1) or Jagged2 cells using N1Fc coated beads to obtain Rupture Force Spectra for each Ligand-bead combination.

CONSTRUCTION OF FORCE – EXTENSION CURVES FROM RUPTURES

The signal traces of peaks from cycles containing the ruptures above 12 pN obtained from the cell bead experiments were analyzed to generate a force versus time plot as shown in Fig. 2.5. After the cell contacts the bead in the forward cycle, it pushes the bead during the millisecond contact observed in the signal as a negative dip. As the stage reverses, the cell now stuck to the bead due to N1-D1 interaction bonds draws the bead through the center of the laser trap focus which is termed as "zero crossing". The cell continues to pull the bead while the laser restoring force acting equal and opposite increases proportional to the

bead displacement and therefore when the restoring force reaches the value at which the N1-D1 interaction fails, i.e., at rupture, the bead quickly falls back into the trap and force drops to low values mediated by viscous forces as the stage continues to move. During the course of interaction, the stage recedes at a constant velocity while the bead displacement lags and the difference of these displacements yield the molecular unraveling of the N1-D1-membrane system known as *Extension*. When the instantaneous laser restoring force, which is the instantaneous tension on the molecule, is plotted over instantaneous extension till rupture, we get a Force versus extension plot (Fig. 2.6). In this plot, we obtain a trace which provides instantaneous Extension Curve (FEC). The equations used to obtain extension is explained in Fig. 2.6. The biophysical energy in terms of work is obtained by integrating the FEC till rupture (shaded region in Fig. 2.6) using trapezoidal rule. Statistical Analysis and graphing was performed in Origin software or Matlab. Mann-Whitney tests were used to compare groups and p value < 0.05 were considered significant to reject the null hypothesis of equal medians.

CLASSIFICATION AND ANALYSIS OF FECs FROM RUPTURE DATA

All Force Extension Curves (FECs) from all conditions were blindly dumped into a data folder and about a 100 random curves (and later to all of the dataset) were chosen to observe curve geometry and frequency. I was able to identify about five classes of FECs which were assigned a class name based on the curve geometry. The curves which showed random voltage signal jumps and aberrations were discarded. Care was taken to consider FECs of ruptures with Rupture forces above 12 pN non-specific cut off. Using this classification scheme, FECs from RFS of each cell line (expressing a Notch1 or its variant) were classified and binned according to their respective classes. Out of the five classes of

FECs, two classes- Class1 and Class4 occurred in varying frequencies across the conditions while all other classes combined comprised less than about 20% of the FEC data. Class1 was renamed as Energy trace1 and Class4 as Energy Trace 2. The occurrence of these to curve types were plotted as pie charts, with the sum of both curve types as total. The value of area under the curve till rupture was computed as "Work". The work values and the FEC frequency was plotted as box plots and pie charts.

STATISTICAL ANALYSIS

Comparisons between groups in FEC analysis were made by applying Mann Whitney tests using the software Origin. Significance level was determined with reference $p < 0.05$ (*).

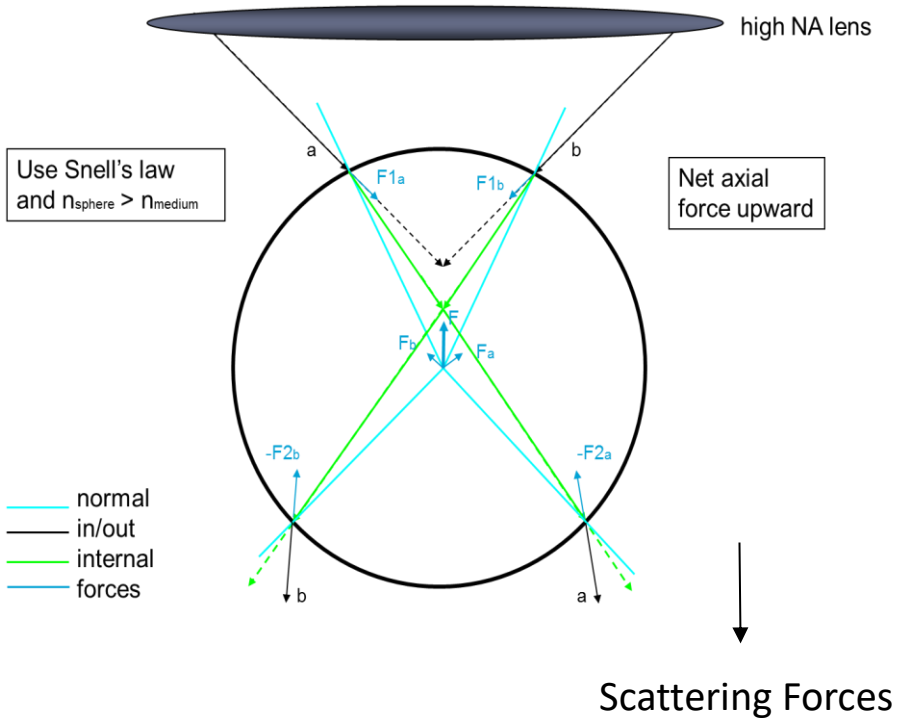

Figure 2.1: Optical Tweezers for biomedical applications. The Ray optics regime of light entering and exiting the microsphere explains the origin of Forces due to photonic conservation. A Gaussian beam coming through a high numerical aperture (NA) exerts a net force levitating the bead while the photonic momentum transfer due to scattering forces push it downwards balancing the upward pull. This generates an optical tweezers which holds polystyrene microbeads in fluid media.

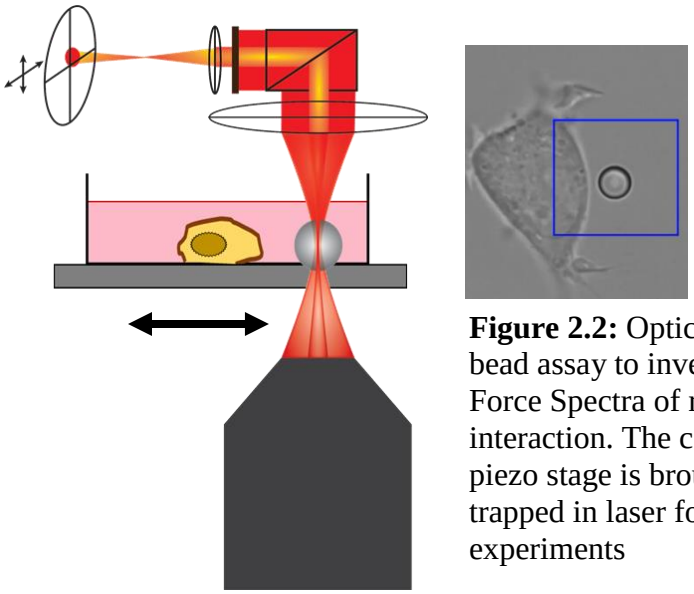

Figure 2.2: Optical Tweezers based cell bead assay to investigate the Rupture Force Spectra of receptor ligand interaction. The cell on a dish housed on a piezo stage is brought close to microbead trapped in laser for touch and release experiments

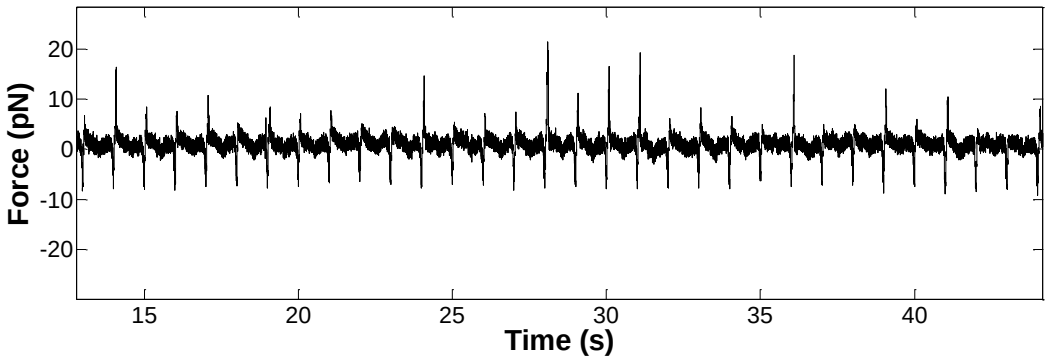

Figure 2.3: Rupture Force Waveform: A sample Force vs Time plot converted from voltage signals of QPD represents a continuous touch and release experiments. As seen from this waveform, stochastic bonds are formed which appear significantly taller than the other peaks

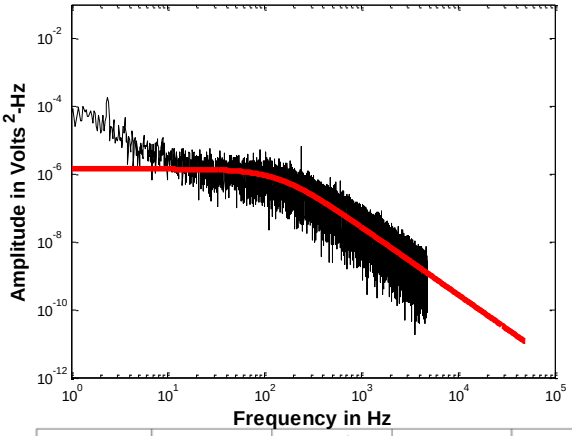

Figure 2.4: A sample power spectrum density plot to obtain corner frequency. The trap stiffness is given from the equation: $\kappa = 2\pi\gamma f_0$, where κ = Trap stiffness, γ= coefficient of viscosity, f_0 = cut off frequency

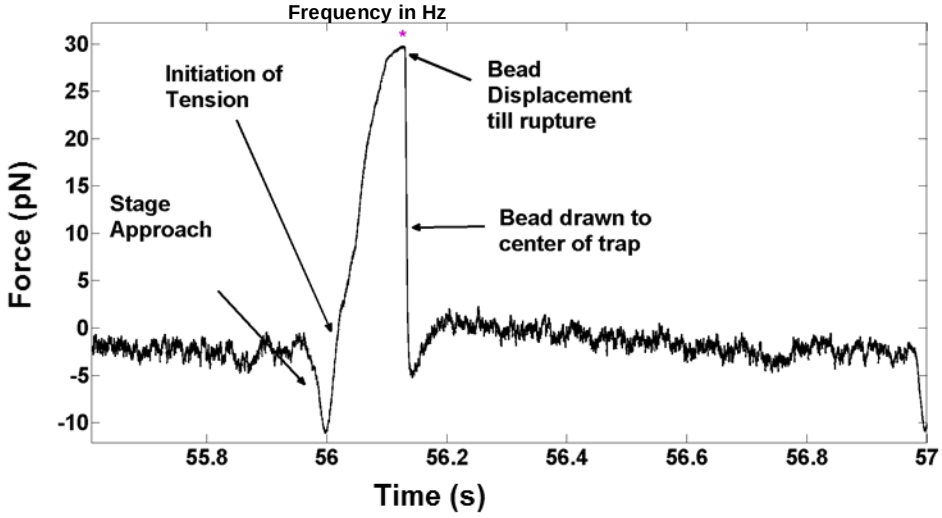

Figure 2.5: A single Rupture: Force vs Time graph of single rupture showing the initiation of tension due to bond formation and displacement of the bead till

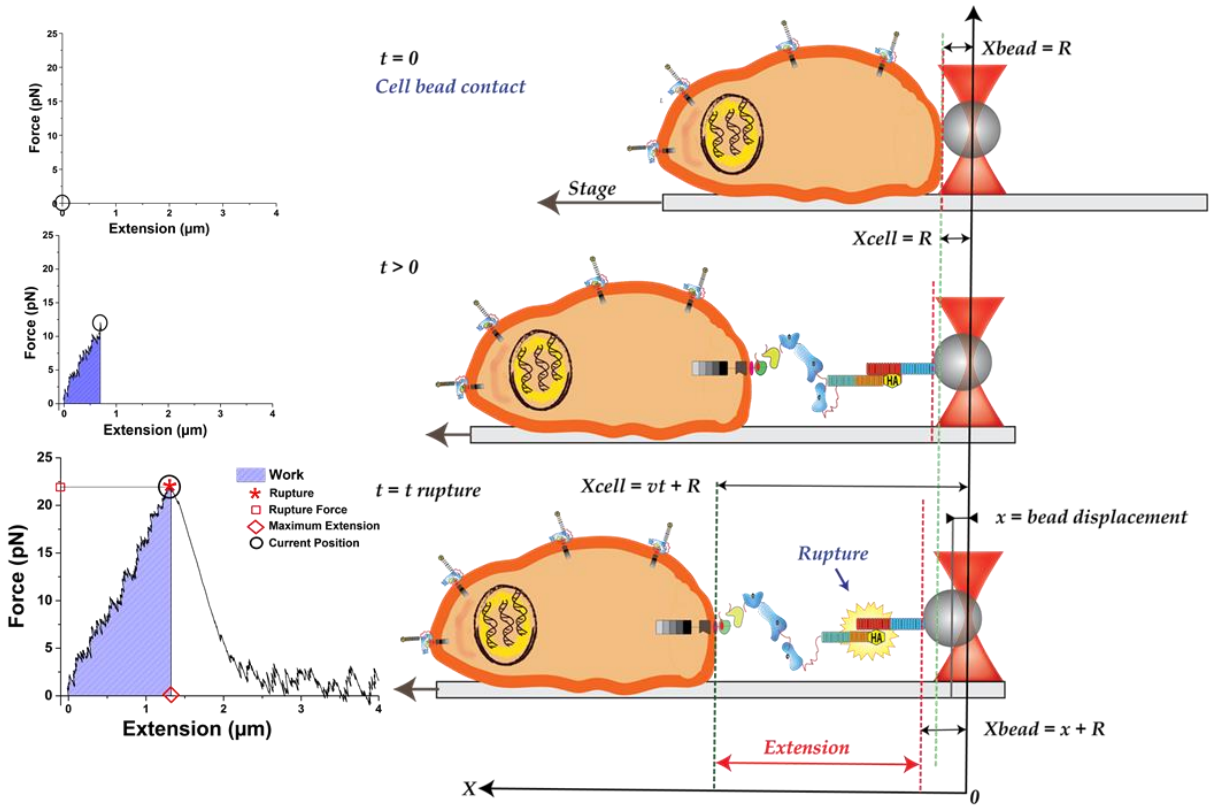

$$Extension = Distance\ between\ cell\ and\ bead\ at\ rupture$$
$$= (Xcell - Xbead) = (vt_{rupture} + R) - (x + R) = vt_{rupture} - x$$

where v is the velocity of the stage , $t_{rupture}$ = time of rupture & x = bead displacement at rupture

Figure 2.6: Generation of Force Extension Curves: Cartoon illustrating the evolution of a FEC from a specific N1-D1Fc interaction. The position of a cell (Xcell) is moved at constant velocity away from a laser trapped bead by a pizeoelectric stage. If a N1-Dll1 bond is established, then tension will act through the interaction to displace the bead from the center of the trap (Xbead) due to forces originating from the piezo stage; this tension acts to unravel N1 and possibly the local cell membrane. We define Extension as the difference in Xcell and Xbead.

CHAPTER 3

DYNAMIC FORCE SPECTROSCOPY OF NOTCH-LIGAND INTERACTION

Ligand endocytosis generates physical pulling force on Notch receptors mediated by the use of endocytic and force generating cytoskeletal components[18]. Mechanotransduction via ligand pulling is therefore, purported to be required for exposure of S2 cleavage for downstream activating proteolysis in Notch receptors[13,18,26]. Ligand binding however, is shown to be independent of the endocytic pulling process, and more importantly force required to break the mammalian N1-Dll1 (Delta-like ligand 1) bond is higher than the force required for S2 exposure[16,26]. In order to directly investigate whether the furin processing of N1 primes the receptor for effective binding to the ligand, I performed OT-based dynamic force spectroscopy similar to Shergill et al.[16] on live cells expressing N1WT or N1ΔFC using Protein-A beads functionalized with D1Fc (Dll1-Fc chimera without the CH2-CH3 hinge). We also compared the forces required for pulling N1 and N1ΔFC to rupture. For these experiments, we generated L-cell lines ectopically expressing either HA tagged wild type N1 (HAN1) or HA tagged N1ΔFC (HAN1ΔFC) as illustrated in Fig. 3.1. During experiments, laser trapped D1Fc beads were brought in contact with an adherent HAN1 or HAN1ΔFC cell in a culture dish housed on a nanopositioning stage to perform cyclic touch and release experiments (Fig. 3.2; details in Methods).

We record the forces acting on the bead in time with a as a force waveform shown in Fig. 3.3 during which the bead and cell are put in contact once per second. Negative forces occur during cell-bead contact, and positive forces occur as the cell moves away from the bead. Cycles in which a specific N1-Dll1 interaction occurs are exhibited as spikes (red stars in Fig. 3.3), whose peak value is the rupture force. Prior to expression levels of N1 and its

mutants on the cell surface was were quantified by FACS after labelling with either fluorescent D1Fc or anti-HA antibody (Fig. 3.4) to detect surface Notch. Reflecting this the FACS data is the specific rupture probabilities of cell lines tested using D1Fc beads (Fig. 3.5). An L cell derived clone expressing Notch1 EGF-like repeats 1-15 in frame with transmembrane domain fused to HA tag named here as N1-EGF-TMHA was also assessed along with the N1 isoforms as an NRR deletion control.

We have previously reported that Dll1 induced Notch activation involves ectodomain dissociation[17,20]. Consistent with this idea we purport that the N1 NECD can dissociate under ligand pulling forces at two different locations, viz., at the S1 chain break in between the HD domains and at the S2 cleavage site within the HD domain (indicated by arrows in Fig. 3.6). Further, in our OT experiments, laser can exert forces equal to or higher than the strength of N1-Dll1 bond occurring at the EGF repeats, so in total allowing three possible regimes of force ruptures (Fig. 3.6) that can contribute to the force spikes in the cell-bead experiments. A probability distribution graph of maximum force for each cycle, known as rupture force spectra (RFS, Fig. 3.7), is plotted to identify the force modes specific to N1-Dll1 interactions. We first performed control experiments with Fc coated beads to find the cut off force value for non-specific interaction between the beads and the cells in the force spectra. For almost all of the clones tested, the respective RFS revealed this cut off force to be at around 12pN (Fig. 3.8), therefore, we posited that any other force above this value is likely to represent N1-Dll1 interaction. RFS for parental L-cells (Fig. 3.9 a) showed forces beyond 12 pN, although at relatively low probability. RFS for HAN1 and HAN1ΔFC (Fig. 3.9 b & c) showed forces beyond 12pN with probability densities higher than that for parental L-cells reflecting the contribution of ectopic N1WT or N1ΔFC

interaction with Dll1. It is important to note that there are no clearly defined force modes typically observed in single molecule force spectroscopy. This reinforces the idea that RFS on these cells are a mixture of multiple rupture modalities as represented in Fig. 3.6. In consideration of these multiple rupture modalities, we mathematically fit a three Gaussian mixture model to the RFS and obtained force mode estimates with computed means at around 13pN, 15 pN and 23 pN. The first two of these modes have values less than 19pN - which we reported as the value of the mammalian N1-Dll1 bond strength in our earlier studies[10]. Interestingly, the 13pN peak found by the fits is approximately half the value of 23pN, which is consistent with single bond-double bond ruptures. However, because of the large overlap of the potential force modes we were unable to identify differences in the way the two molecules isoforms rupture, i.e., where S1 or S2 can be found in the RFS. Therefore, in summary, we were unable to isolate the differences between the RFS of N1WT and that of N1ΔFC under pulling by D1Fc despite similar binding probabilities.

Lastly, we measured the RFS for the mutant N1-EGF-TMHA in which the two modalities of rupture, i.e. the S1 and S2 ruptures, are absent as the molecule lacks NRR, and therefore only interacts with Dll1 at its 1-15 EGF repeats region (Fig. 3.9 d). The RFS revealed a single rupture mode above 12pN, which when mathematical fit with similar Gaussian mixture model showed 19pN peak, which is precisely the force value for N1-Dll1 bond strength observed in our earlier study of Dll1 expressing cells interacting with N1Fc coated beads[10]. When this result is contrasted with the rupture regimes of N1WT and N1ΔFC, it can be inferred that both isoforms are sessile at mechanical pulling forces less than the N1-Dll1 bond strength, which is consistent with the mechanotransduction force model of Notch activation[9,36].

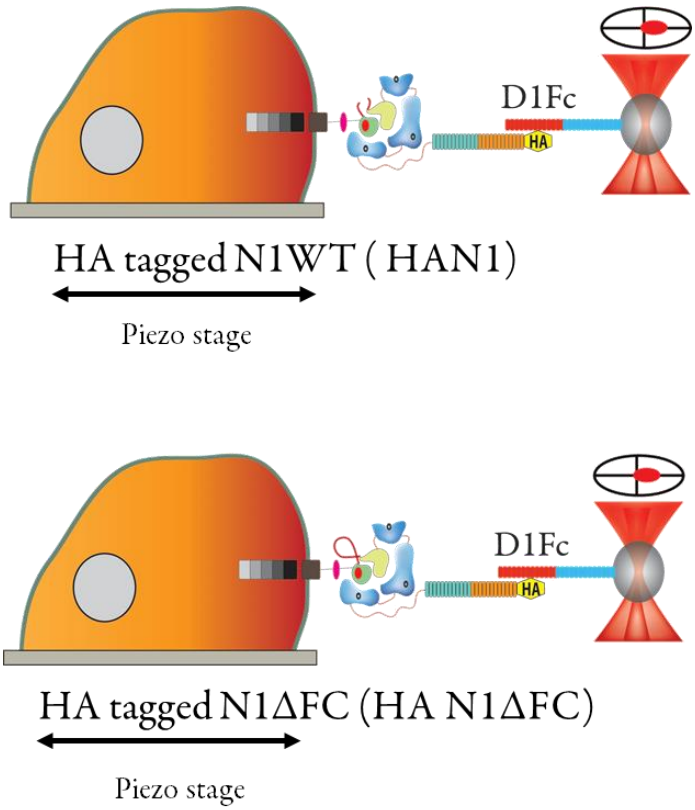

Figure 3.1: Optical Tweezers based studies on cell lines expressing ectopic Wild Type Notch 1 (HAN1WT) or S1 resistant Notch 1 with 36 amino acid ΔFC deletion like the mutant mice discussed in the introduction (HAN1 ΔFC). D1Fc beads were used to probe the Rupture Force Spectra of the WT and ΔFC Notch 1 isoforms.

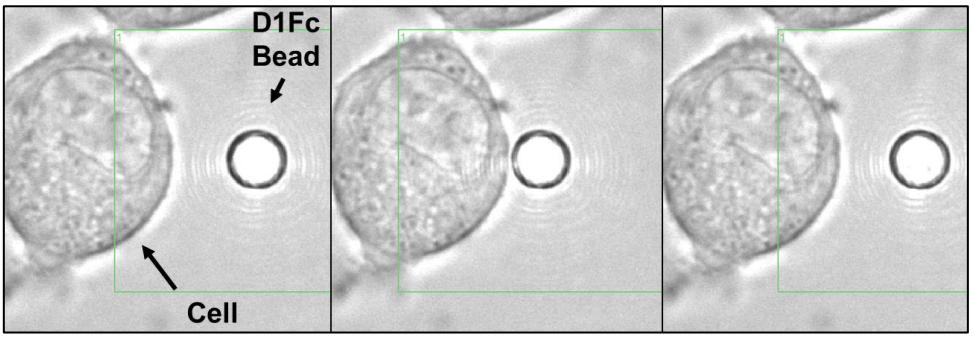

Figure 3.2: Cyclic touch and release experiments with the cell bead configurations of Fig. 3.1 and as described in the Methods.

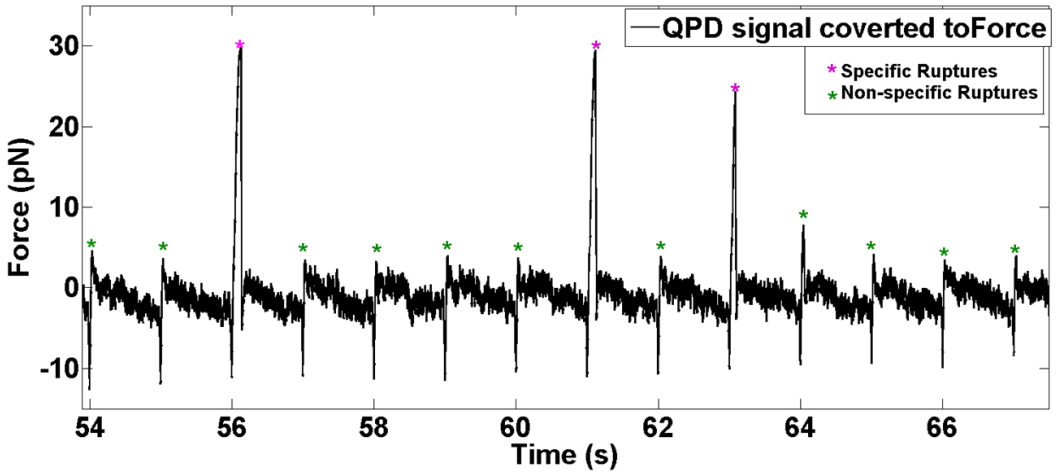

Figure 3.3: Force waveform of serial N1-Dll1 contact and release cycles, where waveform data is recorded by monitoring bead movement using a quadrant photodiode (QPD) as shown in b. Abrupt negative values occur during cell-bead contact and positive values correspond to tensile forces acting through single (with the exception of the rare multiple) N1-D1 interactions. Sharp peaks (red stars) occur when tensed N1-D1 interactions rupture while green stars represent non-specific interactions. A single specific interaction is shown in the expanded plot

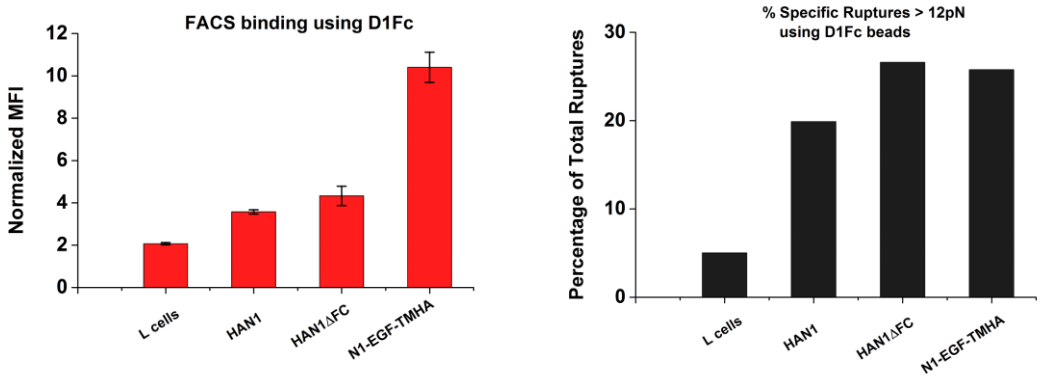

Figure 3.4 (left): Fluorescent D1Fc based FACS analysis of L-cell derived cell lines used in OT force spectroscopy shows similar cell surface expression of HA tagged N1WT (HAN1) and N1ΔFC (HAN1ΔFC). Cell lines are designated with names corresponding to their ectopic expression. Also, all the cell lines - HAN1, HAN1ΔFC (furin cleavage mutant) and N1-EGF-TMHA (NRR deletion mutant) exhibit higher levels of surface expression compared to parental L cells and all of them bind D1Fc.
Figure 3.5 (right): Probability percentage graph. The number of specific ruptures (defined as rupture force > 12pN) correlate with high ectopic expression of wild type or mutant N1 in the cell lines.

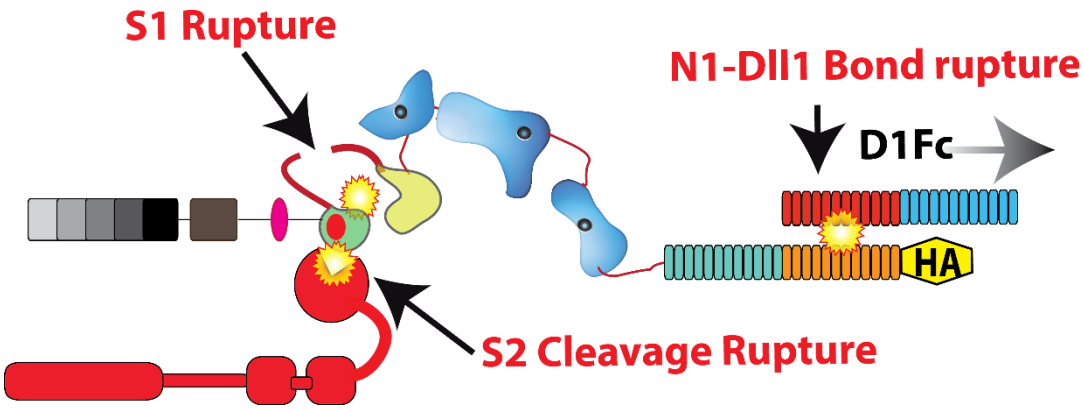

Figure 3.6: Origin of multiple rupture modes in N1: During pulling of interaction, heterodimeric Notch can break or fail at three different regions on the Notch Extracellular Domain (NECD), namely, at the S1 chain break, S2 ADAM 10 cleavage and at the ligand binding EGF repeats.

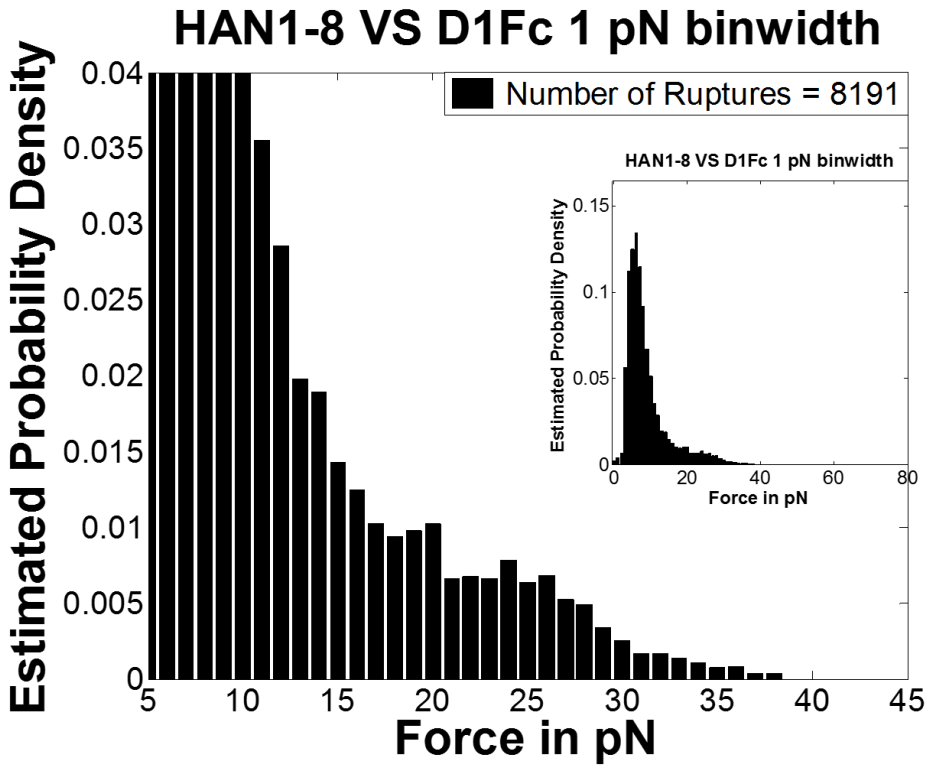

Figure 3.7: A typical rupture force spectra obtained after thousands of cell-bead contact and release cycles. Shown here is the RFS of N1WT cells with trapped D1Fc beads; Inlet shows the RFS in its entirety.

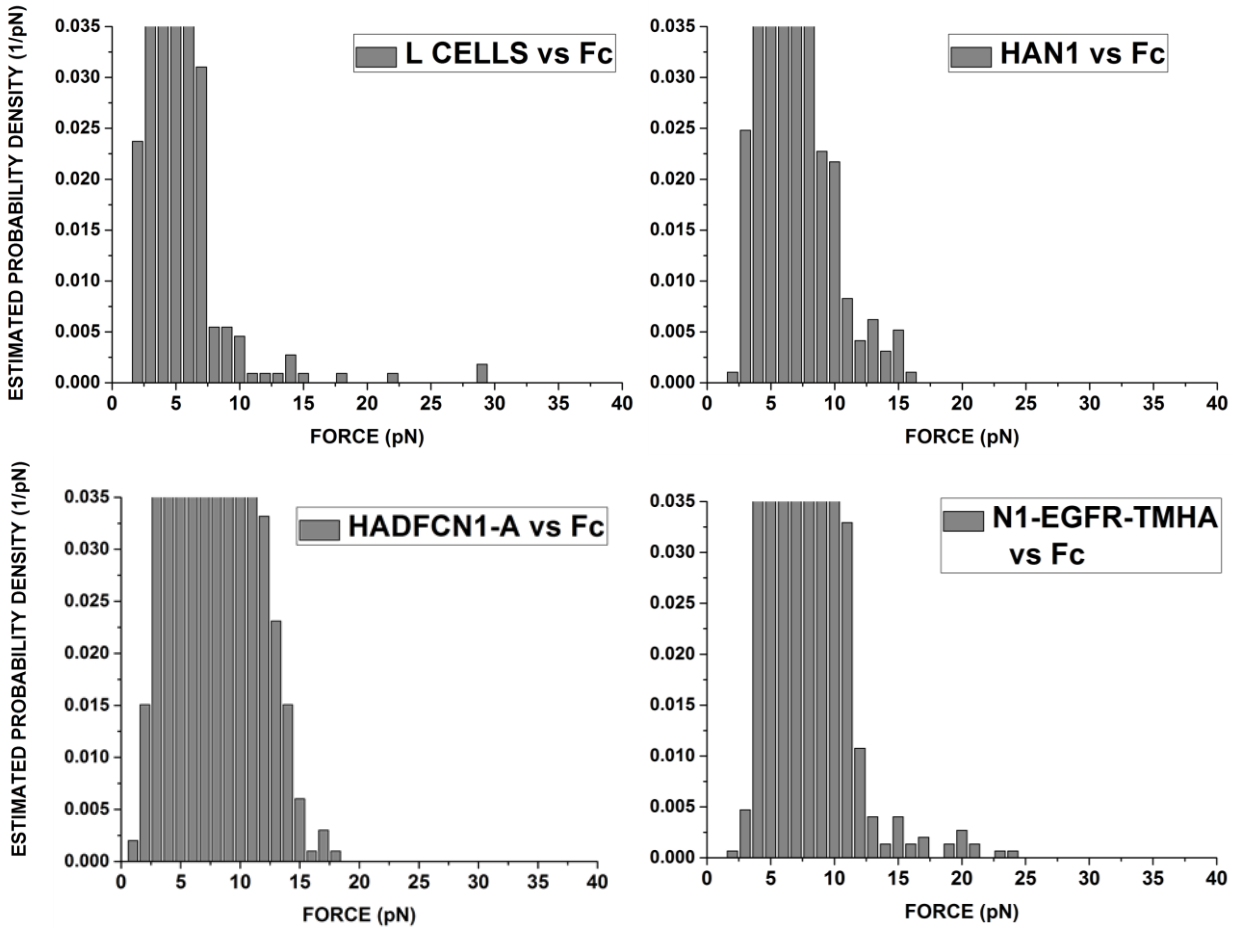

Figure 3.8: RFS of cell lines against D1Fc beads and Fc beads (controls). Notice the diminished presence of forces beyond 12 pN in all of the cell lines in RFS obtained using Fc beads.

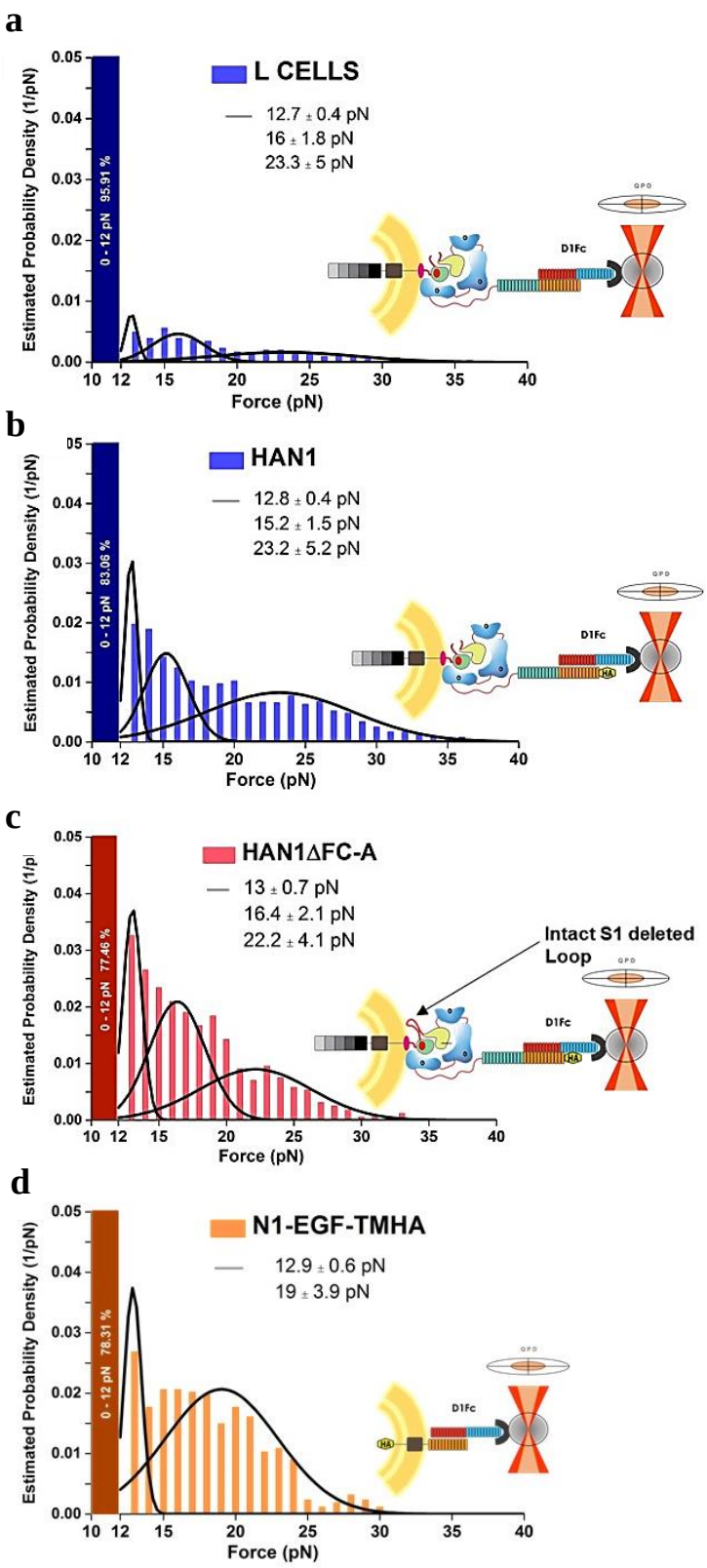

Figure 3.9: Rupture Force Spectra (RFS) of wild type and mutant Notch1 support force model of Notch activation. A three-mode Gaussian mixture model was fit to each rupture force spectra to reflect the three possible rupture points as illustrated in FIG 3F. RFS of **a.** parental L cells **b.** HAN1 and **c.** HAN1ΔFC exhibit three putative rupture modes with peaks around ~13pN and ~16pN. A third 23pN mode possibly representing a double of ~13pN. **d.** Force spectra of N1-EGF-TMHA reveals a force mode at 19-20 pN which was previously identified by Shergill, et. al. Since this mutant is characterized by the absence of NRR, both S1 and S2 ruptures are non-existent and the interaction must fail at the N1-D1 bond.

CHAPTER 4

THE ROLE OF S1 CLEAVAGE IN TRANSACTIVATION ENERGETICS

The primary objective of this chapter is to understand if there are detectable differences between S1 deleted N1ΔFC compared to N1WT. Given that the S1 breakage and S2 cleavage sites are very close to each other, observing forces at which Notch receptors are sessile at these points appears to be futile. Previous experiments performed on intact NRR seem to show this aspect. In AFM studies of unfolding the NRR, the force models at which the NRR breaks and S2 cleavage is initiated is not observed as clear peaks[50,51]. Further, forces applied in these experiments are several tens of pico-newtons which are clearly above the bond strength of a single N1-Dll1 interaction[50,51]. Recent studies on immobilizing NRR on rigid substrate to apply force using magnetic tweezers reported about 4pN of force within the physiological range. The force application brings about S2 cleavage by ADAM17 in these experiments[52]. While these results are interesting, S2 cleavage occurring concomitantly after force application cannot be a linear straightforward conclusion. Whether S1 breakage happens before S2 cleavage or if S2 occurs independent of S1 breakage is ambiguous in these experiments. Further, ligand induced Notch activation requires ADAM10 for cleavage and not ADAM17[53]. While a NRR destabilizes with EDTA treatment can be cleaved by either ADAM10 or ADAM17[53,54]. This is further exemplified by the fact that ADAM10 or Kuz mutation phenotypes overlap a lot of that of Notch pathway[55]. So, if just the S2 exposure allows ADAM17 to cleave, it does not explain the decreased activation by ADAM17[53,56]. However, if Notch is sessile at S1 chain break, leading to NECD shedding independent of S2 cleavage, the exposed S2 site can be easily accessed by ADAM10 or 17 to activate Notch signaling. This would directly impact the signaling

efficiency of the receptors where a heterodimeric Notch sessile at S1 chain break can bind the ligand and shed its extracellular domain upon ligand pulling to expose S2 cleavage site for ADAM10/17 proteolysis. Further, in the absence of ADAMs to cleave and when S1 site is deleted, the molecule may exert mechanical resistance to ligand pulling similar to a rigid molecule. Given that EGF receptors are not extensible at low forces, this tension is likely to transmitted to the cell membrane. In order to investigate all these possibilities, we examined each rupture curves of all mutants and wild type ectopic Notch in our experiments. Further, we chemically inhibited ADAMs or furin in the wild type and the mutant to observe if optical tweezers studies can detect such molecular changes to Notch.

FORCE EXTENSION CURVES REVEAL BIOPHYSICAL CHARACTERISTICS OF THE RUPTURE FORCE DATA

While rupture force spectra for wild type N1 and N1ΔFC were indistinguishable between the two molecules (Fig. 3.9), we next examined the way the molecules, and likely their local membrane, extended under tension. Each specific N1-Dll1 interaction waveform (Fig. 3.6) follows a unique contour in time, which may be unique to each isoform. We can project these waveforms onto force-extension axes using the location of the cell and the bead in time, measured directly by our instrument and where only the portion of the waveform starting with the initiation of tension and ending at rupture is analyzed (Fig. 3.6 & Fig. 2.6). Extension of the interaction is defined as the difference between the positions of the cell and the surface of the bead facing the bead. Fig. 2.6 illustrates the evolution of a Force Extension Curve (FEC). Features of this curve are related to instantaneous molecular unraveling events, and likely membrane extension. A typical FEC is given in Fig. 4.1.

To determine if there are FEC curve types specific to N1 or N1ΔFC, we blindly examined and classified hundreds of FECs such that each curve was presented without identifying the Notch1 isoform it corresponded to. Analysis of all such FECs revealed five FEC classes out of which two were most commonly occurring in the data (Fig. 4.2). After identifying these curves with the molecule being tested, we found that the occurrence of all the other classes remained relatively constant (Fig. 4.3) except for Class1 and Class4 curves. These two highly recurrent curve types as shown in Fig.4.4 a & b, which we term Energy Trace (ET1) and Energy Trace (ET2), displayed unique contours till rupture; ET1 has a near linear rise to rupture while ET2 curves exhibit a steep rise followed by an isotonic plateau. The area under FEC curves till rupture measures mechanical work acting on the bead (Fig. 4.1). This mechanical work acts through the molecular interaction to extend the folded domains of Notch and also likely perhaps the membrane.

N1ΔFC REQUIRES MORE MECHANICAL WORK FOR TRANSACTIVATION BY DLL1 AS COMPARED TO N1WT

Based on the finding that there were two different FECs with markedly different contours, we investigated if FEC distribution correlates with the two Notch variants. We first examined the occurrence of ET1 and ET2 curves in parental L-cells, HAN1, HAN1ΔFC cells and extended this analysis for additional mutants as presented below. Two important observations emerged from the examination of the cell line HAN1, which expresses ectopic N1WT. Firstly, these cells primarily exhibit FECs of ET1 (>70%), as also observed for parental L-cells that express endogenous N1WT on their cell surface (Fig. 4.5). And second, important to transactivation of Notch, ET1 curves correspond to lower mechanical work than do ET2. By contrast, the cell line HAN1ΔFC expressing ectopic N1ΔFC shows a gain of

higher energy ET2 curves and a corresponding loss of ET1 (Fig. 4.5). Taken together these results suggest that the mutant requires more work to pull to rupture. We next examined the NRR deleted mutant, N1-EGF-TMHA, having just 1-15 EGF repeats in its extracellular domain and is directly tethered to the membrane by N1 transmembrane domain (N1TM) lacking a cytoplasmic intracellular domain. We found that FEC analysis of this mutant reports a gain in the percentage of ET2 curves as compared to both N1WT and HAN1ΔFC. The higher percentage of ET2 reflects a likelihood of extensions contributed to by the membrane to a greater degree as compared to WT and N1ΔFC. Considering that the distribution of work for ET2 for both the N1ΔFC and NRR lacking mutants are similar, it is possible that ET2 is dominated by membrane extension, which may be the source of the isotonic contour of the corresponding FECs. This would imply that the wild type N1 can be extended to rupture will much less engagement of the membrane, whereas the N1ΔFC mutant is sufficiently 'stiffer' so that the membrane may be extended as the molecule unfolds until rupture occurs at either the S1 or S2 sites38. To test our supposition, we examined another mutant OCDN1, which had the entire wild type N1 NECD (including the NRR) and N1TM, but no intracellular domain. Interestingly, the percentages of ET1 and ET2 curves are similar to that of the N1WT, as were the work values, supporting our hypothesis that wild type N1, specifically the NRR, can be unfolded without significant involvement of the membrane (Fig. 4.5).

In order to understand if indeed Furin processing of N1 directly contributes to rendering the N1 molecule less "stiffer", we applied out the same FEC analysis to the ruptures obtained from OT experiments on N1WT and N1ΔFC treated with water soluble inhibitors of Furin (Dec-RVKR-CMK/ FI) [36,57,58]and ADAM (TAPI-2)[59] to block S1 or S2 cleavage.

Chemical inhibition of Furin has been shown to prevent S1 processing of N1WT leading to a full length p300 N1 on the cell surface similar to our engineered N1ΔFC[57]. Consistent with this report, we found a marked increase in the occurrence of ET2 after 4 hours of FI treatment on N1WT (Fig 4.6), at levels similar to HAN1ΔFC (Fig. 4.5) or untreated HAN1ΔFC (Fig. 4.6). Further, FI treatment of HAN1ΔFC cells leads to a very minimal change in percentages and median work values of ET1 and ET2 when compared to untreated HAN1ΔFC (Fig. 4.6). In line with the evidence of tissue lysates of the mutant mice, HAN1ΔFC is deficient in Furin processing. Therefore, we postulated that chemical inhibition of Furin processing would lead to occurrence rates of ET1 and ET2 as well as work values for both the treated and untreated HAN1ΔFC would be similar, whereas for the WT, we should observe an increase in both occurrences of ET2 and work, which we did observe.

S2 blockage using TAPI-2 in N1WT cells lead to no shift towards ET2 curves, but a marginal gain in ET1. However, when we inhibited ADAM in N1ΔFC expressing cells, we found very marginal increase in percentages but with significantly higher values of median work values, of note, also for ET1 (Fig. 4.6). Interestingly, we found this the elevation in work values resulted from elevation in rupture force values for both the FECs (Fig. 4.6). To explain this, we consider that when ADAM is inhibited in N1ΔFC mutants, the two possibilities of ruptures S1 and S2 (as explained in FIG 3f) are abrogated leading to the only rupture modality being at the N1-Dll1 bond. This result further reinforces the absolute requirements in Notch mechanotransduction that the N1-Dll1 bond strength must be stronger than forces associated with ectodomain dissociation at the S1 chain break or S2 cleavage for successful transactivation by ligand.

Most of the previous experiments on unfolding of Notch NRR were performed on rigid surfaces with homogenously functionalized Notch. This increases the likelihood of Notch-Ligand interactions. However, this is not the physiological setting Notch receptors and ligands interact in and hence we adopted live cells expressing Notch with ligand. Considering that we observed a large non-specific zone of 12pN for all the cell lines, I raised a question whether the effects of FEC sorting were due to cell membrane and bead interaction rather than Notch and D1Fc interaction. Cell lines created in labs after artificial transformations are prone to exhibit variability in expression levels of proteins due to batch to batch heterogeneity. In order to dissect this question, I tested several other cell lines of N1WT and N1ΔFC generated by Weinmaster lab and found that the results of N1WT versus N1ΔFC were indeed single molecule dependent and not due to cell membrane dynamics or any other contribution (Fig. 4.7). Untagged N1WT proteins labelled as LN1 displayed high ET1 to ET2 ratio similar to HAN1. Whereas, HAN1ΔFC-B a clone similar to HAN1ΔFC (HAΔFCN1-A) displayed higher frequency of ET2 reflective of high expression levels of ΔFC protein compared to HAΔFCN1-A (Fig. 4.8).

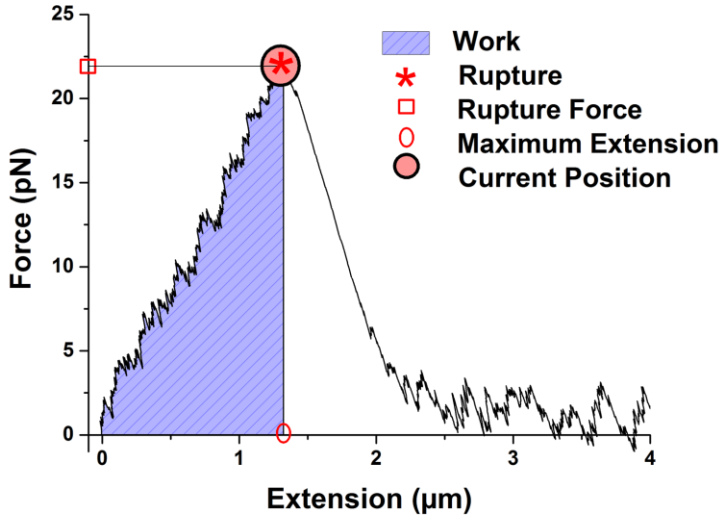

Figure 4.1: Typical Force time waveform from a Rupture plotted over Extension to generate a Force Extension Curve. The shaded region is the Work required to pull the receptors till rupture (red *).

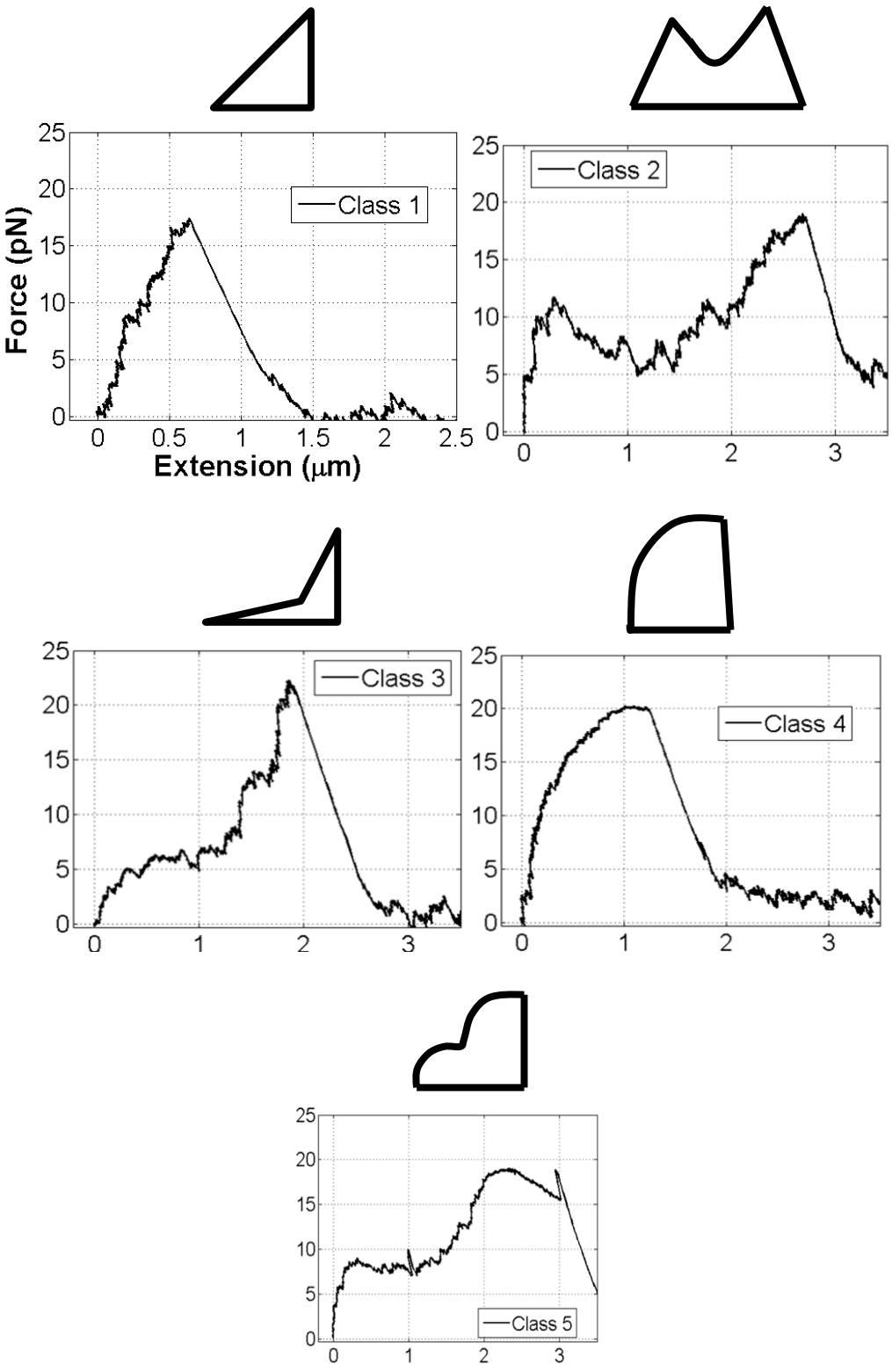

Figure 4.2: The FECs of all the cell lines comprised of five major classes. The corresponding geometry of the classes are shown in inlet cartoons. All other FEC traces which showed abrupt signal jumps and noise were eliminated.

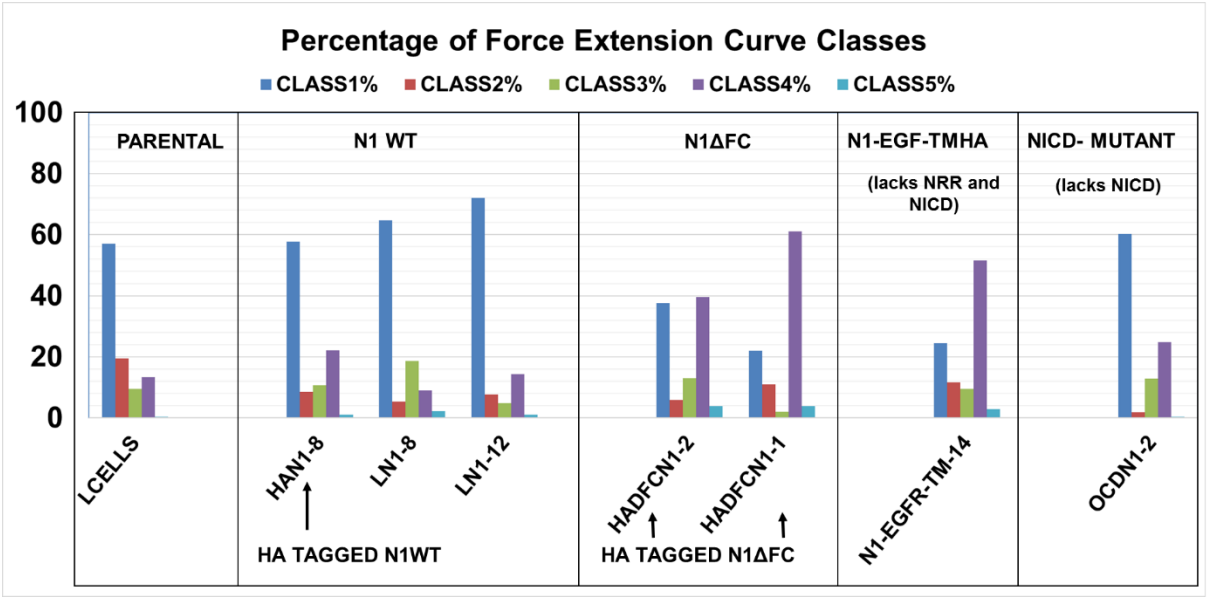

Figure 4.3: Percentage of FECs: The FEC classification in all conditions revealed that the occurrence of Classes 2,3 and 5 were low.

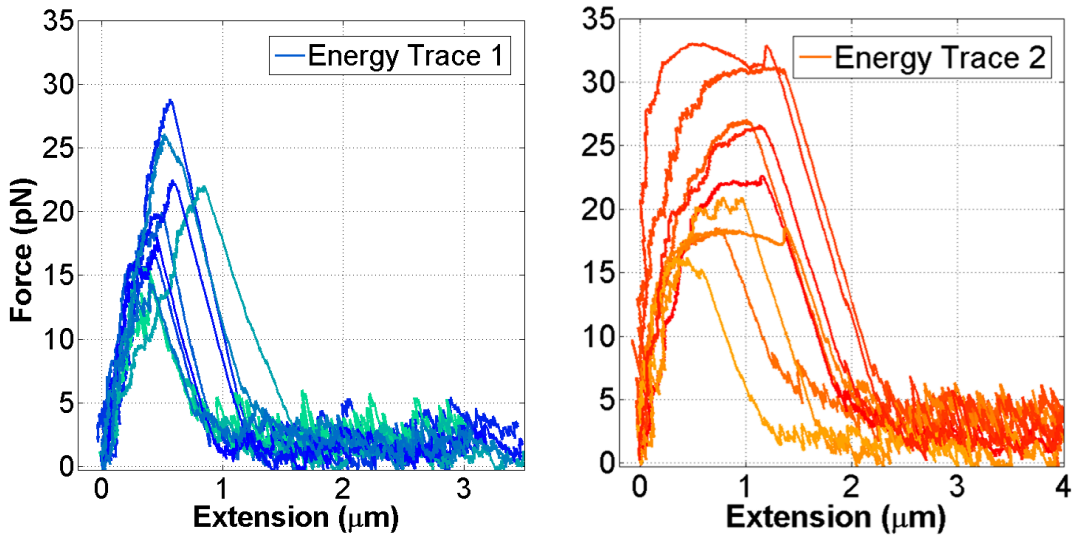

Figure 4.4: Energy traces: Classes 1 and 4 were the predominant classes and were assigned as Energy Trace 1 (ET1) and Energy Trace 2 respectively (ET2).

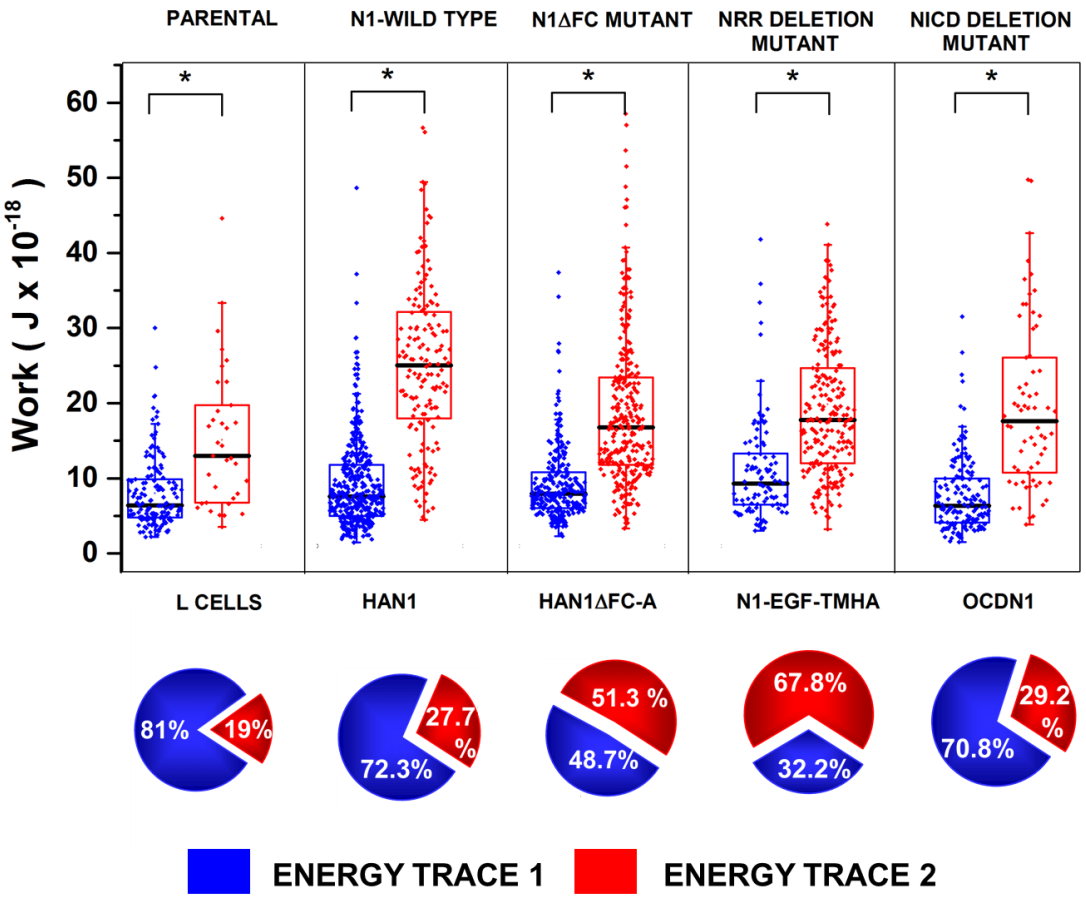

Figure 4.5: Box scatter plot of Work values with ET1 and ET2 classes segregated. Pie charts represent the percenatge of each FEC type for each cell line. Work values for ET2 are larger than for ET1 across all the conditions. N1WT FECs in parental and HAN1 is

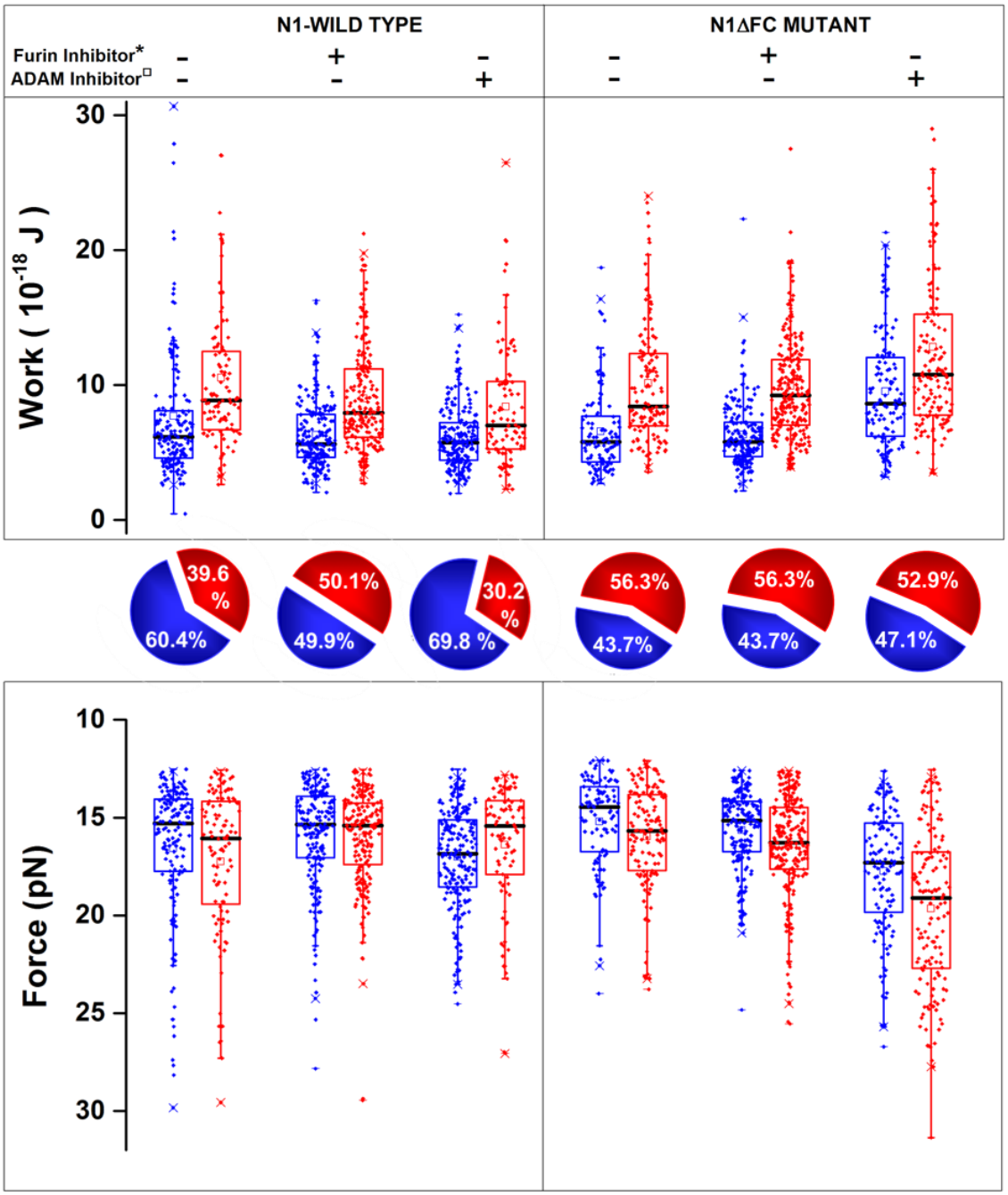

Figure 4.6: N1WT and N1ΔFC drug treatment studies. N1WT treated with FI (*Dec-RVKR CMK) shows increase in the number of ET2 curves compared to untreated control but similar to untreated N1ΔFC, while treatment with ADAM inhibitor (□□TAPI-2) appears to slightly increase the number of ET1 curves. FI treatment of N1ΔFC leads to no detectable change in ET1/2 numbers. Treatment of N1ΔFC with ADAM inhibitor increases ET1 percentage, however, the median work values show a marked increase compared to all other conditions. dominated by high incidence (~70-80%) of ET1, while N1ΔFC (HAN1ΔFC-A) shows increases in incidence of ET2. The number of ET2 curves is predominant in the deleted NRR mutant N1-EGF-TMHA, while the NICD deletion mutant (OCDN1) shows ET1 to ET2 ratio similar to N1WT.

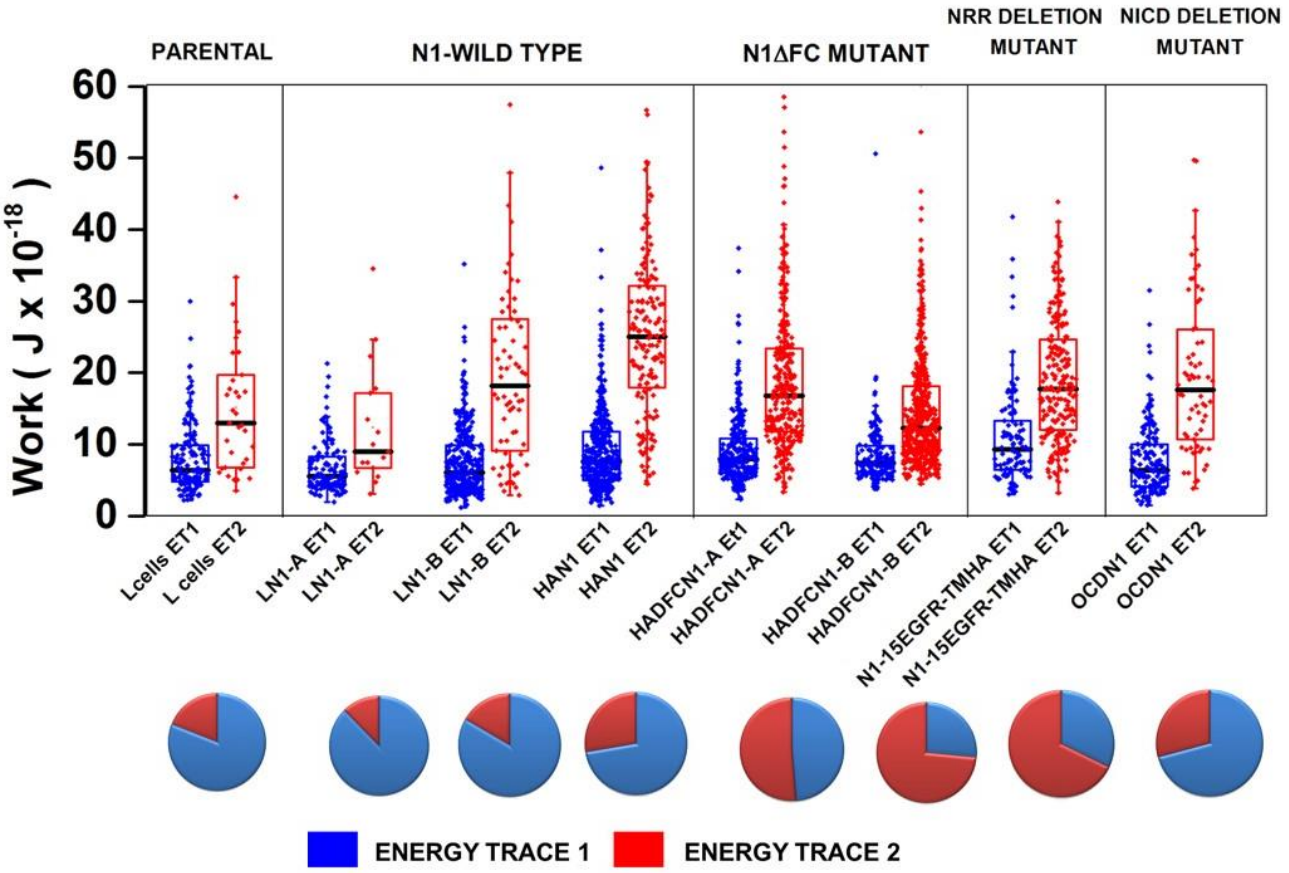

Figure 4.7: Work plot of all cell lines. Additional clones of N1WT and N1ΔFC show biophysical characteristics similar to their isoforms as described in Fig. 4.5. Notice elevated ET2 frequency of N1ΔFC in clone named HADFCN1-B which is reflective of elevated expression of N1ΔFC protein.

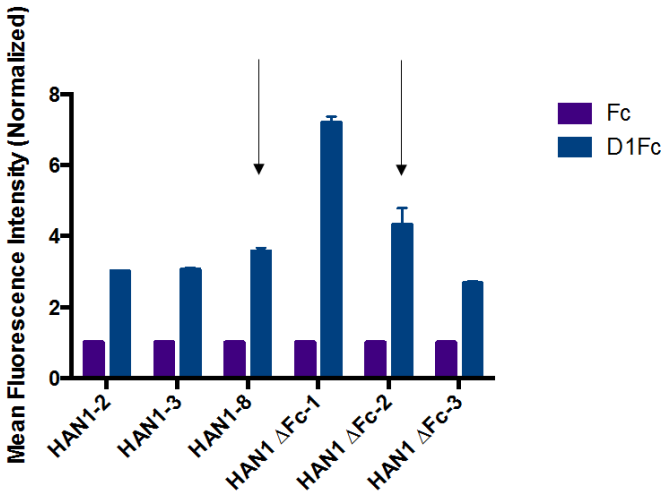

Figure 4.8: Expression levels of cell lines expressing WT and ΔFC isoforms of Notch. Arrows indicate the clones selected for optical tweezers studies. HAN1-1 is HAN1 and HAΔFCN1-2 is the HAΔFCN1 used in Fig. 4.5. HAΔFCN1-1 is interchangeably HAΔFCN1-B as displayed in Fig. 4.6. Notice the expression of HAN1ΔFC-B expression is higher than that of HAN1ΔFC-A which leads to increased ET2 percentage in Fig. 4.7

CHAPTER 5

NOTCH – LIGAND BIOPHYSICS

As mentioned in the introduction, there are two classes of membrane bound ligands that are important for canonical activation of Notch- Delta and Serrate/ Jagged class named after Drosophila Delta and Serrate ligands which differ by the number of EGF repeats. In mammals, the Delta class consists of homologs of Delta- Delta-like ligand (DLL or Dll) 1,3 & 4. While the Serrate class consists of homologs of Jagged (Jag)- Jagged 1 & 2. Each ligand except Dll-3 is capable of generating a signal in Notch in trans while inhibiting in cis[9,29]. The domains on Notch the ligand binds to activate and inhibit are very different nevertheless both regions lie on the EGF repeats region of NECD. The Notch 1 to 15 EGF repeat regions is shown to be critical for ligand binding. Especially, EGF repeats 8, 10, 11,12 and 13 on Notch are known to be critical binding interface for ligands[9,23]. The EGF repeat 8 of Notch has been demonstrated to distinguish the ligands Delta and Jagged[24]. While EGF repeats 11 and 12 are shown to be the most important for binding with the loss of EGF 11 abrogating any binding to the ligands[60]. The Delta and Jagged class primarily differ based on the number of EGF repeats on their extracellular domain. Jagged class of ligands have 16 EGF repeats while Delta class have about 6 to 8 EGF repeats[9,23]. Further, there is a conserved face of ligands at the tip of their extracellular domains named as a *m*odule at the *N*-terminus of *N*otch ligands (MNNL) which is followed by a Delta/Serrate/Lag (DSL) domain which are known to interact Notch repeats 8 to 12 to exercise strong binding[9,22]. Other EGF repeats on the ligands may have unknown functions in stabilizing or destabilizing the Notch -ligand interactions. Similarly, other EGF repeats on Notch from 15- 36 may have a function in

regulating the level of binding to the Notch ligands. Also worth noticing is that some ligands exhibit phospholipid binding on the cell surface which may serve as an additional mechanism to regulate the stability of Notch binding[22].

One of the primary reasons for the study of mammalian Notch ligands is the existence of context dependence and generation of pleiotropy due specific receptor ligand interaction[9,61]. Many receptor ligand pair orchestrate specific signaling states and cell differentiation regimes during development[62]. Further, ligands of the two different classes have opposing functions[63–66] or even within the same class of ligands, different ligands may have reciprocal effects on the same receptor[62,67,68]. In this part of the project my aim was to identify and isolate differences in ligand Notch pairs in relation to the specificity and establish context dependent functional diversity in terms of their interaction biophysics.

BOND STRENGTH AS A MEASUREMENT OF BIOPHYSICAL DIFFERENCES BETWEEN RECEPTOR LIGAND PAIRS

Taking cue from Shergill et al. 2012[16] (Fig. 5.1) that the bond strength of Notch and Delta is independent of ligand cell endocytosis, I pursued to understand bond strength as a possible biophysical identifier of a specific receptor ligand interaction. I performed optical tweezers based dynamic force spectroscopy on L cells expressing the predominant mammalian Notch ligands- Dll1, Dll4, Jag1 and Jag 2. Rupture Force Spectra for different ligands was perfomed by probing with N1Fc (Notch 1 ligand binding domain 1-15 EGF repeats fused in frame with human IgG Fc with hinge). Several thousands of contact and release cycles were performed and peak force values of each cycle was plotted in a normalized histogram called Rupture Force Spectra (RFS) introduced before. As shown in Fig. 5.2, Dll-1 cell

probed with N1Fc reproduced the results by Shergill et al. which when mathematically fit to two Gaussian mixture model identified 19pN and a equally probable 30pN. As described by Shergill et al. due the presence of disulfide hinge in Fc CH2-CH3 region, N1Fc is dimeric molecule with two N1 molecules available for interaction with Dll1. This is because as one Dll-1 molecule on the cell binds to one of N1s on the N1Fc, the dimeric neighboring N1 has increased chance of binding other proximally available Dll-1 on the cell surface increasing the probability of double bond. Therefore, observing 19pN and a near double 30pN is the signature N1-Dll1 bond characterized by our lab. Jagged 1 also exhibited an emerging force mode starting from 15pN with a maximum around 18pN and a reduced 28pN mode which is near the force of double bonds. Further, like Dll-1, the overlap of first and the second bond mode is just enough to reveal the two force modes and the peaks of the respective modes clearly. Surprisingly, N1Fc binding of Dll-1 did not exhibit any obvious force modes beyond 12-15pN cut off force. Given that Dll-4 has been purported to be a stronger binder than Dll-1 to N1 this result was unconventional[69]. N1Fc binding probability to Jag2 was low however, a clear 27pN mode emerged away from the tall non-specific force zone which spanned till about 20pN. This single mode may be representative of weak probability of binding of Jag2 to Notch 1. The Gaussian fits were generated after fitting the RFS beyond 15pN to capture only the specific forces. The 15pN general cut off was chosen based on Dll1- Fc experiments where there are no force values beyond 12-15 pN. The RFS for Fc coated beads probed against ligand cells showed increased presence of forces beyond 12pN for all ligands except Dll-1, however most of the force modes diminish around 18pN (Fig 5.3). This shows that Fc coated beads may be binding non-specifically to cell surface and therefore different protein needs to be chosen as a non-specific control for these

experiments. In summary, RFS of Dll1 and Jag 1 were similar in binding force mode but Jag2 had a higher rupture force of 27pN but within physiological range[16].

ENDOCYTIC PULLING FORCE AS A METHOD TO DISTINGUISH THE N1 LIGAND PAIRS

Next, I observed the pulling force exerted by ligand cells when N1Fc beads were brought in contact with them. Polystyrene Protein A beads incubated with high concentration of N1Fc (5 μg/ml) were used for these endocytic pulling force measurements. As mentioned in the introduction, Notch ligands have to exert pulling force mediated by the ligand cell endocytosis to activate Notch and as such N1Fc beads when placed in contact with ligands experience pulling force[18]. A laser trapped N1Fc bead was brought in contact with ligand cell and observed for about 100s. Endocytic pulling force by the ligand displaces the laser trapped bead and a time dependent endocytic force can be traced as shown in Fig. 5.4. The average value of the force at instantaneous time points gives the average pulling force during the time interval of observation. The maximum value of the force achieved during that time interval was also another variable I took into consideration. As shown in Fig. 5.5, the average pulling force of ligands on N1Fc beads were comparable with statistical tests unable to prove any significant difference between the data samples. However, Jag2 showed remarkably low average pulling force compared to all other ligands showing that Jag2 could be a least potential candidate for Notch 1 signaling in the presence of other ligands. The Fig. 5.6 shows the maximum pulling force graph which closely mirrors the average pulling force showing that positive pulling forces dominate the data points for most of the cell bead pairs. Even though I was unable to distinguish between the ligands using this metric, the critical observation that all ligands exert physical pulling force on N1

is significant in light of the allostery hypothesis proposed for soluble Notch ligands[26]. Another critical observation is that the average pulling force for each ligand cell-bead pair is less than typical bond strength values I could deduce from their respective RFS (Fig. 5.2)

EFFECTS OF LUNATIC FRINGE ON NOTCH LIGAND INTERACTION

Notch receptors undergo glycosylation of the EGF repeats by modified by a set of glycoprotein glycosyltransferases, known as β3-N- acetylglucosaminyltransferases or otherwise known as Fringe, There are three types of Fringe - Lunatic Fringe(LFng), Manic Fringe(MFng) and Radical Fringe (RFng). LFng is associated with segmentation clock during somitogenesis and loss of LFng leads to embryonic defects[9,70–73]. All these Fringes extend an already O-link-fucosylated EGF repeat by adding GlcNAc (N-Acetylglucosamine) sugar[74]. LFng specifically adds fucose residues to the O-glucose modified EGF repeats. The decoration of sugars on the EGF repeats of Notch have been purported to be significant for signal generation and sustenance. Further, glycosylation has also been demonstrated to be an important aspect of context dependent ligand differentiation with Fringe modifications strengthening or weakening ligand binding in trans or cis[66,71,75]. In light of this project, I tried simple experiments to demonstrate that Fringe effects may lead to inactivation of ligand mediated signaling at the receptor ligand interface. Previously, Weinmaster lab had demonstrated that LFng modified N1 is not activated by Jag1 but strongly activated by Dll-1. In other words, LFng acts as a checkpoint to introduce strong ligand preference on Notch to be activated by Delta class of ligands. This is significant because there are many instances in which Delta and Jag classes of ligands have divergent and also opposing effects[63,64,76,77].

First, I generated LFng modified N1Fc conditioned media to functionalize it on protein A beads. I performed dynamic force spectroscopy on ligand Dll1 and Jag 1 and graphed the respective RFS for differences. As shown in Fig. 5.7, the RFS for N1Fc on Dll1 cells showed enhanced rupture force mode with peak at around 30pN almost double that of its unglycosylated mode of 19pN previously reported. Jag1 also showed an enhancement of rupture force peak to around 25pN when fitted with a Gaussian model. However, this bond strength was still weaker than the enhancement for N1-Dll1 bonds. Next, I observed the endocytic pulling force of Dll1 and Jag1 cells by comparing the average positive pulling force of the unglycosylated and glycosylated N1Fc. As shown in Fig. 5.8, I found that Jag1 fails to effective exert pulling force on Fringe glycosylated N1Fc compared to its unglycosylated form. Further, the raw waveform of pulling force exerted by Dll1 expressing cells on N1Fc vs time and Fringe modified N1Fc, I could observe the push-pull dynamics of the cells on the beads. Jag1 expressing cells, however, exhibited push/ pull on N1Fc coated beads but failed to show detectable push pull interactions with Lunatic Fringe coated N1Fc as shown in Fig. 5.9.

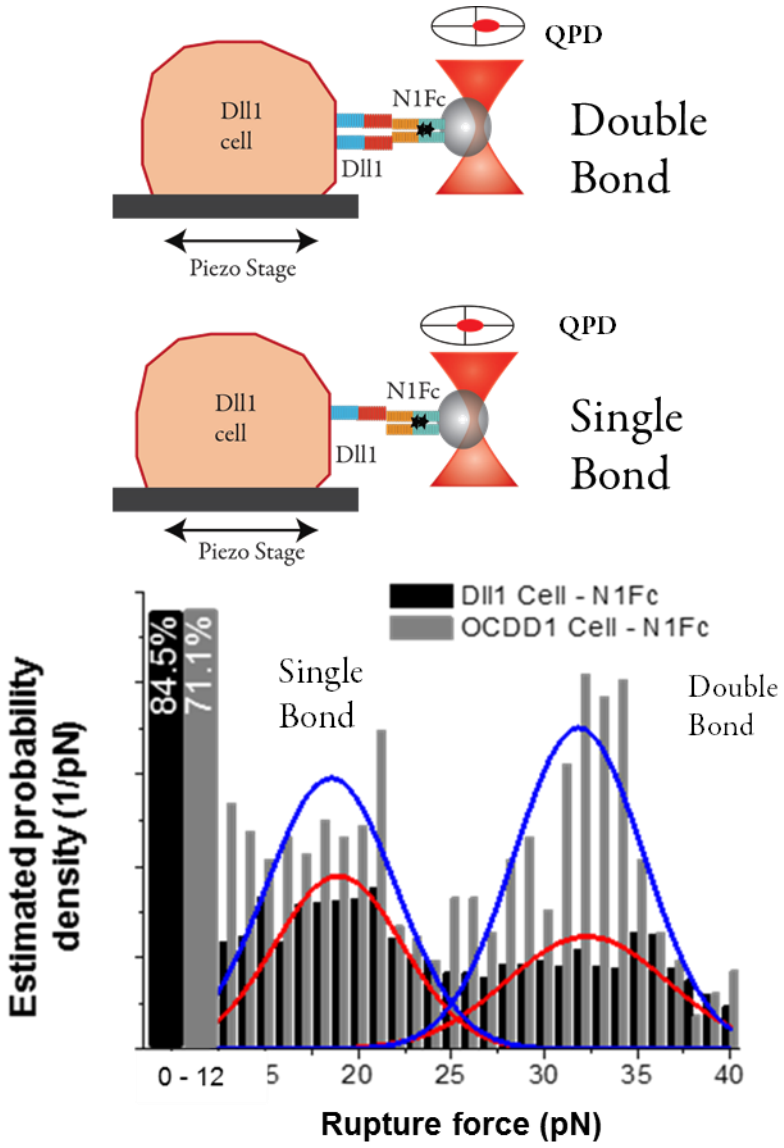

Figure 5.1: The Rupture Force Spectra of Notch 1 (N1Fc) beads and Dll1 expressing cells identifying the most probable force of rupture as observed by Shergill et al. 2012[16]. A two Gaussian mixture model differentiates single and double bond mode, with the later occurring almost at two times the force value of the former. The elevated probability of the second bond mode is due to the increased change of two N1-Dll1 pairs binding caused due to hinge in the Fc region.

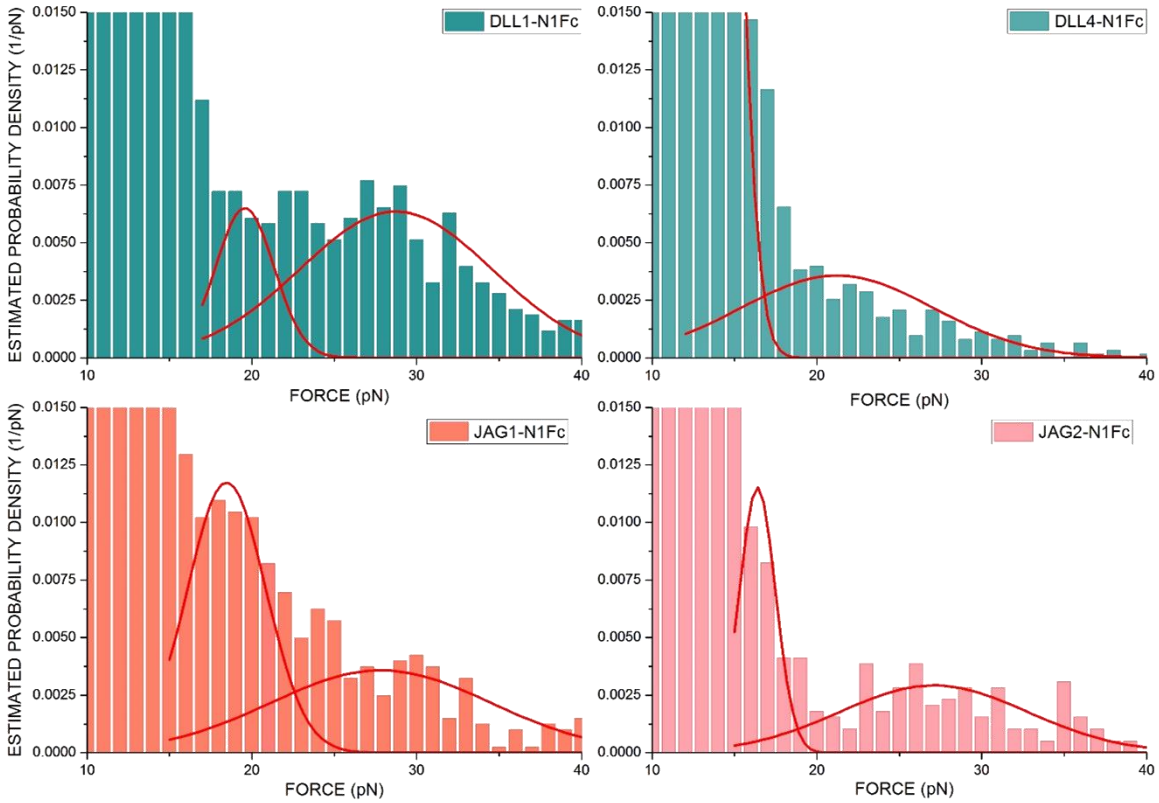

Figure 5.2: The Rupture Force Spectra of N1Fc beads against cells expressing ligands Dll-1, Dll-4, Jag1 and Jag2. Dll-1 and Jag1 showed single bond rupture at around 19pN and double bond around 30pN. The double bond mode was diminished for Jag1 compared to Dll-1. Jag2 displayed a clearly isolated mode at around 27pN- much higher than Dll-1 or Jag1 but at a lesser probability nevertheless. The 17pN mode of Jag1 is likely a non-specific shoulder. Dll-4 surprisingly does not show high probability of binding to N1Fc.

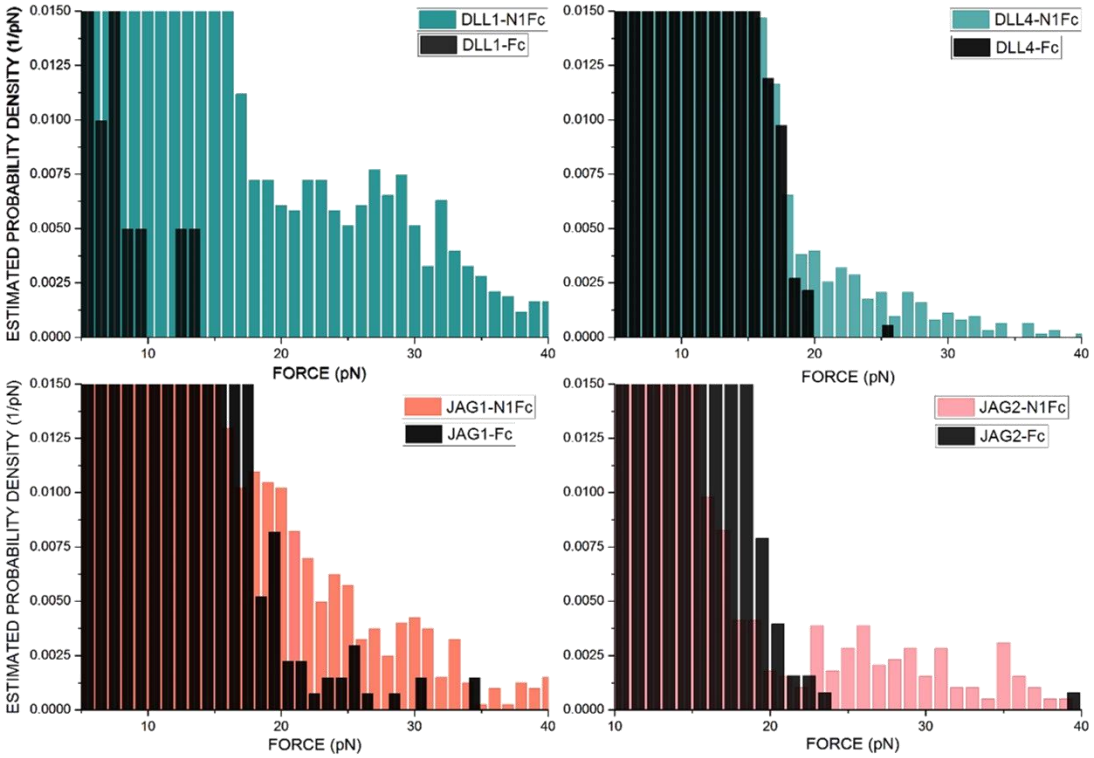

Figure 5.3: Fc Control RFS. The Rupture Force Spectra of N1Fc beads against cells expressing ligands Dll-1, Dll-4, Jag1 and Jag2 compared with Fc beads against the same. Fc RFS here extends more than 15pN in Jag 1, Jag2 and Dll4 cell lines showing non-specific interaction of Fc with these cell lines at these force ranges. Nevertheless, forces beyond 18pN can be accounted for specific ligand-N1Fc interaction

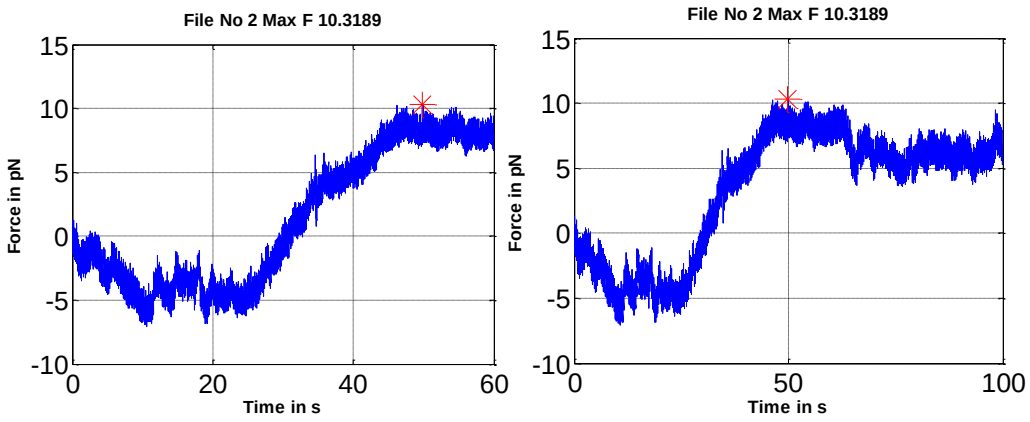

Figure 5.4: Typical Pulling Force waveforms for laser trapped N1Fc beads pulled by ligand cells.

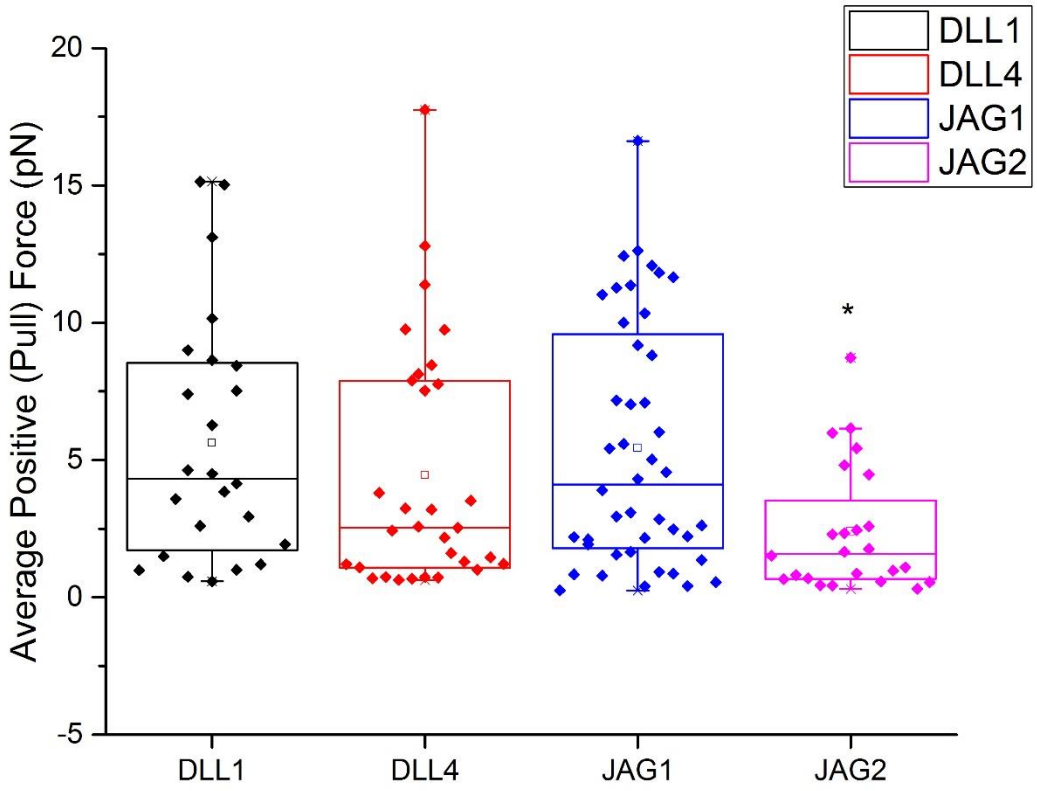

Figure 5.5: Endocytic Pulling Force is the net force exerted by ligand cells on laser trapped N1Fc beads. The median values for average positive pulling force for these ligands appear to be the same except for Jag2. This data reflects the understanding that Dll1, Dll4 and Jag 1 and common candidates for signaling through N1Fc.

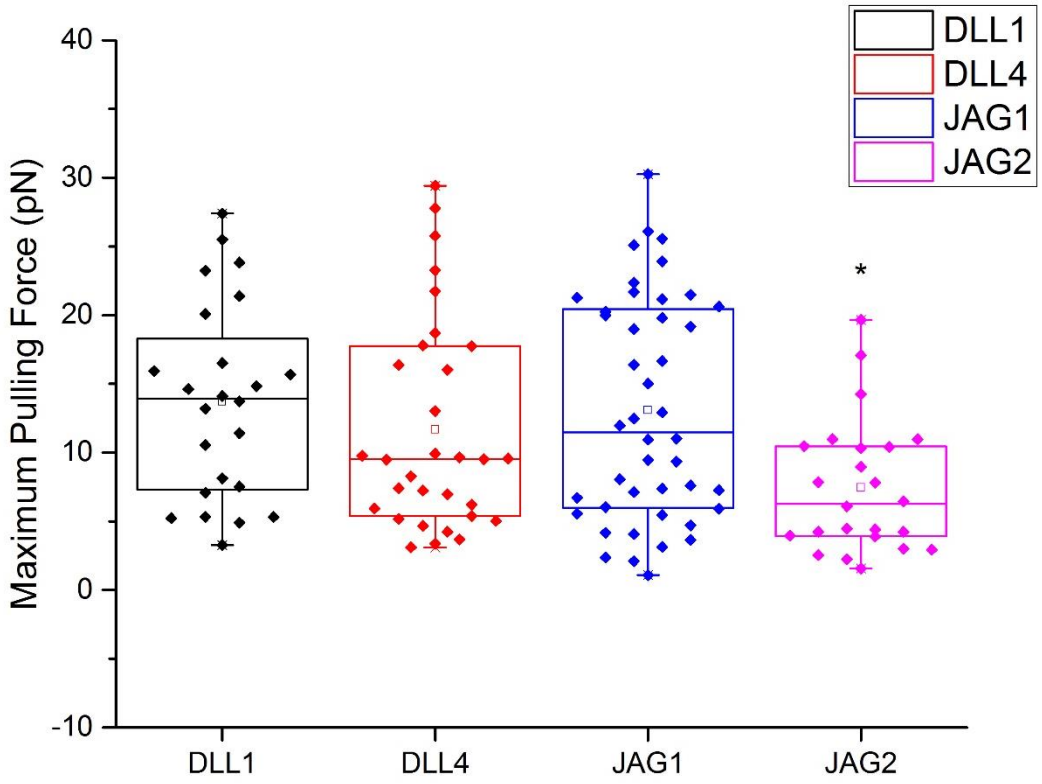

Figure 5.6. Maximum Pulling Force Box plots. The Maximum force achieved during a 100s pulling experiment constitutes the Maximum Pulling Force. The plot recapitulates the Average Pulling Force reinforcing the idea that the majority of the force waveform is "pulling" in nature than pushing.

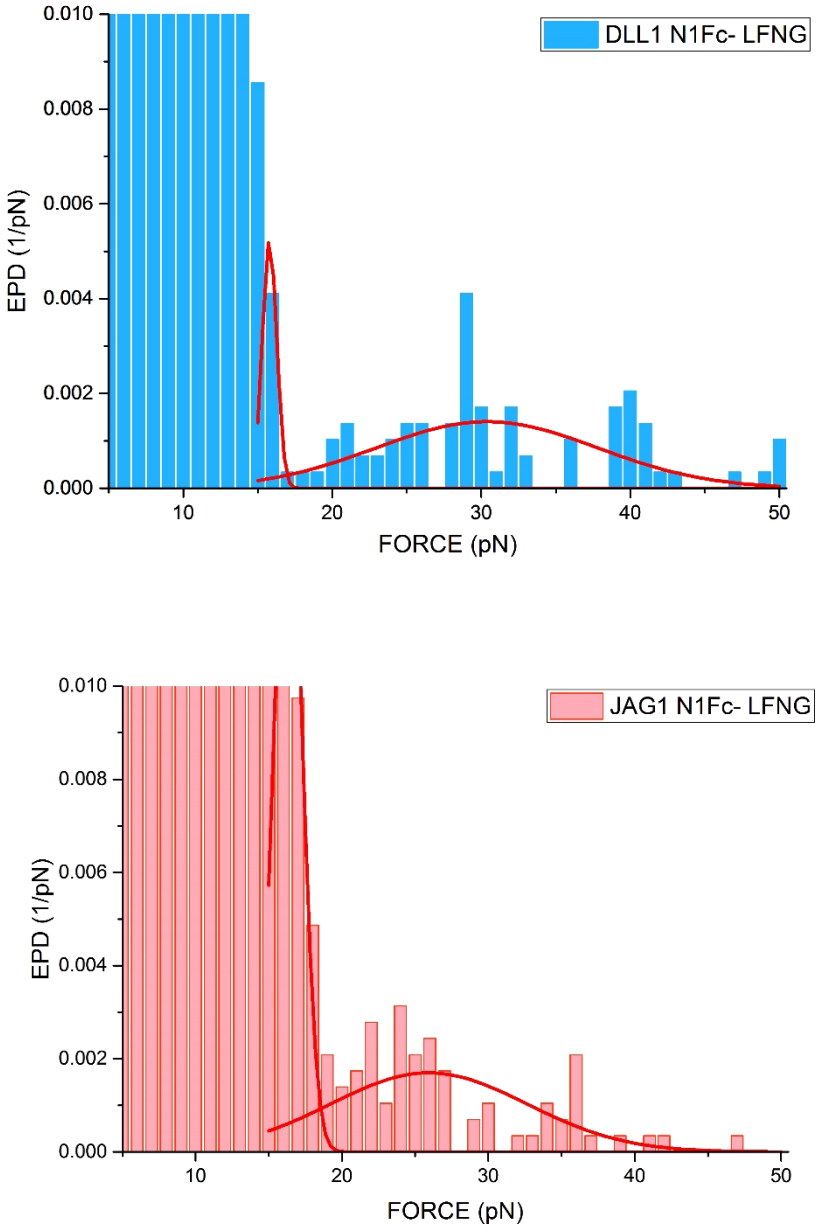

Figure 5.7: Role of glycosylation in bond strength enhancement. Rupture Force Spectra of N1Fc modified by Lunatic Fringe (LFng) shows peak force mode at around 30pN which is greater than the unglycosylated N1Fc- Dll-1 bond. Similar enhancement is observed for Jag1 but the bond strength is still smaller than that for glycosylated N1Fc and Dll-1.

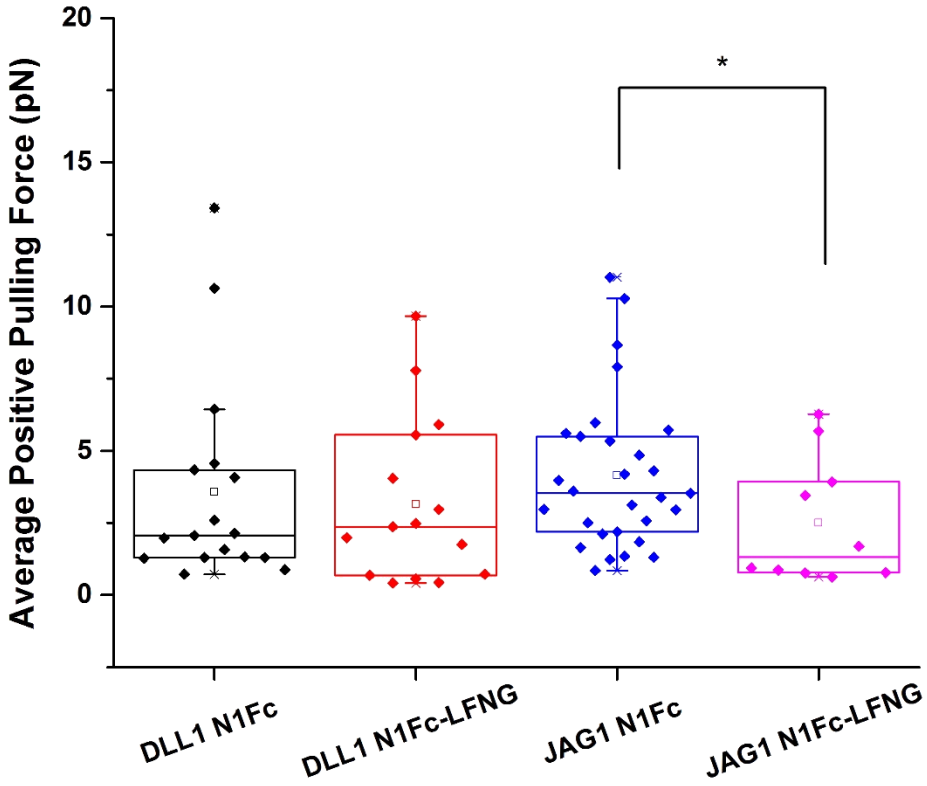

Figure 5.8: The Role of glycosylation in Pulling Force. LFng modified N1Fc is not sufficiently pulled by Jag1. Unglycosylated N1Fc is pulled by Jag1 at higher forces while the pulling force is significantly smaller for glycosylated Notch. Dll1 cells do not seem to decrease the endocytic pulling for glycosylated versus unglycosylated N1Fc.

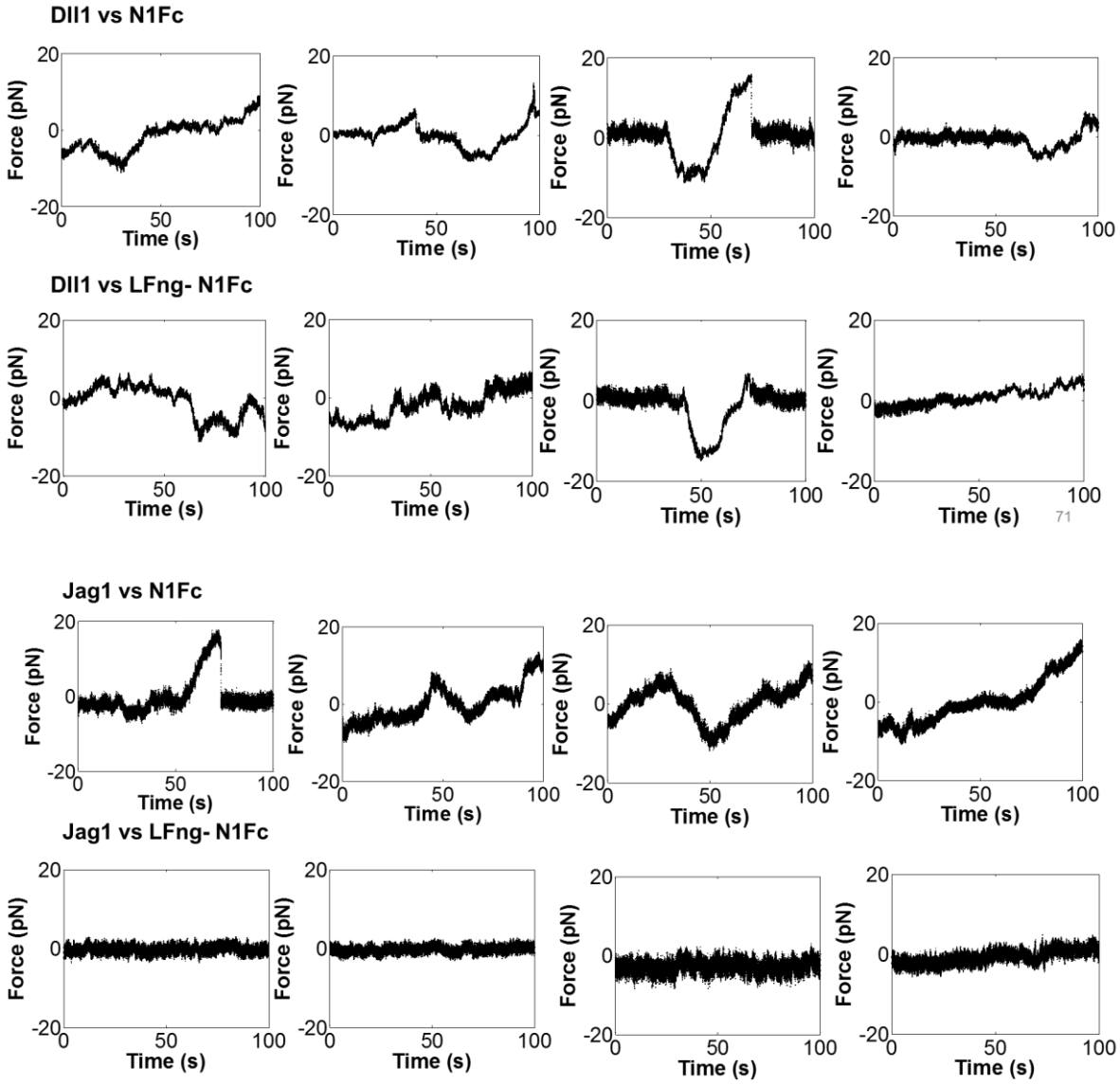

Figure 5.9: Sample pulling force vs time graphs. When the N1Fc coated beads are placed next to Dll1 or Jag1 expressing L cells, the pulling forces exerted by the cells can be monitored in time. The ability of Dll1 cells to interact with both N1Fc and Lunatic Fringe (LFng) modified N1Fc (first and second rows) is clearly observable in these graphs. While Jag1 cells pull and push N1Fc beads (third row), they do not exhibit incremental pulling force when in contact with Lunatic Fringe modified N1Fc beads.

DISCUSSION

FURIN PROCESSING OF NOTCH IS REQUIRED FOR BIOPHYSICAL EFFICIENCY

Here we provide evidence for the role of Furin processing of Notch in titrating the level of transactivated Notch signals with specific emphasis on mammalian embryonic development. We generated mutant mice in which abrogation of S1 cleavage of N1 leads to insufficient signals post mid-gestation resulting in vascular remodeling abnormalities and therefore partial lethality. The knocked-in engineered ΔFC mutation leads to no loss of Notch phenotype especially with N1WT background. However, the homozygous N1ΔFC/ΔFC mice are born with major septal defects and dysplastic aortic valves indicative of hypomorphic development. Presence of a single copy N1ΔFC against a Notch null background (N1ΔFC/NULL) increases embryonic survivability in mice which reflects the fact many Notch dependent processes are still ongoing in N1ΔFC till E14.5, surpassing E9.5 -the embryonic stage of lethality associated with N1NULL 18, however, N1ΔFC/NULL mutants fail to survive till birth. These findings demonstrate that although N1ΔFC is still a functional mutant capable of orchestrating most Notch dependent processes, it does not necessarily recapitulate the high Notch signaling levels provided by N1WT, which is predominantly an S1 cleaved heterodimeric receptor. We therefore, attempted to establish the molecular basis for the requirement of S1 cleavage for maintenance and sustenance of such high signaling levels by analyzing the surface expression and cleavage products of mutant receptors compared to wild type in cells extracted from the mice of both homozygous genotypes (N1WT/WT and N1ΔFC/ΔFC). Embryonic analyses of mice reveal

that the S1 deleted N1ΔFC traffics to the cell surface in tissues isolated from yolk sacs as a full length 300kDa molecule supporting the idea that the disruption of Furin processing did not greatly affect the transport of this collinear N1 isoform to the cell surface. Further, it is important to note that our 36 a.a. knocked-in mutation does not overlap with any of the flanking consensus sequences reported in the S1 loop that does not directly involve S1 cleavage[35]. Also, the deleted sequences show no residual amino acid sites reported to be involved in the binding of other proteins[58,78]. When we co-cultured MEFs from N1ΔFC/ΔFC in presence of L cells expressing Dll1, we found detectable NICD release in the mutants albeit at lower levels as compared heterozygous N1WT/ΔFC or N1WT/WT MEFs which is coherent with the understanding that S1 cleavage affects the ligand dependent activation on the cell surface and not the signal transduction through downstream S3 cleavage (data not shown). Moreover, it illustrates that the mutant N1ΔFC is capable of binding the ligand in trans and signaling as a collinear 300kDa surface protein.

In order to find how exactly does S1 play a role in effective transactivation so as to eventuate sufficient signal transduction downstream, we decided to perform optical tweezers based force spectroscopy on live cells to find out if the biophysical requirements for pulling the NRR of heterodimeric and collinear N1 are different. Several recent studies on forces required for activation and ADAM cleavage of Notch have been reported, however, none have aimed to isolate the difference between the two isoforms[26,51,79]. Here, we directly compare the ligand pulling mechanics of N1WT with that of our engineered mutant protein N1ΔFC expressed in L-cells. Importantly, the L-cell derived N1WT (HAN1) and N1ΔFC (HAN1ΔFC-A) cells used in these assays were similar in cell surface expression levels (Fig. 3.4). Reflecting this is our observation that the specific rupture probabilities

between the two isoforms are similar (Fig. 3.5) and are greater than that for parental L-cells which have background endogenous N1WT. RFS analysis of N1WT and N1ΔFC displayed unclear force modes, which are mathematically revealed by Gaussian mixture model fitting (Fig. 3.7). The single bond force mode inferred from such Gaussian fits displayed forces less than ~19pN, the force that is equal to N1-Dll1 bond strength[16]. These results suggest that ligand exerts similar force to expose both the isoforms for ADAM cleavage, and most importantly that there are no measurable differences in the affinity of ligand binding between the isoforms. FEC analysis of these ruptures show that as compared to N1ΔFC , there is an inherent bias to undergo cleavage at lower energy for N1WT as well as parental L-cells and NICD deletion mutant OCDN1 (Fig. 4.5).

The cartoons in Fig. 6.1 illustrate a simple physical model of the origin of the ET1 and ET2 classes of FECs. When we consider N1WT, the predominant isoform is heterodimeric. When ligand engages with the heterodimer, the molecule unravels at its LNR domains and gets disengaged at the S1 chain break making it analogous to a "soft" spring attached to a much stiffer spring – the plasma membrane (Fig. 6.1, i). Therefore, the tension exerted by ligand pulling is sufficient to allow the molecule to disengage and expose S2 cleavage site for activation before the membrane is engaged. On the other hand, when ligand pulls on N1ΔFC molecule, which is predominantly collinear, it encounters a resistance to pulling owing to the loss of easily detachable link at the S1 and thus is analogous to a "stiff" spring attached to the membrane (Fig. 6.1, ii) and allows for membrane extension. Other membrane bound receptor-ligand interaction pairs have been shown to elongate either the membrane or the structures to which they are attached[80–82]. For example, P-Selectin and PSGL-1 interaction extends the membrane upon force loading when a critical tension is

reached[80]. This membrane extension is considered to be possible because of local detachment of the membrane from the cortical cytoskeleton[81]. The ET2 curves from our experiments closely resemble the P-Selectin and PSGL-1 force curves, which show an initial elastic deformation followed by isotonic plateau attributed to membrane tether formation. Abrogation of furin processing could produce an N1 isoform having an extracellular domain that is capable of detaching the membrane from the cytoskeleton upon ligand pulling and thereby elevating the mechanical work of transactivation. This membrane extension hypothesis is further supported by the analysis of FECs for N1-EGF-TMHA cells in which the ET2 curves dominate. The N1-EGF-TMHA isoform is a short rigid molecule exclusively comprising EGF repeats shown to be almost inextensible at the level of forces applied during optical tweezers experiments[83]. Thus, we hypothesize that forces acting through the molecule will cause membrane deformation, ultimately leading to the formation of FEC plateaus once a critical level of tension is applied (Fig. 6.1, iii). To further illustrate that this 'membrane-extension' hypothesis is due to the increasing rigidity of the N1 isoforms from wild type to N1-EGF-TMHA, we tested a mutant receptor with heterodimeric NECD but with no NICD (OCDN1). If the OCDN1 NECD were to be softer than N1-EGF-TMHA, then ligand engagement of OCDN1 should result in a decreased ET2 frequency and a gain in ET1. Indeed, OCDN1 FECs showed high ET1 presence as compared to ET2 (at relative frequencies similar to N1WT), demonstrating that the tension generated by the ligand is primarily utilized to unravel and shed NECD. Our data suggests that furin acts to facilitate Notch signaling by rendering the NECD to be easily dissociated before the membrane can detach from the cytoskeleton due to the tension generated by ligand pulling.

This establishes the biophysical basis for efficient signal generation in activating heterodimeric N1.

High steady levels of Notch signals require steady NICD generation, which in turn depends on the extent of transactivation by ligand at the cell surface. NECD shedding at lower energy may perhaps enhance signal generation downstream due to ready access of S2 cleavage site. In that case, efficiency of NICD generation is directly related to energetic efficiency of receptor transendocytosis, and as a corollary, the reduction in signalling observed in N1ΔFC mutants causing hypomorphic phenotypes can be attributed to decrease in this efficiency. We, therefore, purport that S1 cleavage of Notch serves as an important modulatory process for tightly regulating sufficient Notch signalling levels by controlling the efficiency of ligand induced transactivation in developmental contexts which are heavily dependent on high Notch dosage.

NOTCH RECEPTOR -LIGAND COMBINATORICS HAVE SOME COMMON AND SOME UNIQUE BIOPHYSICAL PROPERTIES

Notch signaling mechanics is orchestrated by ligand binding and ligand cell endocytosis by the application of pulling force on Notch. From the ligand Notch bond strength studies, I was able to observe single bond and double bond modes at similar probabilities for N1-Dll1 interaction recapitulating previous findings[16]. The Jag1 -N1 bond strengths were similar to that observed for Dll-1 -N1 while Jag2- N1 was the strongest bond I could isolate from the RFS, albeit at a low rupture probability. Dll4 surprisingly did not exhibit any peak bond strength value beyond 15pN raising speculation whether Dll4 is acts through avidity more than affinity. Further, a total of 4pN was just enough to active Notch receptors in

recently reported studies in which Dll4 was used to transactivate N1[26]. If Dll4 binding predisposes Notch to be activated at lower forces, high bond strength of Dll4 and Notch1 would be unnecessary. But if low bond strength and activation at low forces are the mechanism of Dll4, then perhaps this is one way to allow only Dll4 as the potent ligand for activation in certain contexts. Either way further studies are required to fully investigate the role of Dll4 in Notch activation.

The second important deduction I could obtain from analyzing the Endocytic pulling force plots is that all ligands exert pulling force with average forces lesser than high bond strengths. This finding is significant in the light of Mechanotransduction model of Notch as force of transactivation must be lower than the Notch ligand bond strength to allow NRR exposure and NECD shedding. Jag 2 however, exhibited significantly lower forces compared to other ligands on N1 which is reminding of the fact that Jag2 activation of Notch is very specific while other ligands are potent activators relevant in many different contexts. Further, it also exemplifies a position that Jag2 activation may not supersede activation by other ligands.

Lunatic Fringe modification of Notch has an extraordinary relevance in somitogenesis and therefore, its importance in understanding Notch signaling is noteworthy. Lunatic Fringe is known to predispose Notch to execute selectivity for Delta class of ligands and not Jagged class. The exact mechanism of how glycosylation helps in accomplishing this preferential ligand receptor pair selection is only partially known. LFng modified N1 exhibits high bond strength with respect to Dll1 compared to its unglycosylated counterpart. Also, LFng modified N1-Dll1 bond strength is higher than the bond strength of LFng modified N1-Jag1.

Jag1 cells fail to exert significant pulling force on laser trapped LFng modified N1Fc beads compared to unmodified N1Fc beads. Perhaps the LFng modification on N1Fc was meant to reduce the potential of Jag1 to pull on Notch than to bind Notch. This is in line with the fact that Jag1 still binds glycosylated Notch receptors but generates significantly lower signal compared to Dll1 or when compared to its signaling potential on the unmodified Notch[84].

CONCLUSIONS

Notch signaling pathway is intrinsically complex with part of its complexity arising from careful modulation of forces involved in its activation cascade. The level of Notch signaling is context dependent and is directly proportional to the transactivation mechanics at the cell surface. Furin cleavage of Notch ensures high efficiency by reducing the mechanical energy expenditure of ligands leading to high signaling levels (Fig. 6.2). Almost all ligands exert pulling force on Notch and is in line with the fact that Notch transactivation is not allosteric . Lunatic Fringe modified N1 is unable to be effectively pulled by Jagged 1 corroborating the fact that effects of LFng modification is to affect ligand based transactivation so as to predispose Notch to activation only by the Delta class of ligands.

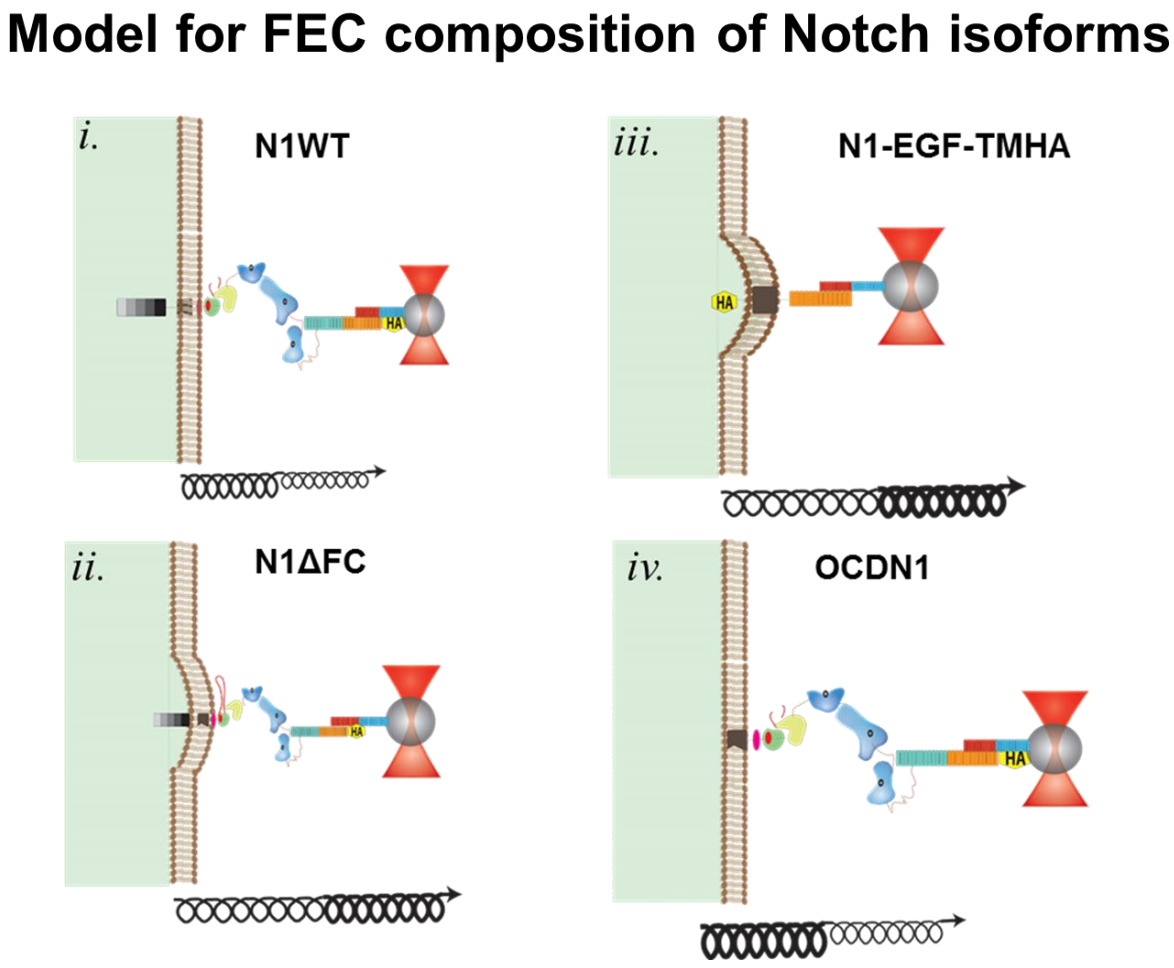

Figure 6.1: Model to understand the FEC composition of the different Notch isoforms. Illustrative model to explain the ET1 and ET2 FECs that serve as biomechanical fingerprint of ligand induced transactivation. (*i*) N1WT is predominantly heterodimeric and acts a 'soft' sessile spring attached to membrane allowing easy ectodomain shedding. (*ii*) furin resistant N1ΔFC likely engages the membrane before rupture that relaxes the tension which possibly delays activation. (*iii*) Transmembrane mutant N1-EGF-TMHA is rigid molecule

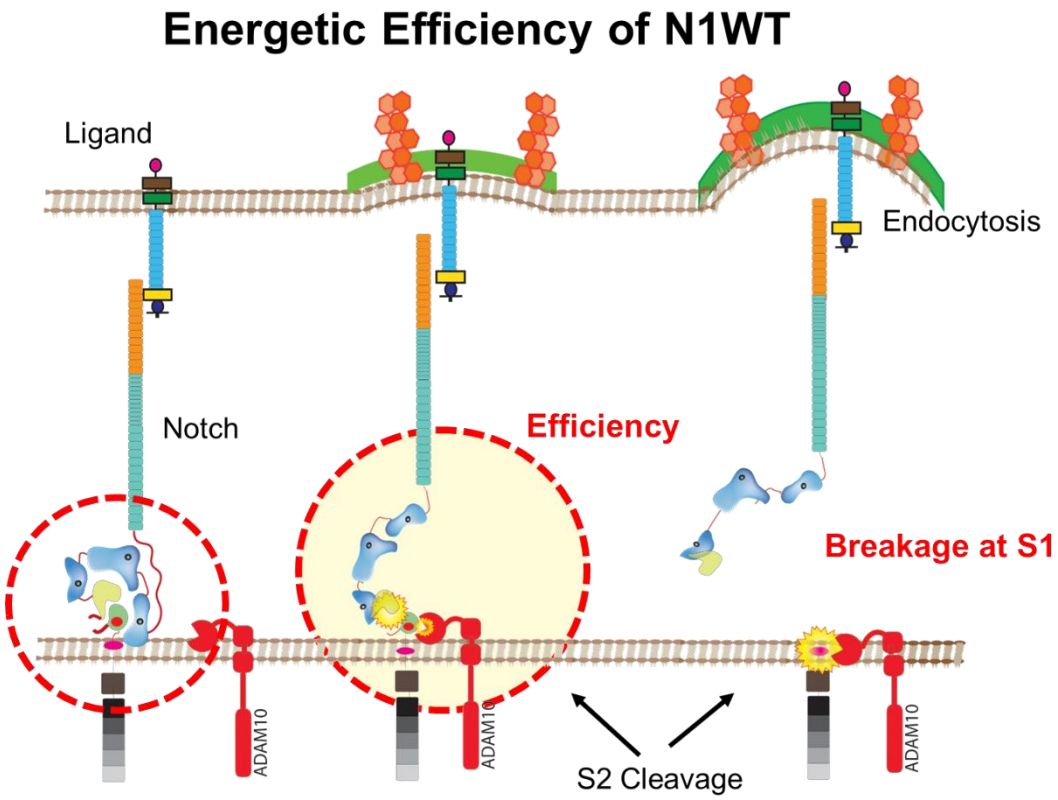

Figure 6.2: Pictorial summary of Aim1 of my studies in which I investigated the effects of furin processing on Notch on signal transduction. Heterodimeric Notch receptor takes an energetic 'path of least resistance' upon ligand engagement leading to ectodomain shedding and efficient cleavage of the receptor. Over a range of cellular forces available, Notch mechanotransduction is limited by ligand exerted pulling forces which are lesser than the force required to break the Notch-ligand bonds. Under such low forces of transactivation, furin processing further channelizes ectodomain shedding at lowest possible energy, thereby increasing the chances of productive signaling.

APPENDIX I

Rupture Force Spectra of cell lines expressing Notch isoforms

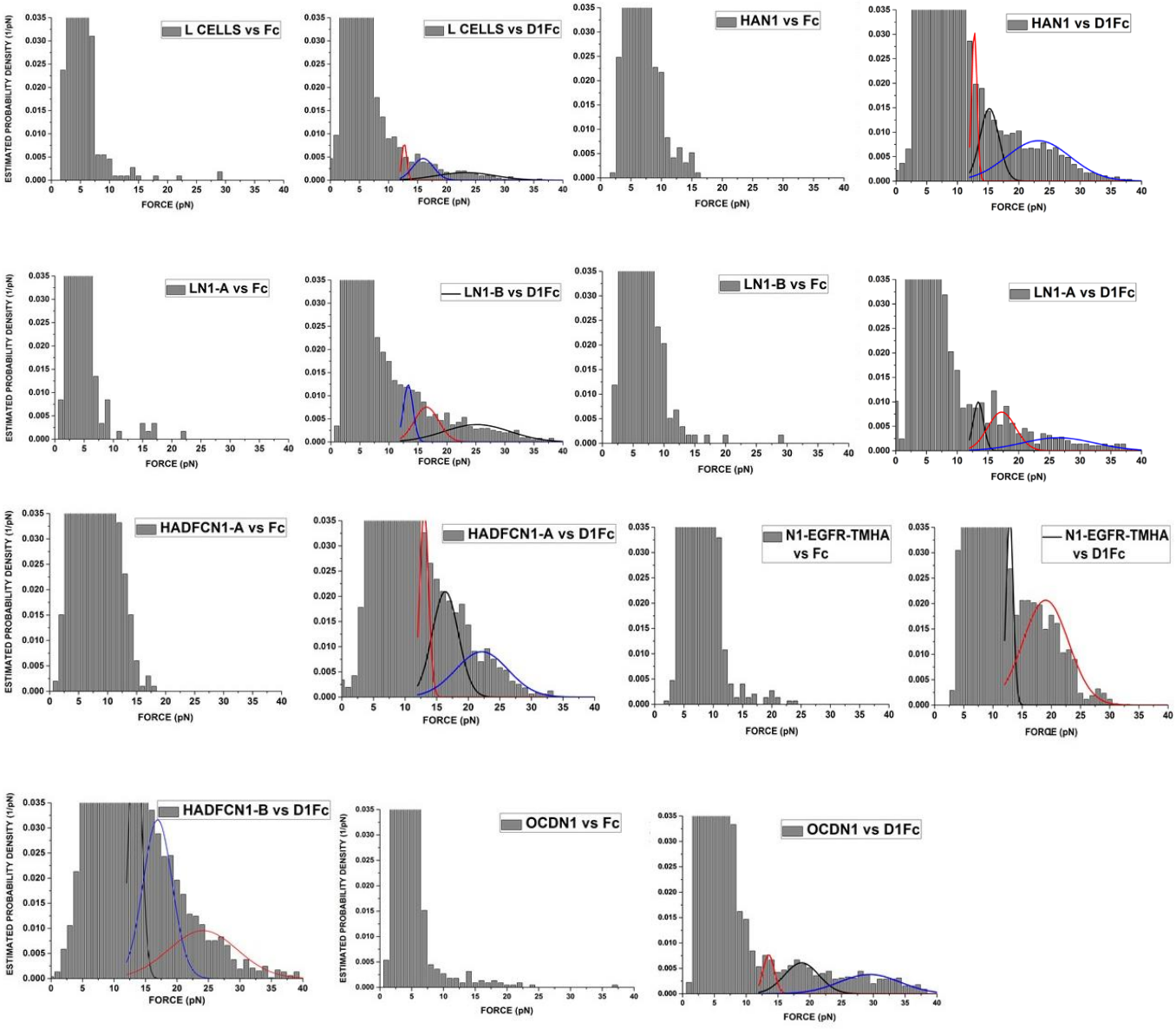

APPENDIX II

Summary of Optical Tweezers based cell-bead assay

Original Cell Line Name	Interchangeable Name	Ectopic Expression	Number of Cell Bead Pairs (using D1Fc beads)	Number of Ruptures(using D1Fc beads)	Number of Cell Bead Pairs (using Fc beads)	Number of Ruptures (using Fc beads)
L-Cells	L-Cells	Parental	125	10529	17	1096
HAN1-8	HAN1	HA tagged N1WT	129	8191	13	967
N1-8	LN1-A	N1WT	45	2873	7	593
N1-12	LN1-B	N1WT	85	7525	9	591
HAN1ΔFC-2	HAN1ΔFC-A	HA tagged N1ΔFC	88	8265	12	995
HAN1ΔFC-1	HAN1ΔFC-B	HA tagged N1ΔFC	77	5308	--	--
N1-EGFR-TMHA-14	N1-EGF-TMHA	N1with only 1-15 EGFrepeats-Transmembrane domain	152	6897	18	1488
OCDN1-2	OCDN1	N1WT without NICD	58	4503	22	2243

Summary of FEC analysis for cell lines

Original Cell Line Name	Interchangeable Name	Ectopic Expression	Number of FECs	Number of ET1 curves	Number of ET2 curves
L-Cells	L-Cells	Parental	261	149	35
HAN1-8	HAN1	HA tagged N1WT	705	407	156
LN1-8	LN1-A	N1WT	187	121	17
LN1-12	LN1-B	N1WT	489	352	70
HAN1ΔFC-2/ HADFCN1-A	HAN1ΔFC-A	HA tagged N1ΔFC	743	279	294
HAN1ΔFC-1/ HADFCN1-B	HAN1ΔFC-B	HA tagged N1ΔFC	718	158	438
N1-EGFR-TMHA-14	N1-EGF-TMHA	N1with only 1-15 EGF repeats-Transmembrane domain	421	103	217
OCDN1-2	OCDN1	N1WT without NICD	266	160	66

Summary of FEC analysis for N1WT and N1ΔFC chemical inhibition of ADAM and Furin					
Cell line	**Ectopic Expression**	**Number of cell Bead pairs**	**Number of FECs**	**Number of ET1 curves**	**Number of ET2 curves**
HAN1-8 N1WT	Untreated	47	340	165	108
	Furin Inhibitor	45	479	203	204
	TAP-2 (ADAM Inhibitor)	40	385	217	94
HAN1ΔFC-2 N1ΔFC	Untreated	36	300	111	143
	Furin Inhibitor	42	491	193	249
	TAP-2 (ADAM Inhibitor)	29	324	130	146

APPENDIX III

Rupture Force and Extension values of FECs

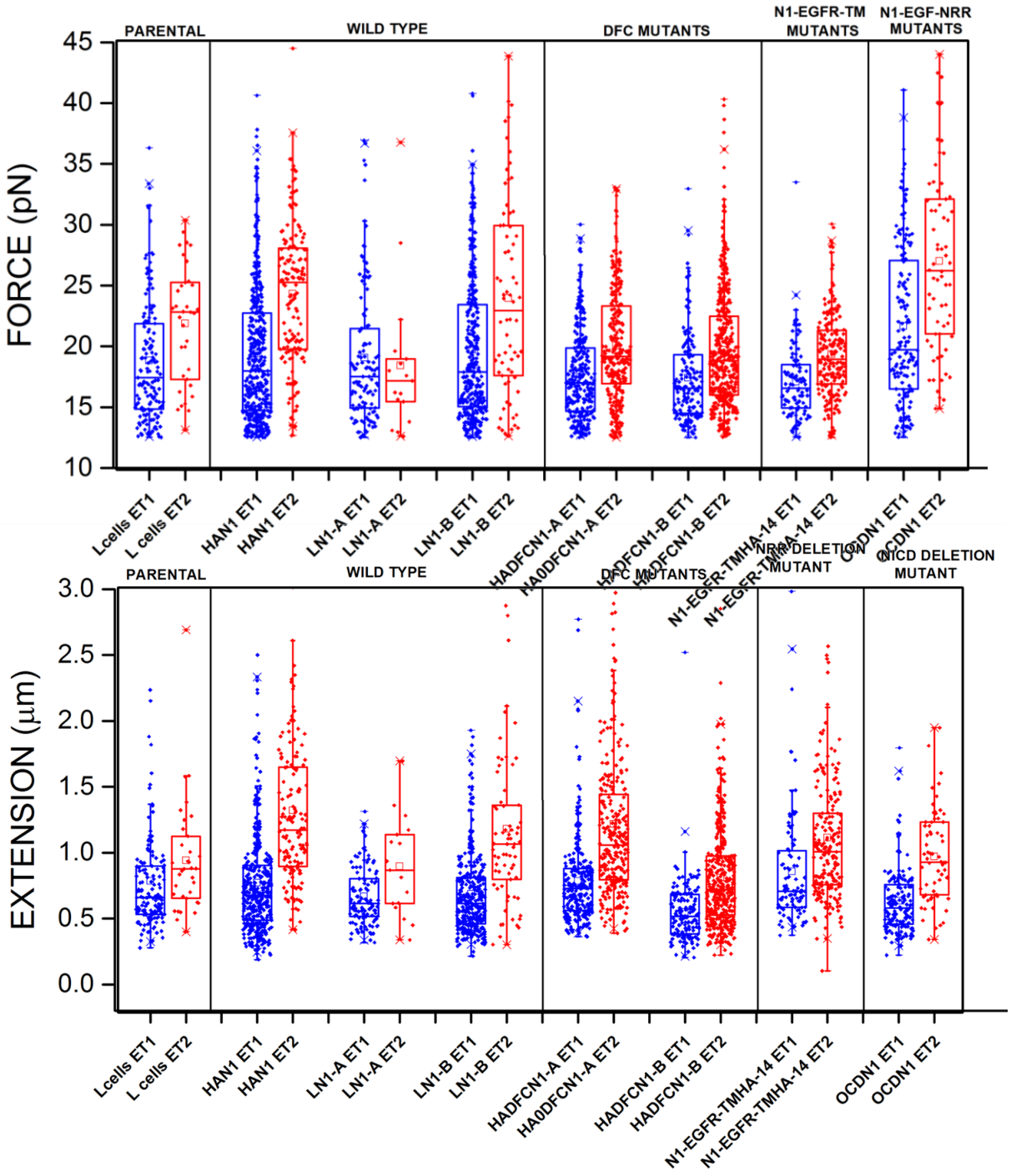

APPENDIX IV

EXTENDED MATERIALS AND METHODS

Materials

Item	Make	Catalog Number
Advanced DMEM	Gibco by ThermoFisher Scientific	12491023
DMEM	Gibco by ThermoFisher Scientific	11995040
PBS (phosphate buffered saline)	Gibco by ThermoFisher Scientific	10010031
FBS (Fetal Bovine Serum)	Atlanta Biologicals	S11150, lot# D13057
Trypsin-EDTA (0.05%), phenol red	Gibco by ThermoFisher Scientific	25300062
CO_2 Independent Medium	Gibco by ThermoFisher Scientific	18045088
BSA (Bovine Serum Albumin)	Sigma-Aldrich	A5611-10G
DMSO (Dimethyl sulfoxide)	Sigma-Aldrich	D2650-5X5ML
Ethanol	Gold Shield	serial# D1-15686
Protein A Coated Microspheres	Bangs Laboratories, Inc.	CP02N
1.5mL microcentrifuge tubes	VWR	20170-038
TAPI-2 (Inhibitor of TNF-α processing)		BML-PI135-0001
Furin convertase inhibitor (chloromethylketone)	Enzo Life Sciences, Inc.	ALX-260-022-M005
35MM Glass Bottom Dishes uncoated	MatTek Corporation	P35G-1.5-20-C
OriginPro 9.1 Student Software	OriginLab	
MATLAB R2012	Matlab	
LabView	National Instruments	
Nano-precision (Piezostage) Stage	Physik Instrumente GmbH & Co. KG, Karlsruhe, Germany	

Methods

Performing a Rupture Experiment

Cells expressing Notch or the Ligand were cultured on 35 mm glass bottom dishes (MatTek) and placed on the piezo stage in the custom-built laser tweezers instrumentation, as shown in cartoon in Fig 2.2. Cells were seeded at a seeding density that allowed single isolated cells spread across the glass cover slip on the dish. I optimized the cell plating density to be 40,000 cells per 35 mm dish seeded for an overnight growth to allow for Notch or ligand expression. It was essential to obtain a single cell spread and yet a good number of cells for two reasons. First, choosing a cell which is adhered to another cell or group of cells for rupture experiment may impact rupture probability as available Notch (or ligand) on the surface may accumulate unevenly on the cell contact free surface. Secondly, clustering of the ligands or Notch receptors of cells on their counterparts on beads may lead to interactions that deviate from single molecule. After the dish was taken from incubator, the media was supplanted with 2 mls of CO_2 independent media and the dish is carefully placed in the slot of the piezo stage. The incubator around the piezo in the microscope set up enables to maintain the temperature at 37°C. However, as the oil objective is used to focus the cells, the oil acts as a heat sink reducing the dish temperature to 33°C. Once the cells are in focus, they can be viewed in an installed Live Video program that takes input from microscope camera. The rupture experiment program written in LabView which is saved as 'Shreyas_RuptureForce' and the interface looks as shown in the Fig 7.1 & 7.2. The program can run the experiment as well as perform data acquisition from QPD through a DAQ device. The program has a space for input of file directory in which the collected data needs to be saved. Notch or Ligand coated beads were added (according to

the experiment) and a bead was trapped and brought close to the cells. The 'Uprate' and 'Downrate' fields in the LabView program refer to the approach and rectraction velocities of the piezo stage. A value of 1.2 corresponds to 24μm/s stage speed which was measured from tracking a stuck bead movement at the same height. Once the bead was positioned near the cell, the 'Start' button was pressed to run cyclic touch and release experiment. The piezo stage moves corresponding to a sawtooth waveform. A small time vs QPDx signal window shows live QPD signal recording so observer can have an estimation of the number of ruptures and make sure that the cycles are uniformly recurring without artefacts (Fig. 7.1). The signal appears inverted in the QPD signal window on the LabView program and occasional deviations (labelled as 'bond' in Fig. 7.1) are stochastic bond formation during an approximate 60s run of the touch and release experiments.

Calibration and Conversion of QPD into Force

The raw QPD signals were extracted from LabView generated '.bin' files in Matlab and QPD X, Y and sum were computed. QPD X provides the rupture voltage waveform corresponding the cell bead contact experiments. For calibration, QPD X signals corresponding to Brownian displacements of a laser trapped bead away from a cell were recorded for 60s which is applied to compute a power spectra as shown in Fig. 2.3. The corner frequency of the power spectra was extracted from a fit to the Lorentzian equation[16], $S(f) = \frac{S_0 f_0^2}{f_0^2 + f^2}$ … (1)

Where f_0 is Corner frequency, S(f) is the power spectral density as a function of frequency. The Corner frequency f_0 is used to compute the trap stiffness κ using the equation,

$\kappa = 2\pi\gamma f_0$ … (2)

Where γ is the Drag Coefficient which is, further, computed after Faxen's correction[49] from the equation

$\gamma = \frac{3\pi\eta d}{1-\frac{9r}{16d}+\frac{1}{8}(\frac{r}{d})^3}$, …(3)

where d is the distance of the bead from the glass bottom, η is the coefficient of viscosity and r is the radius of the bead. The voltage waveforms for 60s contact release experiments are converted to Force by $Force = \kappa * Displacement$. The Displacement is computed from voltage by calibrating bead movement in time and converting voltage of QPD corresponding to the movement from the fit to the graphs as shown in Fig. 6.4. The meters moved by the bead per voltage of QPD recorded is termed as V2m. Displacement then is V2m times the QPD X voltage normalized to QPD sum.

The laser tweezer system is a dual beam set up[48,85] and can be used to precisely monitor the bead movement in time by oscillating the trapping laser while keeping the detection laser, which is coaligned to the trapping laser, centered to the bead. First, the trapping 1064nm laser beam which is of high power (200 to 250 mW) is co-aligned with a 785nm detection laser of very low trapping power. The coaligned beam collected from the objective through culture dish is expanded by a condenser lens into a beam splitter which dumps the trapping beam while only detection beam is collected onto the QPD. Therefore, the trapping beam is primarily used for trapping the bead while the detection beam is used for detecting the movement of the trapped bead. Thus when trapping beam is oscillated with the help of a pair of perpendicular mirrors known as galvanometers mentioned by

Kotlarchyk et al. 2011, the bead moves in media following the trapping beam focus. This movement can be detected by the detection laser with precise co-alignment. A known voltage to galvanometers was applied in a square wave form to move the bead through a distance as shown in Fig. 7.3a and the bead movement for per mV of galvanometer voltage is obtained by calculating the bead movement through a centroid-detection image processing algorithm written in Matlab as shown in Fig, 7.3 b & c. When a 2mV triangular oscillation voltage is applied to galvanometers, it oscillates the bead in space which is recorded by detection laser as a triangular QPD X voltage (Fig. 7.5). A QPD X voltage recorded vs Position graph is plotted using the equation

$$Position = V2mg * Vg \ldots (4)$$

Where V2mg is the bead movement per volt sent to galvanometers obtained from square wave analysis shown in Fig. 7.3 a. Vg is the Triangular voltage amplitude applied to galvanometers to move the trapped bead in a triangular wave and QPD X is the voltage recorded on the QPD X. The inverse slope of the linear fit of the linear-most region of the triangular wave in Fig. 7.4 gives meters moved by bead per volts recorded on QPD X which is the V2m. This way of calculating the bead position after movement by laser through galvanometers was very reproducible and convenient than previous methods[16].

Classification of Force Extension Curves

The ruptures above 12pN cut off were converted to Force Extension Curves (FECs) as described in the main methods and stored in a 'Dump' folder. The curves were classified by my undergraduate Janelle Halog using a custom written, user friendly program in Matlab as shown in Fig, 7.5. The program prompts to input the initial number of curves already

classified – a functionality that allows the observer to continue from previously saved work. In the case of classifying from the beginning, the initial values for the number of classified curves for each class would be 0. After inputting the number of curves for each class, the program prompts new curve sequentially from the FEC Dump folder. The program also takes input from the user as to which curve number should be prompted from the Dump to continue from previously saved work; in case of beginning the classification, this number would be 0. The new curve is prompted to the user as shown in Fig. 7.6 and the user is allowed to "select" the button corresponding the class which the user thinks the prompted curve belongs. In the example shown in Fig. 7.6, I would select the Class 5 option as the curve resembles Class 5 described in Fig. 4.2. The information of classification and the curve is both then stored in a different folder under the classified name.

Figure 7.1: A snapshot of the LabView program to conduct Rupture experiment 1: The LabView program "Shreyas_RuptureForce" shows the user interface for performing a rupture experiment. The program has fields to input the File directory to save recorded files, approach and retraction piezo stage velocities, sampling rate and time steps. The QPD signal monitoring window shows the continous signal generation in cyclic touch and release experiments for user to gauge the signal characteristics and bond formation.

Figure7.2: A snapshot of the LabView program to conduct Rupture experiment 2:
The trapped bead placed away from the cells at a sufficient distance to start the rupture experiment

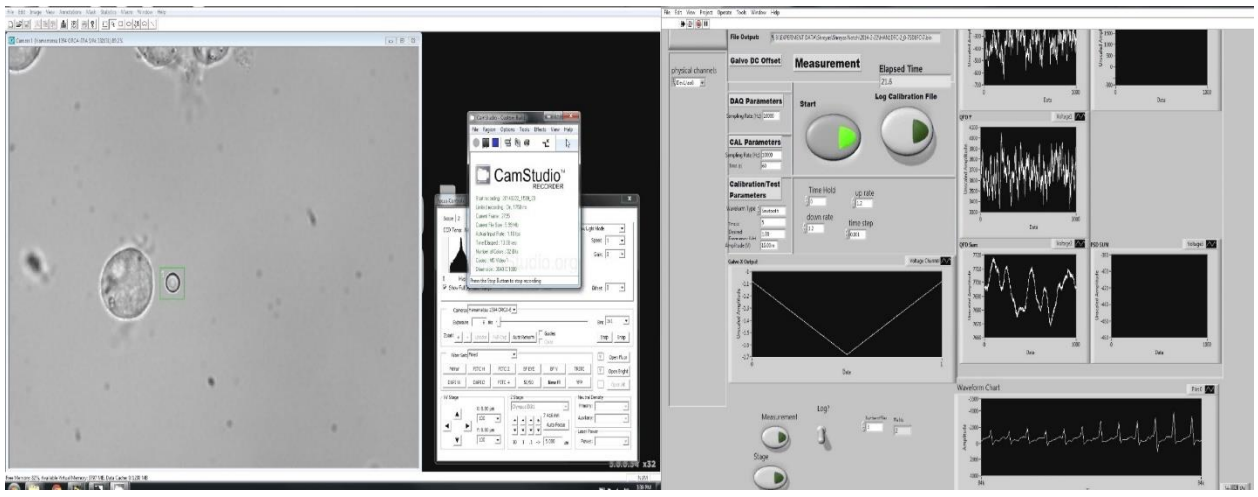

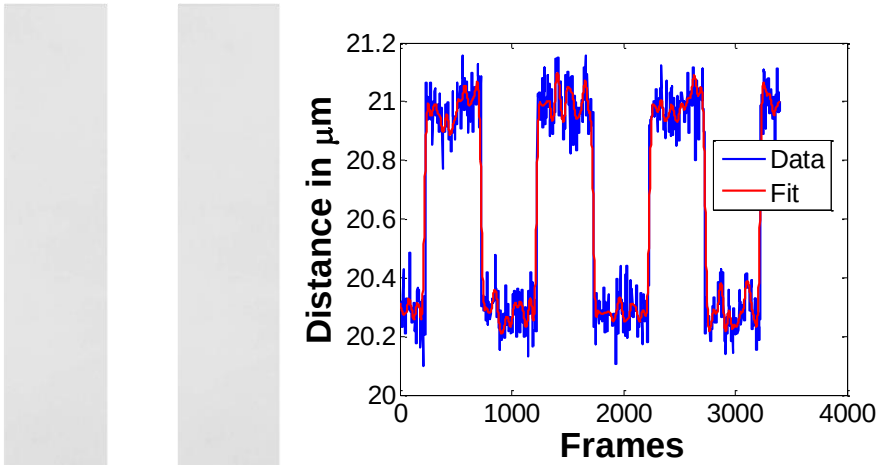

Figure 7.3: V2mg - Distance moved by bead per volt applied to galvanometers. **a.** Image processing of the bead moved by a square wave of a known voltage applied to galvanometers which steer the trap focus thereby steering the trapped bead. The position of the bead is computed from locating the centroid of the bead and its movement relative to the field of view whose measurements in meters are obtained from the specifications of the camera. **b.** The position of the bead extracted from the image processing shows the bead moves in a square waveform reflecting the square waveform of volts applied to the galvanometers.

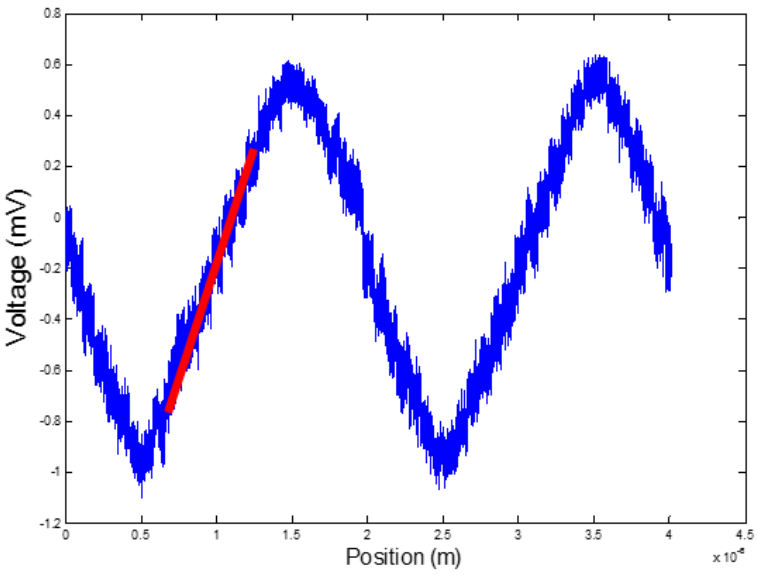

Figure 7.4: QPD volts to meters Calibration. The galvanometers are used to move a trapped bead in a triangular oscillation and the corresponding QPD X response is recorded. From the galvanometer volts to bead displacement square waveform from Fig. 6.3, we can know the meters moved by the bead per volt applied to galvanometers (V2mg). Using V2mg, the position of the bead in time is calculated and a plot of QPD X vs bead position is generated. The inverse of slope of the linear fit gives QPD Volts to meters.

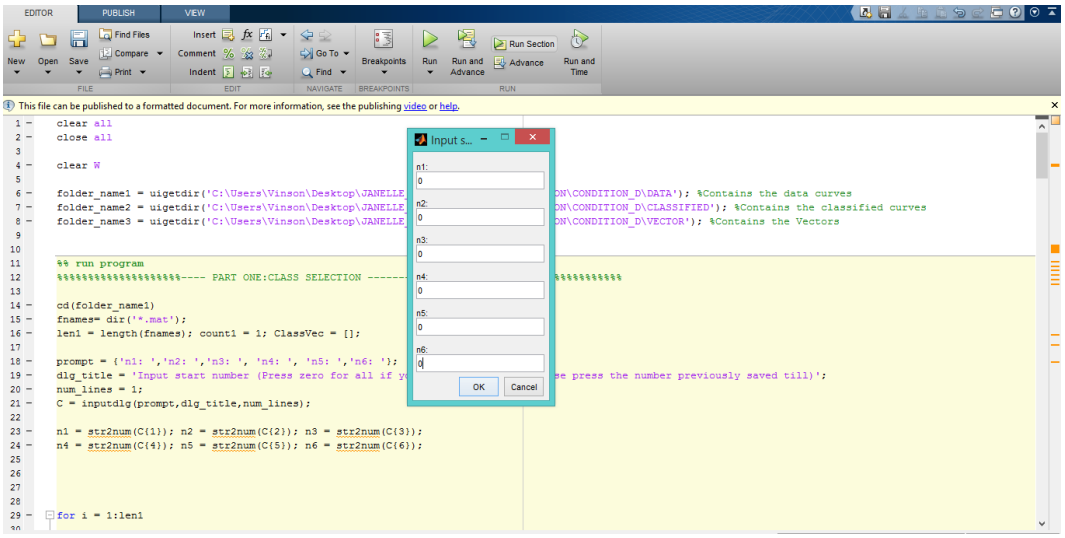

Figure 7.5: A snapshot of FEC Classification program1: The program asks for inputs of number of curves already classified for each curve type.

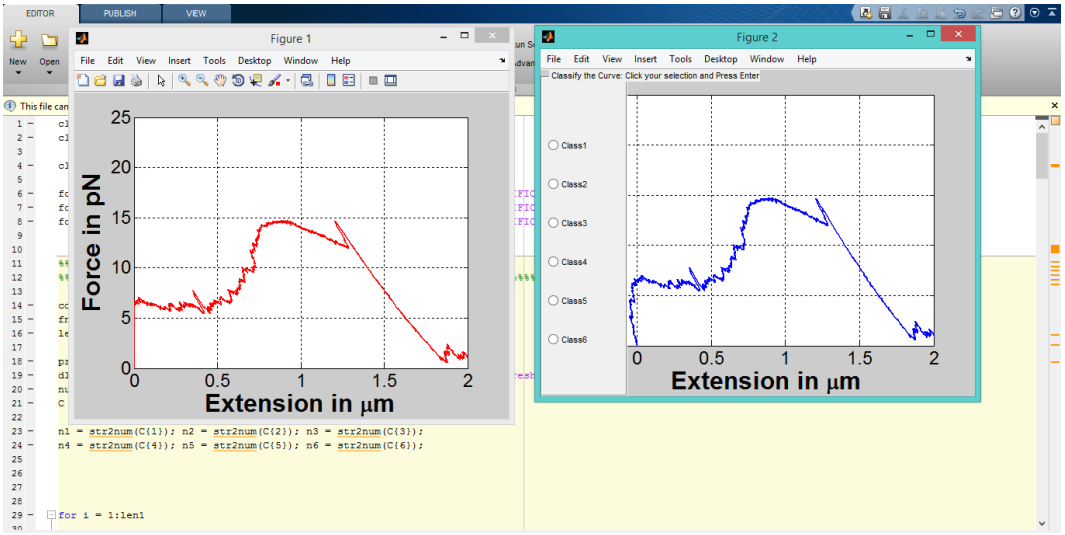

Figure 7.6: A snapshot of FEC Classification program 2: The program prompts fresh curves from a stored folder and displays for the user to identify and classify based on geometry described in Fig. 4.2

REFERENCES

1. Morgan, T. H. The Theory of Gene. *Sch. Publ.* **14,** 43–59 (1917).

2. Kimble, J. & Simpson, P. THE LIN-12 / Notch SIGNALING. (1997).

3. Ellisen, L. W. *et al.* TAN-1, the human homolog of the Drosophila Notch gene, is broken by chromosomal translocations in T lymphoblastic neoplasms. *Cell* **66,** 649–661 (1991).

4. Demarest, R. M., Ratti, F. & Capobianco, a J. It's T-ALL about Notch. *Oncogene* **27,** 5082–5091 (2008).

5. Hansson, E. M., Lendahl, U. & Chapman, G. Notch signaling in development and disease. *Semin. Cancer Biol.* **14,** 320–328 (2004).

6. Kopan, R. & Turner, D. L. The Notch pathway: Democracy and aristocracy in the selection of cell fate. *Curr. Opin. Neurobiol.* **6,** 594–601 (1996).

7. Le Gall, M., De Mattei, C. & Giniger, E. Molecular separation of two signaling pathways for the receptor, Notch. *Dev. Biol.* **313,** 556–567 (2008).

8. Minter, L. M. & Osborne, B. A. Canonical and Non-Canonical Notch

Signaling in CD4 + T Cells. 99–114 (2012). doi:10.1007/82

9. D'Souza, B., Miyamoto, a & Weinmaster, G. The many facets of Notch ligands. *Oncogene* **27,** 5148–67 (2008).

10. Kopan, R. & Ilagan, M. X. G. The canonical Notch signaling pathway: unfolding the activation mechanism. *Cell* **137,** 216–33 (2009).

11. Guruharsha, K. G., Kankel, M. W. & Artavanis-Tsakonas, S. The Notch signalling system: recent insights into the complexity of a conserved pathway. *Nat. Rev. Genet.* **13,** 654–66 (2012).

12. Weinmaster, G. Notch signal transduction: a real rip and more. *Curr. Opin. Genet. Dev.* **10,** 363–9 (2000).

13. Musse, A. a, Meloty-Kapella, L. & Weinmaster, G. Notch ligand endocytosis: mechanistic basis of signaling activity. *Semin. Cell Dev. Biol.* **23,** 429–36 (2012).

14. Del Álamo, D., Rouault, H. & Schweisguth, F. Mechanism and significance of cis-inhibition in notch signalling. *Curr. Biol.* **21,** 40–47 (2011).

15. Sprinzak, D. *et al.* Cis Interactions between Notch and Delta Generate Mutually Exclusive Signaling States. **465,** 86–90 (2010).

16. Shergill, B., Meloty-Kapella, L., Musse, A. a, Weinmaster, G. & Botvinick, E. Optical tweezers studies on notch: single-molecule interaction strength is independent of ligand endocytosis. *Dev. Cell* **22,** 1313–20 (2012).

17. Le Borgne, R., Bardin, A. & Schweisguth, F. The roles of receptor and ligand endocytosis in regulating Notch signaling. *Development* **132,** 1751–62 (2005).

18. Meloty-Kapella, L., Shergill, B., Kuon, J., Botvinick, E. & Weinmaster, G. Notch Ligand Endocytosis Generates Mechanical Pulling Force Dependent on Dynamin, Epsins, and Actin. *Dev. Cell* **22,** 1299–1312 (2012).

19. Weinmaster, G. & Kintner, C. Modulation of notch signaling during somitogenesis. *Annu. Rev. Cell Dev. Biol.* **19,** 367–95 (2003).

20. Gordon, W. R. *et al.* Structure of the Notch1-negative regulatory region: Implications for normal activation and pathogenic signaling in T-ALL. *Blood* **113,** 4381–4390 (2009).

21. Rebay, I. *et al.* Specific EGF repeats of Notch mediate interactions with Delta and Serrate: implications for Notch as a multifunctional receptor. *Cell* **67,** 687–99 (1991).

22. Chillakuri, C. R. *et al.* Structural Analysis Uncovers Lipid-Binding Properties of Notch Ligands. *Cell Rep.* **5,** 861–867 (2013).

23. Vincent C. Luca, Kevin M. Jude, Nathan W. Pierce, Maxence V. Nachury, Suzanne Fischer, K. C. G. Structural basis for Notch1 engagement of Delta-like 4. **347,** (2015).

24. Yamamoto, S. *et al.* A mutation in EGF repeat-8 of Notch discriminates between Serrate/Jagged and Delta family ligands. *Science* **338,** 1229–32 (2012).

25. Ahimou, F., Mok, L. P., Bardot, B. & Wesley, C. The adhesion force of Notch with Delta and the rate of Notch signaling. *J. Cell Biol.* **167,** 1217–1229 (2004).

26. Gordon, W. R. *et al.* Mechanical Allostery: Evidence for a Force Requirement in the Proteolytic Activation of Notch. *Dev. Cell* 729–736 (2015). doi:10.1016/j.devcel.2015.05.004

27. Jaekel, R. & Klein, T. The Drosophila Notch inhibitor and tumor suppressor gene lethal (2) giant discs encodes a conserved regulator of endosomal trafficking. *Dev. Cell* **11,** 655–69 (2006).

28. Dunwoodie, S. L., Henrique, D., Harrison, S. M. & Beddington, R. S. Mouse

Dll3: a novel divergent Delta gene which may complement the function of other Delta homologues during early pattern formation in the mouse embryo. *Development* **124,** 3065–76 (1997).

29. Ladi, E. *et al.* The divergent DSL ligand Dll3 does not activate Notch signaling but cell autonomously attenuates signaling induced by other DSL ligands. *J. Cell Biol.* **170,** 983–992 (2005).

30. Logeat, F. *et al.* The Notch1 receptor is cleaved constitutively by a furin-like convertase. *Proc. Natl. Acad. Sci. U. S. A.* **95,** 8108–12 (1998).

31. Thomas, G. Furin at the cutting edge: from protein traffic to embryogenesis and disease. *Nat. Rev. Mol. Cell Biol.* **3,** 753–66 (2002).

32. Blaumueller, C. M., Qi, H., Zagouras, P. & Artavanis-Tsakonas, S. Intracellular cleavage of Notch leads to a heterodimeric receptor on the plasma membrane. *Cell* **90,** 281–291 (1997).

33. Kidd, S. & Lieber, T. Furin cleavage is not a requirement for Drosophila Notch function. *Mech. Dev.* **115,** 41–51 (2002).

34. van Tetering, G. & Vooijs, M. Proteolytic cleavage of Notch: 'HIT and RUN'. *Curr. Mol. Med.* **11,** 255–69 (2011).

35. Gordon, W. R. *et al.* Effects of S1 cleavage on the structure, surface export, and signaling activity of human Notch1 and Notch2. *PLoS One* **4,** e6613 (2009).

36. Bush, G. *et al.* Ligand-induced signaling in the absence of furin processing of Notch1. *Dev. Biol.* **229,** 494–502 (2001).

37. Gordon, W. R., Arnett, K. L. & Blacklow, S. C. The molecular logic of Notch signaling: a structural and biochemical perspective. *J Cell Sci* **121,** 3109–3119 (2009).

38. Lake, R. J., Grimm, L. M., Veraksa, A., Banos, A. & Artavanis-Tsakonas, S. In Vivo analysis of the Notch receptor S1 cleavage. *PLoS One* **4,** (2009).

39. Gridley, T. NIH Public Access. **2153,** (2010).

40. High, F. a & Epstein, J. a. The multifaceted role of Notch in cardiac development and disease. *Nat. Rev. Genet.* **9,** 49–61 (2008).

41. Laboratories, B. Optical trapping and manipulation of neutral particles. **94,** 4853–4860 (1997).

42. Felgner, H., Müller, O. & Schliwa, M. Calibration of light forces in optical tweezers. *Appl. Opt.* **34,** 977–982 (1995).

43. Litvinov, R. I., Shuman, H., Bennett, J. S. & Weisel, J. W. Binding strength and activation state of single fibrinogen-integrin pairs on living cells. *Proc. Natl. Acad. Sci. U. S. A.* **99,** 7426–31 (2002).

44. Nichols, J. T. *et al.* DSL ligand endocytosis physically dissociates Notch1 heterodimers before activating proteolysis can occur. *J. Cell Biol.* **176,** 445–58 (2007).

45. Le Gall, S. M. *et al.* ADAM17 is regulated by a rapid and reversible mechanism that controls access to its catalytic site. *J. Cell Sci.* **123,** 3913–3922 (2010).

46. Hicks, C. *et al.* A secreted Delta1-Fc fusion protein functions both as an activator and inhibitor of Notch1 signaling. *J. Neurosci. Res.* **68,** 655–667 (2002).

47. Meloty-Kapella, L., Shergill, B., Kuon, J., Botvinick, E. & Weinmaster, G. Notch ligand endocytosis generates mechanical pulling force dependent on dynamin, epsins, and actin. *Dev. Cell* **22,** 1299–312 (2012).

48. Kotlarchyk, M. a *et al.* Concentration independent modulation of local micromechanics in a fibrin gel. *PLoS One* **6,** e20201 (2011).

49. Leach, J. *et al.* Comparison of Faxén's correction for a microsphere

translating or rotating near a surface. *Phys. Rev. E - Stat. Nonlinear, Soft Matter Phys.* **79,** 1–4 (2009).

50. Stephenson, N. L. & Avis, J. M. Direct observation of proteolytic cleavage at the S2 site upon forced unfolding of the Notch negative regulatory region. *Proc. Natl. Acad. Sci. U. S. A.* **109,** E2757-65 (2012).

51. Ploscariu, N. *et al.* Single molecule studies of force-induced s2 site exposure in the Mammalian notch negative regulatory domain. *J. Phys. Chem. B* **118,** 4761–70 (2014).

52. Gordon, W. R. *et al.* Mechanical Allostery: Evidence for a Force Requirement in the Proteolytic Activation of Notch. *Dev. Cell* 1–8 (2015). doi:10.1016/j.devcel.2015.05.004

53. Bozkulak, E. C. & Weinmaster, G. Selective use of ADAM10 and ADAM17 in activation of Notch1 signaling. *Mol. Cell. Biol.* **29,** 5679–5695 (2009).

54. Rand, M. D. *et al.* Calcium depletion dissociates and activates heterodimeric notch receptors. *Mol. Cell. Biol.* **20,** 1825–35 (2000).

55. Glomski, K. *et al.* Deletion of Adam10 in endothelial cells leads to defects in organ-specific vascular structures. *Blood* **118,** 1163–1174 (2011).

56. Hartmann, D. *et al.* The disintegrin/metalloprotease ADAM 10 is essential for Notch signalling but not for alpha-secretase activity in fibroblasts. *Hum. Mol. Genet.* **11,** 2615–2624 (2002).

57. Chi, Z. *et al.* Botch promotes neurogenesis by antagonizing Notch. *Dev. Cell* **22,** 707–20 (2012).

58. Watanabe, K. *et al.* Enhancement of Notch receptor maturation and signaling sensitivity by Cripto-1. *J. Cell Biol.* **187,** 343–353 (2009).

59. van Tetering, G. *et al.* Metalloprotease ADAM10 is required for Notch1 site 2 cleavage. *J. Biol. Chem.* **284,** 31018–31027 (2009).

60. Rebay, I. *et al.* Specific EGF repeats of Notch mediate interactions with Delta and Serrate: implications for Notch as a multifunctional receptor. *Cell* **67,** 687–699 (1991).

61. Andersson, E. R. & Lendahl, U. Therapeutic modulation of Notch signalling--are we there yet? *Nat. Rev. Drug Discov.* **13,** 357–78 (2014).

62. Preusse, K. *et al.* Context-Dependent Functional Divergence of the Notch Ligands DLL1 and DLL4 In Vivo. *PLoS Genet* **11,** e1005328 (2015).

63. Benedito, R. *et al.* The notch ligands Dll4 and Jagged1 have opposing

effects on angiogenesis. *Cell* **137,** 1124–35 (2009).

64. Kume, T. Novel insights into the differential functions of Notch ligands in vascular formation. *J. Angiogenes. Res.* **1,** 8 (2009).

65. Besseyrias, V. *et al.* Hierarchy of Notch-Delta interactions promoting T cell lineage commitment and maturation. *J. Exp. Med.* **204,** 331–43 (2007).

66. Abe, N., Hozumi, K., Hirano, K., Yagita, H. & Habu, S. Notch ligands transduce different magnitudes of signaling critical for determination of T-cell fate. *Eur. J. Immunol.* **40,** 2608–17 (2010).

67. Cappellari, O. *et al.* Dll4 and PDGF-BB Convert Committed Skeletal Myoblasts to Pericytes without Erasing Their Myogenic Memory. *Dev. Cell* **24,** 586–599 (2013).

68. Rios, A. C., Serralbo, O., Salgado, D. & Marcelle, C. Neural crest regulates myogenesis through the transient activation of NOTCH. *Nature* **473,** 532–535 (2011).

69. Andrawes, M. B. *et al.* Intrinsic selectivity of notch 1 for delta-like 4 over delta-like 1. *J. Biol. Chem.* **288,** 25477–25489 (2013).

70. Zhang, N. & Gridley, T. Defects in somite formation in lunatic fringe-deficient mice. *Nature* **394,** 374–377 (1998).

71. Rampal, R. *et al.* Lunatic fringe, manic fringe, and radical fringe recognize similar specificity determinants in O-fucosylated epidermal growth factor-like repeats. *J. Biol. Chem.* **280,** 42454–63 (2005).

72. Takeuchi, H. & Haltiwanger, R. S. Significance of glycosylation in Notch signaling. *Biochem. Biophys. Res. Commun.* **453,** 235–242 (2014).

73. Haltiwanger, R. S. & Stanley, P. Modulation of receptor signaling by glycosylation : fringe is an. **1573,** 328–335 (2002).

74. Taylor, P. *et al.* Fringe-mediated extension of O-linked fucose in the ligand-binding region of Notch1 increases binding to mammalian Notch ligands. *Proc Natl Acad Sci U S A* **111,** 7290–7295 (2014).

75. Hicks, C. *et al.* Fringe differentially modulates Jagged1 and Delta1 signalling through Notch1 and Notch2. *Nat. Cell Biol.* **2,** 515–20 (2000).

76. Jubb, A. M. *et al.* Expression of vascular Notch ligands Delta-like 4 and Jagged-1 in glioblastoma. *Histopathology* **60,** 740–7 (2012).

77. Sheldon, H. *et al.* New mechanism for Notch signaling to endothelium at a

distance by Delta-like 4 incorporation into exosomes. *Blood* **116,** 2385–94 (2010).

78. Chi, Z. *et al.* Botch Promotes Neurogenesis by Antagonizing Notch. *Dev. Cell* **22,** 707–720 (2012).

79. Wang, X. & Ha, T. Defining single molecular forces required to activate integrin and notch signaling. *Science* **340,** 991–4 (2013).

80. Evans, E., Heinrich, V., Leung, A. & Kinoshita, K. Nano- to microscale dynamics of p-selectin detachment from leukocyte interfaces. I. Membrane separation from the cytoskeleton. *Biophys J* **88,** 2288–2298 (2005).

81. Heinrich, V., Leung, A. & Evans, E. Nano- to microscale dynamics of P-selectin detachment from leukocyte interfaces. II. Tether flow terminated by P-selectin dissociation from PSGL-1. *Biophys. J.* **88,** 2299–2308 (2005).

82. Forero, M., Yakovenko, O., Sokurenko, E. V., Thomas, W. E. & Vogel, V. Uncoiling mechanics of Escherichia coli type I fimbriae are optimized for catch bonds. *PLoS Biol.* **4,** 1509–1516 (2006).

83. Oberhauser, a F., Marszalek, P. E., Erickson, H. P. & Fernandez, J. M. The

molecular elasticity of the extracellular matrix protein tenascin. *Nature* **393,** 181–185 (1998).

84. Yang, L.-T. *et al.* Fringe glycosyltransferases differentially modulate Notch1 proteolysis induced by Delta1 and Jagged1. *Mol. Biol. Cell* **16,** 927–42 (2005).

85. Kurup, A. *et al.* Novel insights from 3D models: the pivotal role of physical symmetry in epithelial organization. *Sci. Rep.* **5,** 15153 (2015).